Chemical analysis of thin films for applications in organic electronics

Angefertigt am *Max Planck Institut für Polymerforschung, Mainz* in der Arbeitsgruppe von Prof. Dr. Paul Blom

Angefertigt von	Carla Volkert
Matrikelnummer	2723540
Studiengang	Master Chemie, Johannes Gutenberg Universität Mainz
Fachbereich	Chemie, Pharmazie, Geographie und Geowissenschaften
Erstgutachter	Dr. Ulrike Kraft
Zweitgutachter	Prof. Dr. Pol Besenius
Bearbeitungszeit	sechs Monate
Eingereicht	30. Juli 2021

Ich, Carla Nicola Volkert, Matrikelnummer 2723540, versichere, dass ich meine Masterarbeit selbstständig verfasst und keine anderen als die angegebenen schriftlichen und elektronischen Quellen, sowie andere Hilfsmittel, benutzt habe. Alle Ausführungen, die anderen Schriften wörtlich oder sinngemäß entnommen wurden, habe ich kenntlich gemacht.

Datum, Ort

Unterschrift

List of abbreviations

approx.	approximately
CB	chlorobenzene
CP	cross polarization
CTC	charge transfer complex
DCB	*ortho*-dichlorobenzene
DCM	dichloromethane
DDQ	2,3-dichlor-5,6-dicyano-1,4-benzochinon
DFT	Density functional theory
EPR	electron paramagnetic resonance
ESR	electron spin resonance
F_4TCNQ	2,3,5,6-tetrafluor-7,7,8,8-tetracyanoquinodimethan
F8BT	poly(9,9-dioctylfluoren-*alt*-benzothiadiazol)
eV	electron volts
h	hours
HETCOR	heteronuclear correlation
IDT-BT	indacenodithiophen-*co*-benzothiadiazole
IR	infra red
K	Kelvin
L	liter
m	milli
M	molar
MALDI	matrix-assisted laser desorption/ionization
MeCN	acetonitrile
MeOH	methanol
min.	minutes
MS	mass spectrometry
m/z	mass-to-charge ratio
NaOH	sodium hydroxide
NMR	nuclear magnetic resonance
OFET	organic field effect transistor
OSC	organic semiconductor
ppm	parts per million
rt	room temperature (approx. 297 K)
TBAB	tetra-*N*-butylammonium bromide
TCNQ	7,7,8,8-tetra-cyanochinodimethan
TEMPO	2,2,6,6-tetramethylpiperidonyloxyl
THF	tetrahydrofuran
TOF	time of flight
UV/vis	ultraviolett/ visible

Contents

1 Zusammenfassung

In den letzten Jahren haben organische Halbleiter, die in elektronischen Bauelementen verwendet werden, viel Aufmerksamkeit erhalten. Vorteile sind, unter anderem, ihre Verarbeitbarkeit bei niedrigen Temperaturen und zu geringen Kosten, ihre mechanischen Flexibilität, ihr geringes Gewicht und die Möglichkeit, ihr chemisches Design individuell anzupassen.[1–3] In organischen Bauelementen, wie organischen Feldeffekttransistoren (OFETs), werden organische Halbleiter manchmal dotiert, um ihre Leitfähigkeit durch das Einfügen von Ladungsträgern zu verbessern und dadurch die Kenngrößen und Betriebsstabilität des Bauelements zu erhöhen.[1] Nikolka et al.[3] veröffentlichten 2017 eine Arbeit, in der sie über verbesserte OFET-Eigenschaften durch die Zugabe von molekularen Additiven zum konjugierten Polymer berichten. Aufgrund der nicht übereinstimmenden Energieniveaus von Polymer und Additiv sollte eine Dotierung des Polymers nicht stattfinden. Der bauelementverbessernde Effekt wird auf die Passivierung von Ladungsträgerfallen zurückgeführt, was durch weitere Studien gestützt wurde.[3–5] Als extrinsische Ladungsträgerfallen werden insbesondere Wasser und Sauerstoff diskutiert. Deren Passivierung wird auf die Verdrängung von Wasser aus nanoskopischen Zwischenräumen im Polymerfilm durch die Additive zurückgeführt. Alternativ könnte auch eine chemische Reaktion der Additive mit Wasser und/oder Sauerstoff zu der beschriebenen Passivierung führen.[3–5] Nikolka et al. verwendeten unter anderem die Polymere Indacenodithiophen-*co*-benzothiadiazole (IDT-BT) und Poly(9,9-dioctylfluoren-*alt*-benzothiadiazol) (F8BT) und das nicht-dotierende Additiv 7,7,8,8-Tetracyanochinodimethan (TCNQ).[3] Da es sich als schwierig erwies, die passivierenden chemischen Reaktionen, an denen TCNQ in den dünnen Schichten beteiligt sein könnte, nachzuvollziehen, wurden bisher keine Beweise für das Stattfinden selbiger beobachtet. Daher war es das Ziel dieser Arbeit, diese potenziell stattfindenden Reaktionen genauer zu untersuchen. Ursprünglich war geplant, dies hauptsächlich mit Hilfe von Matrix-unterstützten Laser-Desorption/Ionisation (MALDI) Spektrometrie zu tun. In einer kürzlich publizierten Arbeit von Horatz et al.[6] wurden konjugierte Polymere als duale MALDI-Matrizen vorgestellt. Basierend auf diesen Ergebnissen sollten die Polymere IDT-BT und F8BT als MALDI-Matrizen eingesetzt werden und somit den Nachweis von TCNQ-Reaktionsprodukten mit z.B. Wasser und/oder Sauerstoffbildung in den Filmen ermöglichen. Aufgrund der COVID-19-Pandemie war der Zugang zu dem Gerät jedoch sehr eingeschränkt. Daher wurde beschlossen, zusätzlich die Kernspinresonanzspektroskopie (NMR) und die Elektronenspinresonanzspektroskopie (ESR) als Analysemethoden zu verwenden.

In dieser Arbeit wurden die Polymere IDT-BT und F8BT sowie die Additive TCNQ, 2,3,5,6-Tetrafluor-7,7,8,8- tetracyanoquinodimethan (F_4TCNQ) und 2,3-Dichlor-5,6-dicyano-1,4-benzochinon (DDQ) untersucht. Die Verwendung der Polymere IDT-BT und F8BT als duale MALDI-Matrizen wurde untersucht, wobei sich herausstellte, dass beide lediglich im positiven Ionenmodus verwendet werden können. MALDI-Studien mit Kombinationen aus Polymer, Additiv und H_2O oder D_2O zeigten keine eindeutigen Anzeichen von TCNQ-H_2O-Reaktionsprodukten. Die lösungsmittel-, temperatur- und aggregatszustandabhängige Bildung von radikalischen Anionen von TCNQ, F_4TCNQ und DDQ sowie in verschiedenen Kombinationen aus Polymer und Additiv, wurden mittels ESR-Spektroskopie sowohl im festen als auch im flüssigen Zustand untersucht. Es wurde festgestellt, dass die molekularen Additive häufig Radikalanionen bilden, obwohl kein Elektronentransfer zu erwarten oder erkennbar ist. Es wird ein Zusammenhang mit der Polymeranwesenheit und dem Aggregatszustand vermutet. Mit-

tels Festkörper-NMR-Spektroskopie wurden IDT-BT/F_4TCNQ-Filme und die F_4TCNQ-Lösungsmittelabhängigkeit untersucht. Letzteres zeigte die lösungsmittel- und temperaturbedingte Bildung von neuartigen, nicht eindeutig zuzuordnenden F_4TCNQ-Spezien. Abschließend sollten mithilfe von Festkörper- und Lösungs-^{2}H NMR-Spektroskopie Reaktionsprodukte von TCNQ und D_2O untersucht werden. Es wurden keine eindeutigen Hinweise auf Reaktionsprodukte unter Beteiligung von Deuteronen beobachtet.

Abschließend ist zu sagen, dass die chemische Reaktion von TCNQ mit Wasser und/ oder Sauerstoff nicht eindeutig nachweisbar war. Das häufige Detektieren von Radikalen in Polymer/Additiv-Filmen, so wie in den reinen Additiven, legt die Vermutung nahe, dass die Radikalanionen des Additivs zur Verbesserung der Transistoreigenschaft beitragen könnten.

2 Abstract

In recent years, organic semiconductors used in electronic devices have received a lot attention due to their low-temperature and low-cost processability, mechanical flexibility, light weight, and the possibility to customize their chemical design.[1–3] In organic devices, such as organic field-effect transistors (OFETs), organic semiconductors are sometimes doped to improve their conductivity by inserting charge carriers, thereby improving the device performance and operational stability.[1] Nikolka et al.[3] published a paper in 2017 reporting improved OFET properties by adding molecular additives to conjugated polymers. Due to mismatched energy levels of polymer and additive, doping of the polymer should not occur. The device improving effect is attributed to the passivation of charge carrier traps, which was supported by further studies.[3–5] Water and oxygen, in particular, are discussed as extrinsic charge carrier traps.[1–3] The passivation of the same is attributed to the displacement of water from nanoscopic interstices in the polymer film by the additives. Alternatively, a chemical reaction of the additives with water and/or oxygen could lead to the described passivation.[3–5] Nikolka et al. used, among others, the polymers indacenodithiophen-*co*-benzothiadiazole (IDT-BT) and poly(9,9-dioctylfluoren-*alt*-benzothiadiazole) (F8BT) and the non-doping additive 7,7,8,8-tetracyanoquinodimethane (TCNQ).[3] Since it proved difficult to trace the passivating chemical reactions in which TCNQ might be involved inside the thin films, no evidence of the same has been observed so far. Therefore, this work aimed to investigate these potentially occurring reactions in more detail. Originally, it was planned to do this mainly using matrix-assisted laser desorption/ionization (MALDI) spectrometry. In a recent paper by Horatz et al. conjugated polymers were presented as dual MALDI matrices.[6] Based on these results, the polymers IDT-BT and F8BT ought to be used as MALDI matrices and thus facilitate the detection of TCNQ reaction products with e.g. water and/ or oxygen forming in the films. However, due to the COVID-19 pandemic, access to the instrument was very limited. Therefore, it was decided to additionally use nuclear magnetic resonance spectroscopy (NMR) and electron spin resonance spectroscopy (ESR) as analytical methods.

In this work, the polymers IDT-BT and F8BT and the additives TCNQ, 2,3,5,6-tetrafluoro-7,7,8,8-tetracyanoquinodimethane (F_4TCNQ) and 2,3-dichloro-5,6-dicyano-1,4-benzoquinone (DDQ) were investigated. The use of the polymers IDT-BT and F8BT as dual MALDI matrices was investigated, and it was found that both can only be used in positive reflectron mode. MALDI studies with combinations of polymer, additive, and H_2O or D_2O showed no clear evidence of TCNQ-H_2O reaction products. The solvent-, temperature-, and aggregate-state-dependent formation of radical anions of TCNQ, F_4TCNQ, and DDQ, as well as various combinations of polymer/additive blends, were investigated by ESR spectroscopy in both, solid and liquid state. It was found that the molecular additives often form radical anions, although no electron transfer is expected or apparent. A relationship between polymer presence and aggregate state is suspected. Solid-state NMR spectroscopy was used to study IDT-BT/F_4TCNQ films and F_4TCNQ solvent dependence. The latter showed the solvent- and temperature-induced formation of novel F_4TCNQ species that could not be clearly assigned. Finally, solid-state and solution ^{2}H NMR spectra were recorded to study reaction products of TCNQ and D_2O. No clear evidence of reaction products involving deuterons was observed.

In conclusion, chemical reactions of TCNQ with water and/ or oxygen were not clearly detectable. The frequent detection of radicals in polymer/additive films, as in the pure additives, suggests that the radical anions of the additive might contribute to the improvement of the transistor properties.

3 Theory

3.1 Organic semiconductors

OSCs are materials that are widely used in modern electrical devices such as organic field effect transistors (OFETs), solar cells, and diodes. With semiconductors, it is the bandgap that makes them unique and different from metal. In recent years, much research has been done on OSCs, which offer several advantages over inorganic semiconductors, such as low-temperature processing, mechanical flexibility, light weight, and the ability to specifically tailor the polymer design to any situation. In some applications, the OSC is doped to improve conductivity or to shift the Fermi level. In organic materials, it is not appropriate to speak of conduction and valance bands as in inorganic semiconductors, because the electronic states are much more tightly bound. Therefore, in OSCs, electrons are either added to the lowest unoccupied orbital (LUMO) to induce n-type doping or removed from the highest occupied orbital (HOMO) to induce p-type doping. There are many molecules and ionic species that can serve as dopants: Brønsted acids, Lewis acids and bases, and neutral dopants with a high electron affinity (EA or HOMO with reversed sign) for p-type doping or a low ionization energy (IE or LUMO with reversed sign) for n-type doping.[1] In this work, only p-type doping with neutral dopants will be discussed.

Doping organic semiconductors

In general, there are two doping mechanisms for neutral dopants: Ion pair formation (IP, Figure 3.1) and charge transfer complex (CTC) formation. In the case of an IP, charge is transferred, resulting in ionized species and free charge carriers. CTC occurs when the degree of charge transfer is < 1. For systems including the often used polymer poly(3-hexylthiophen-2,5-diyl) (P3HT), IP seems to be a sufficient model for thiophene-based polymers with dopants such as TCNQ,[1,7] but there are cases of CTC formation known as well.[8] This shows that the doping process of polymers is complex and system-dependent. For p-type doping, IP should occur when $EA_{dopant} > IE_{OSC}$. However, these values do not take into account any interaction between dopant and OSC, since they refer to vacuum and consider well-separated molecules only. Therefore, it is not possible to predict the doping behavior by considering only EAs and IEs.[1,7] This circumstance will be discussed in more detail below. The doping efficiency is usually below 100 %, for which there are several reasons, such as dopant aggregation, CTC formation, coulombic bonding of IPs, and local trapping of free charges. Recent studies also suggest that miscibility, molecular packing of the dopant, and OSC morphology play a role in doping efficiency as well.[1] It should be noted that oxygen

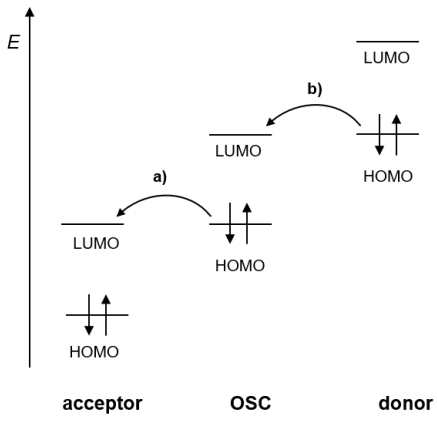

Figure 3.1: **a)** p-type doping and **b)** n-type doping.[1]

O_2 can also act as a dopant in an OSCs. The effects of oxygen on the stability of OSCs have been studied extensively. In general, reactions or electron transfers appear to occur between the OSC and O_2, making encapsulation necessary.[1]

Donor-acceptor-polymers

Conjugated polymers in general are an attractive material due to their flexibility, low weight, and processing costs, and biocompatability.[2] In recent years, donor-acceptor-polymers (D-A) with alternating electron-donor and electron-acceptor units have attracted a lot of attention.[9,10] These polymers exhibit in-chain donor-acceptor-interactions, low band-gaps[9] and high mobilities.[10] Additionally, they offer a large variety in structures as their molecular design of side chains and backbone can be tailored.[9] In D-A polymers the high mobility cannot be assigned to a very high degree in crystallinity, as it is a necessary condition for small molecule conductors or polymeric systems with a relatively simple repeat unit design.[10,11] A lot of factors influence the high mobility properties of D-A-polymers in organic devices, such as a co-planar backbone with minimum torsion and steric hindrance between donor and acceptor units, but also attractive electronic interactions between donor and acceptor units. Furthermore, a high degree of in-plane alignment, which facilitates the transport along the polymer backbone is of importance, as is the side chain design, which ideally should make the polymer flexible and solubilizing. Lastly, face-on or edge-on orientation of the polymer chains with respect to the substrate plane needs to be considered.[10]
Despite all the advantages, polymers tend to contain defects that interrupt conjugation. Due to this fact, polymers are not uniform, but differ in conjugation length and thus in energy states, resulting in energy distribution or so-called energetic disorder.[2] This fact makes the correct prediction of doping based on the HOMOs and LUMOs even more difficult.

Traps in organic semiconductors

When it comes to charge carrier transport in OSCs, so-called charge carrier traps, that often result in decreased performances of organic electronic devices, are an important issue. Traps can be structurally or energetically disorganized. Since there is no change in the covalent bonding in this type of trap, the defect energy is low, resulting in a high defect density. Traps can originate from residual impurities introduced during chemical synthesis, sample preparation, or measurements. Common external impurities are oxygen or water. In addition, defects can be introduced into OSCs by self-ionization of conjugated bonds. Since in most OSCs positively charged defects are much more delocalized than negatively charged defects, OSCs can appear to be slightly p-doped even though no dopant is introduced.[1] Nicolai et al. found that polymers with EAs lower than -3.6 eV exhibit trap-free electron transport.[12]
There are two common methods to remove different types of defects: By either filling the voids with dopants or passivating external impurities through chemical reactions with additives.[3–5,13,14] Voids containing water and/ or oxygen within the polymer structure are thought to be essential when it comes to charge trapping and device degradation. Molecular additives may replace water inside these voids and thereby enhance the OFET performance.[3] Chemical passivation is required for charged defects and impurities: OSCs cannot be purified by sublimation like small molecules, and thus often have some level of impurities.[1]

Transistors are important electrical components that are used, for example, in logic circuits or sensors. OFETs in particular utilize organic semiconductors, such as polymers, for charge transport. Generally speaking, there are three types of OFETs: n-type, p-type, and ambipolar. To operate an OFET, a gate voltage between source and gate electrode is applied.[2] In 2017, a paper was published by Nikloka et

al.[3] in which, among others, the polymers IDT-BT and F8BT were used in OFETs with incorporated additives such as TCNQ (see Figure 3.4 for chemical structures). Since the energy levels are unsuitable for p-type doping, the authors argue that the improved transistor performances result from chemical passivation or trap filling induced by the additive TCNQ. This theory is also supported by the fact that the authors describe finding the same device-improving effect when no additives are added but the annealing time during the transistor fabrication is shortened to leave residual solvent remaining in the film. Here, the hypothesis is that the solid-state additives or the residual solvent fill the nanoscale gaps between the polymer chains and prevent water from entering the films. However, the performance improvement through residual solvent is not permanent. Following the authors' reasoning, this could be due to evaporation of the solvent.[3]

The same group has investigated this topic further: There are studies on the effect of leaving various solvent residues in the film as well as studies on other device-enhancing additives. The first study found that azeotropic solvents lead to device enhancement, while non-azeotropic solvents do not. The authors attributed this effect to hydrogen bonding between water-induced traps and the solvent.[4] In the second study, a large number of additives were screened (see Figure 3.2 for a selection). The device-improving molecules vary in size, raising doubts on the hypothesis that the molecules fill nanoscale voids in the polymer films. However, all but one device-improving additive possess nitrile groups and are expected to have high electron affinity. Again, the authors attribute the effect to a possible reaction with water or filling of the voids as indicated above.[5] Following this argument, it is surprising that when it comes to the device improving additives, size does not seem to matter, as it varies significantly (see Figure 3.2). Since a reaction with water is difficult to show inside the film, no reaction products yet were found for the possible reaction of additive and water.[3–5] It was therefore the aim of this work to take a closer look into these suspected reactions.

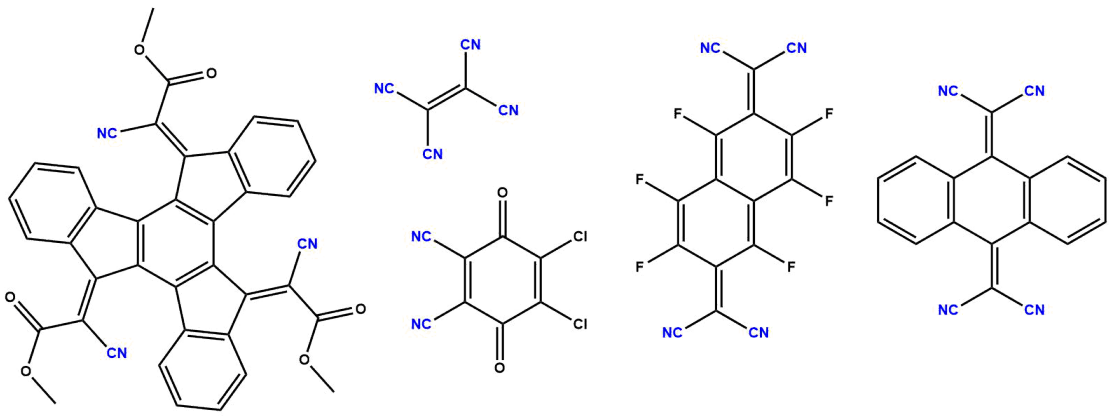

Figure 3.2: Selection of molecular additives leading to improved device charceristics, reproduced from [5].

3.2 In this work investigated polymers and additives

In this work, the p-type dopants F_4TCNQ, TCNQ, and DDQ as well as the D-A-polymers IDT-BT and F8BT have been used. They were selected to ensure the comparability of the systems to the publication of Nikolka et al.[3] Their chemical structures are shown in Figure 3.3. Since the conclusion that molecular additives passivate charge carrier traps is based on mismatched energy levels, a closer look at the HOMO and LUMO levels is crucial. They are displayed in Figure 3.3, left side. Energy levels with arrows represent HOMO levels and levels without LUMO energy levels. Theoretically, only the transfer of one electron from the polymer IDT-BT to the dopant F_4TCNQ is expected to

take place, leading to an anion radical and a cation radical. It should be noted that the second electron transfer is not expected (EA^-). TCNQ with an EA^0 of −4.7 eV is not able to dope most OSCs effectivley,[1] therefore any doping reactions involving TCNQ and IDT-BT or F8BT should not occur.[3] However, as mentioned earlier, HOMO and LUMO levels are not the only factors to consider when looking at possible doping reactions.[1,2,7]

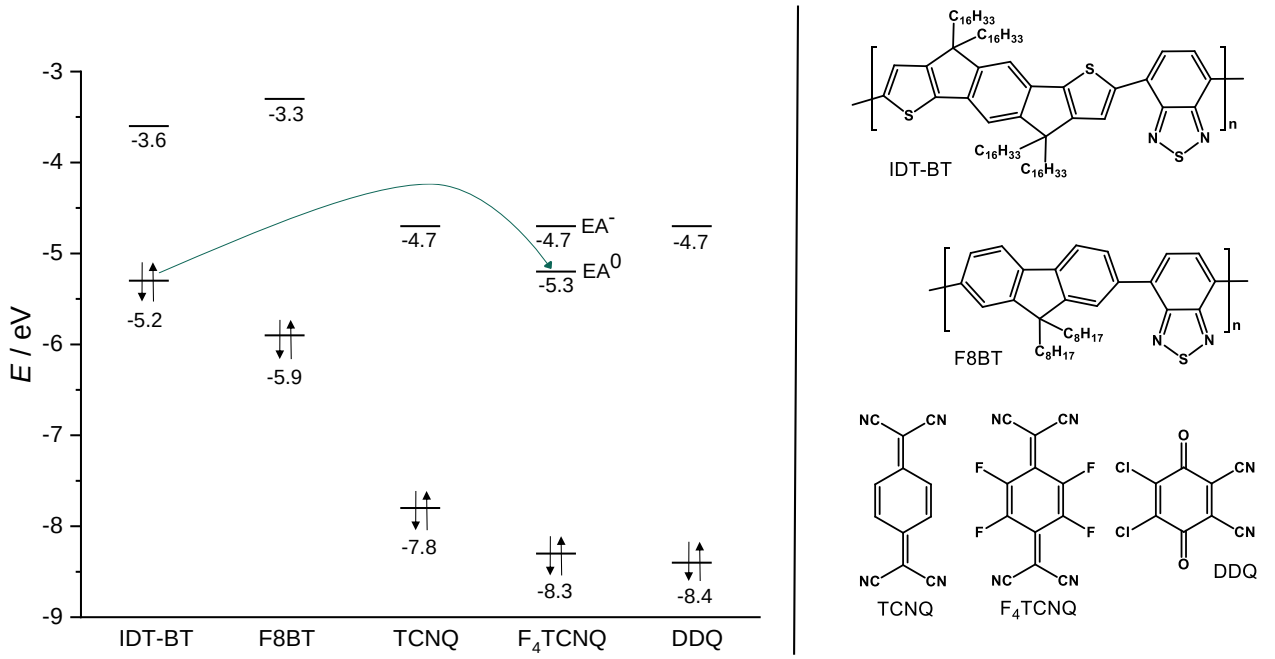

Figure 3.3: Left: HOMOs and LUMOs of IDT-BT,[3,15] F8BT,[16] TCNQ,[1] F_4TCNQ[17] and DDQ[18] as well as the possible doping reactions marked by a green arrow and second ionization energy EA^- for F_4TCNQ.[17] Energy levels with arrows represent HOMOs and energy levels without LUMOs. Right: Chemical structures of IDT-BT, F8BT, F_4TCNQ, TCNQ and DDQ.

Reactions of TCNQ and F_4TCNQ

TCNQ and F_4TCNQ are widely studied molecules due to their structural, chemical, and physical properties.[1,19] Because of their ability to accept up to two electrons they are often used as p-type dopants in solar cells, diodes, or OFETs.[17] In Figure 3.4 there is an overview of the most important reaction pathways of TCNQ and F_4TCNQ displayed. In general, this overview applies to both molecules if not marked otherwise. However, reaction probabilities might vary and if so will be mentioned. To apply to both molecules the rest "R" is introduced, standing for either fluorine or hydrogen atoms.
Starting with the unreacted quinoid form R_4TCNQ on the lefthand side in the middle: For this molecule, it is possible to describe a benzenoid resonance structure containing two radicals and no charge. By DFT calculations it has been shown that neutral TCNQ exhibits a quinoid and benzenoid character in the lowest singlet and triplet state.[20] However, by Raman spectroscopy the benzenoid form has not been found.[21] Aromatization can be seen as a driving force behind the formation of the proposed benzenoid structure. For F_4TCNQ this diradical species has been found to form when being irradiated with light of 405 nm in acetonitrile. The authors could furthermore show the reaction with THF coming from this state, leading to F_4TCNQ with a proton added to the carbon between the

cyanide groups on the one side and the residual THF added on the opposite side.[22] Theoretically, an additional ionic R_4TCNQ form can be formulated that carries both a positive and negative charge. This form, however, has not been discussed in literature.

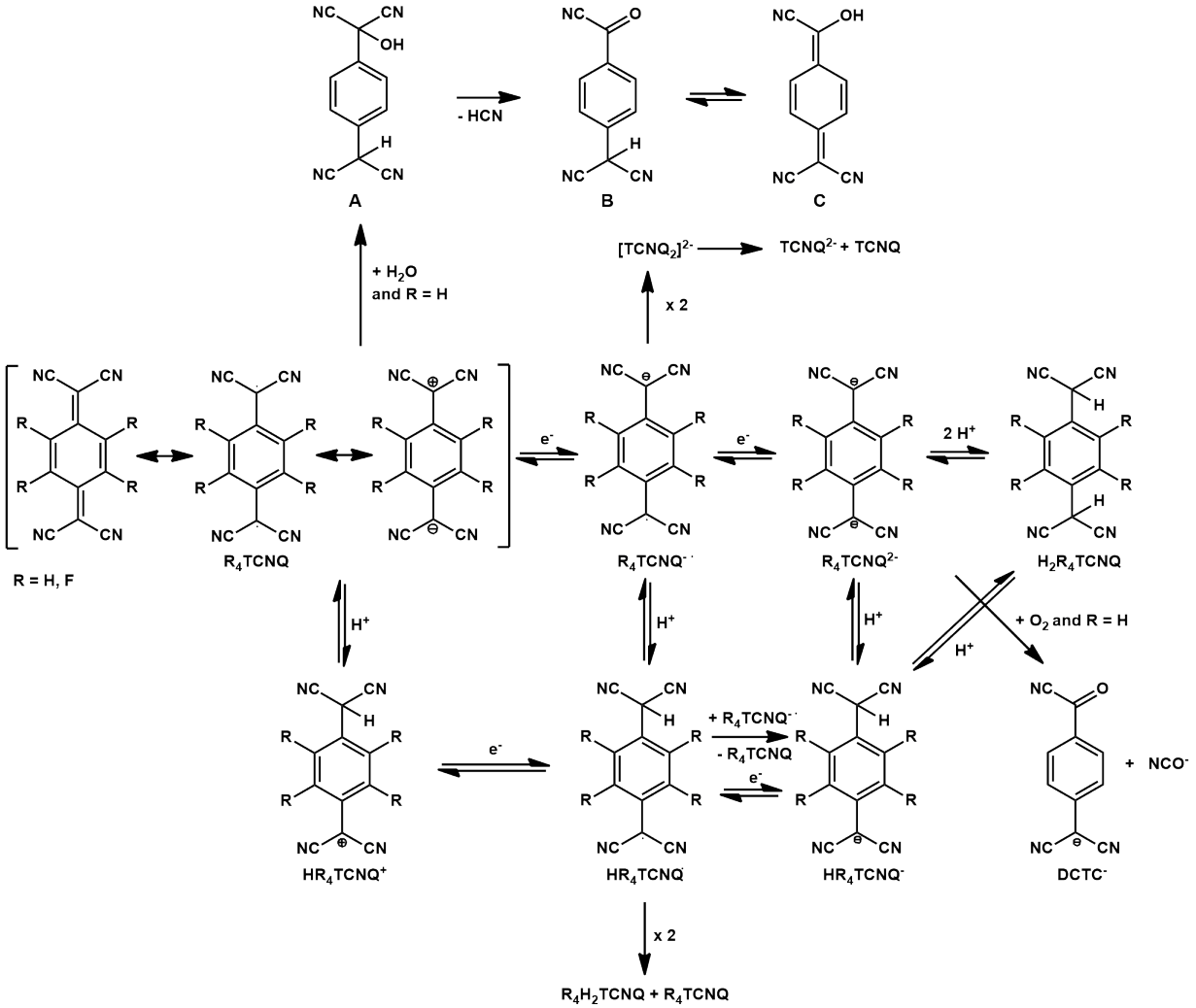

Figure 3.4: Overview over the reversible redox-chemistry,[19,23] reversible acid-base-chemistry[19,23,24] and dimerizations[19,23,25–27] for TCNQ and F_4TCNQ and additionally reactions with water[28] and oxygen[29] for TCNQ only. The rest "R" either refers to fluorine or hydrogen.

As mentioned before, the quinones are known for their one-electron reversible redox-chemistry.[19,23] The electron affinities have been described previously and apply (Figure 3.3). The neutral species can accept an electron, leading to the radical anion $R_4TCNQ^{\bullet -}$. These radical anions are highly stable, even after a long storage time in air.[19] When accepting a second electron the dianion R_4TCNQ^{2-} is formed. Due to the electron-withdrawing effect of the fluorine atoms F_4TCNQ has a higher electron affinity than TCNQ and making F_4TCNQ^{2-} thermodynamically more stable.[19] Coming from this redox-chemistry reversible acid-base-chemistry is possible: Either two protons can be added forming the diprotonated form H_2R_4TCNQ or one forming the monoprotonated anionic form HR_4TCNQ^-. The equilibrium constants for the reaction leading to H_2R_4TCNQ is much higher for $TCNQ^{2-}$ than for F_4TCNQ^{2-}, because it is the stronger base due to the lack of fluorine atoms.[19,23] It was also shown that F_4TCNQ^{2-} can be protonated by the weak base H_2O, yielding HF_4TCNQ^-.[24] In case of $TCNQ^{2-}$ an irreversible reaction with oxygen can take place producing α,α-dicyano-p-toluylcyanide

($DCTC^-$) and making the dianion air-unstable.[19,29]
For the neutral form R_4TCNQ and the radical anion $R_4TCNQ^{\cdot -}$ proton-adding has been reported, also. Both species can accept one proton.[19,23] This protonation with hydrochloric acid has been studied for salts of the radical anion of $TCNQ^{\cdot -}$ in alcohols and acetonitrile in more detail.[25] Additionaly, $HR_4TCNQ^{\cdot}$ can undergo dimersation reactions: Either with a second $HR_4TCNQ^{\cdot}$ to form neutral R_4TCNQ and H_2R_4TCNQ[23,25] or with $R_4TCNQ^{\cdot -}$ to form also neutral R_4TCNQ and anionic HR_4TCNQ^-.[19] For the radical anion it is furthermore known that it forms $[TCNQ_2]^{2-}$ dimers, which then can react to $TCNQ^{2-}$ and TCNQ.[26,27]
Lastly, the addition of water to TCNQ needs to be mentioned: By adding it, **A** is formed and by elimination of hydrocyanic acid **B**, which can tautomerize to **C**. Note that the authors established these reactions by measuring UV/vis-spectra in MeCN. There were no products isolated. The authors furthermore describe the formation of carboxylic acids due to hydrolysis of the nitrile groups. Again, those proposed products were observed by UV/vis-spectroscopy and not isolated.[28]
In summary TCNQ and F_4TCNQ can undergo reversible redox-chemistry,[19,23] reversible acid-base-chemistry,[19,23,24] dimerisations[19,23,25–27] and for the TCNQ reactions with water[28] and oxygen.[29] This summarizes the most important reactions to the best of my knowledge. Due to the extensive studies on these additives, not all reactions may have been mentioned.

3.3 Electron spin resonance

Principles and basic theory

Electron spin resonance (ESR), also called electron paramagnetic resonance (EPR), is the study of samples containing one or more unpaired electrons, making them paramagnetic.[30] Both EPR and ESR refer to the same technique. In this work, the term ESR will be used. In general, the underlying principles of ESR spectroscopy are similar to those of nuclear magnetic resonance (NMR) spectroscopy in that they study the interaction between electrons or nuclei with an applied magnetic field and electromagnetic radiation of appropriate wavelength.[31,32] In ESR spectroscopy, the applied frequency, which is microwaves, is higher than in NMR spectroscopy, which uses radio waves. In turn, the magnetic field strength required for ESR spectroscopy is lower.[32] Generally, ESR spectroscopy is more sensitive than NMR spectroscopy[32] due to the higher magnetic moment of electrons compared to nuclei.[33] ESR spectrometers are named according to the wavelength they use. The most common is the X-band, which uses a wavelength of about 9.3 GHz and a magnetic field of about 0.3 T.[32] Based on the technical setup, the first derivative of absorption spectra are recorded and presented.[33]

Electron Zeeman interaction

Elelctrons as being elementary particles contain an intrinsic mechanical angular momentum, which is called spin S and is controlled by quantum mechanic rules. A spin can be in two states, most commonly named α and β, describing the different possible angular orientations in space. The spin S possess moments along the x-, y- and z-axis, but by convention the spin state describes different components along the z-axis (in the cartesian frame). In units of $\hbar$ and according the rules of quantum mechanics S_z can either have a value of $\frac{1}{2}$ (α- state) or $-\frac{1}{2}$ (β-state).[30]
The magnetic moment μ_e is neecessarily associated with the electron spin angular momentum S since they are proportional to one another and parallel vectors:

$$\mu_e = g\mu_B S \tag{3.1}$$

with g being the Landé factor and μ_B being the Bohr magneton. Because of the association between the electron spin and the magnetic moment, there is an energy difference between the α and β spin state. When applying a constant magnetic field the electron spin energy will depend on the orientation of μ_e with respect to B. When choosing the frame in such way that the z-axis is aligned with B the equation of the energy is:

$$E = g|\mu_B|B_0 S_z \tag{3.2}$$

where B_0 is the intensity of the magnetic field. When further taking into account the spin can be in two possible states Equation 3.2 transforms to:

$$E = \pm\frac{1}{2}|\mu_B|gB_0 \tag{3.3}$$

which is referred to as the Zeeman interaction. In other words, the Zeeman effect describes the interaction between an electron and an applied external magnetic field.[30] This interaction is graphically shown in Figure 3.5. The g_e-value for a free electron without any interactions is 2.00231930437378.[33]

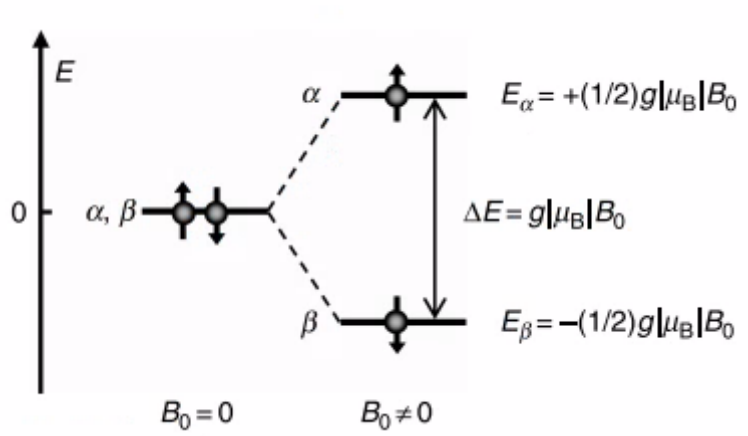

Figure 3.5: Electron Zeeman interaction: Without any applied external field no splitting is observed. The α and β state, displayed by the up and down arrows, possess the same energy. When applying a magnetic field B_0 the β state shifts to lower energy and the α state to higher energy.[30]

Since the g-value is independent of the spectrometer used, it is an ideal value for comparisons. It can be seen as similar to the chemical shift in NMR spectroscopy although the shifts in g-values exceed the NMR shift by a couple of magnitudes.[32,33] The g-values obtained during an ESR experiment vary from those of a free electron g_e. This is mainly due to the coupling between spin and angular momentum of the electron. Because the spin-orbit-coupling (SOC) is a relativistic effect, the g-value shifts more or less compared to g_e, depending on the nucleus. For transition metals the effect is large and for purely organic radicals the effect is rather small. This contribution is added to g_e. Due to the energy levels contributing to the transition a positive shift is more common.[33]
The spin-orbit interaction is anisotropic since it is related to orbital motion. Therefore the g-value is dependent on the molecule orientation with respect to the external magnetic field. When a paramagnetic species with a spherically symmetric center is considered, only one g-value is observed, since the orientation to the external magnetic field is always the same. If the paramagnetic center does not possess spherical symmetry, g-anisotropy is observed. When for example considering a system with axial symmetry two g-values can be found: $g_x, g_y = g_\perp$ and $g_z = g_\parallel$. If there is no symmetry at all, three different g-values are observed and the spectrum is called orthorhombic. Both types of spectra, absorption, and first derivative are displayed in Figure 3.6.[30,33]

Although multiple g-values might be expected from looking at the molecule of interest it is possible that not all of them can be determined. This is often the case in liquid samples. Here, due to the Brownian motion and fast tumbling, the g-anisotropy can be averaged out. In this case only the averaged isotropic spectrum is detected: $g_{\text{iso}} = (g_x + g_y + g_z) \cdot \frac{1}{3}$. In solid-state the situation is different: When looking at a single crystal with a paramagnetic center, possessing no symmetry, the crystal would have to be rotated inside the spectrometer to obtain all g-values. However, it is more common to either record spectra of a powder or frozen solutions, which also act as powder spectra. Because in these powder spectra all possible orientations are present, the signals typically broaden, which may again lead to not all g-values being detected.[33]

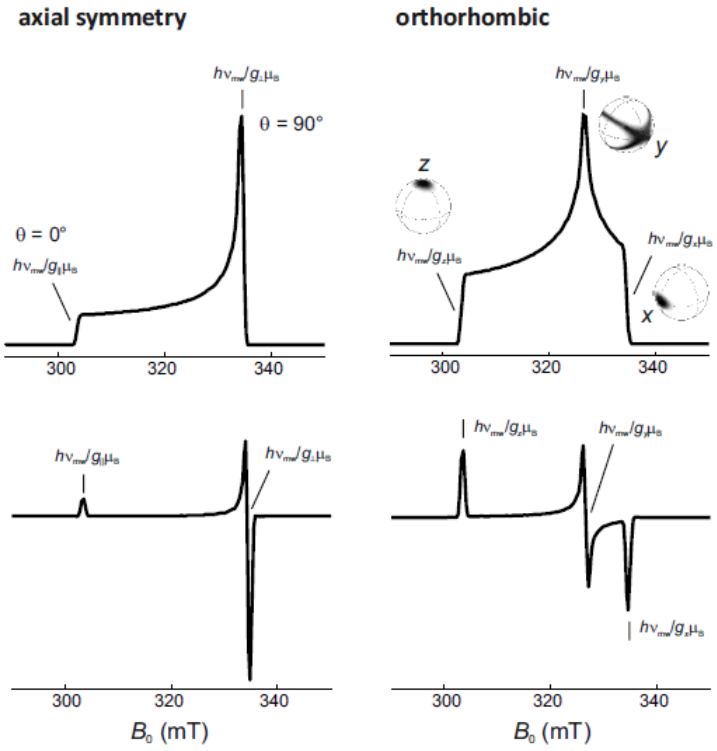

Figure 3.6: Simulated X-band ESR spectra for systems with g-anisotropy only. The upper spectra show the absorption spectra and the bottom ones the first derivative. On the left, the spectra for a paramagnetic center with axial symmetry are displayed and on the right for orthorhombic symmetry. The highlighted points show the principal g-values.[33]

Hyperfine interaction

Another, rather frequently observed interaction is the hyperfine interaction. This is the electron nuclei interaction and possesses an isotropic and an anisotropic part. The isotropic part describes the probability of finding the electron at the position of the nucleus and is a through-bond interaction.[32] Due to this interaction the energy levels already split by the Zeeman effect are split further. The amount of splitting depends on the nucleus spin I. In general, there will be $2I+1$ lines. The hyperfine energy contribution E_{hf} is:[30]

$$E_{hf} = aS \cdot I \tag{3.4}$$

with the hyperfine coupling constant a, the electron spin S, and the nuclear spin angular momentum I. Because the nuclei themselves exhibit the nuclear Zeeman effect when being brought into an

external magnetic field, the electrons will experience an additional magnetic field. This affects the resonance conditions. Therefore the energy E_n for a rapidly tumbling molecular system in solution can be described by combining the nuclear Zeeman interaction and the isotropic contact hyperfine ineraction:[30,31]

$$E_n = -g_N \mu_N B_0 I_z + aS \cdot I \tag{3.5}$$

where g_N is the nuclear g-value, μ_N is the nuclear magneton, I_z is the nuclear spin angular momentum component along z-direction of the magnetic field and B_0 is the magnetic field. Since both terms in Equation 3.5 are much smaller than the electron Zeeman interaction (high field approximation, $|a| << g|\mu_B|B_0$), E_n is a small perturbation on the electron spin energy. The total energy E_{tot} (former Equation 3.2), after taking the electron nuclei interaction into account, can be written as:

$$E_{tot} = g|\mu_B|B_0 S_z - g_N \mu_N B_0 I_z + aS \cdot I \tag{3.6}$$

Using Equation 3.6 and considering all possible combinations, there will be four energy levels for an electron interacting with a nucleus with $I = \frac{1}{2}$. Graphically, these enegry levels are shown in Figure 3.7:

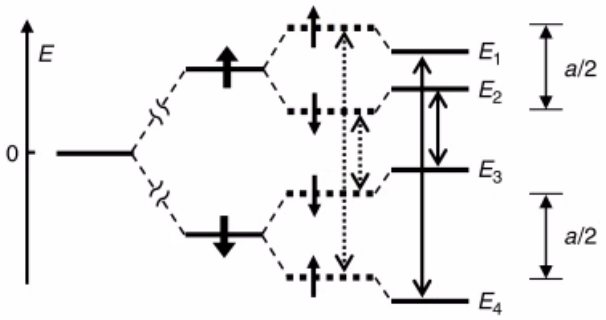

Figure 3.7: Schematic energy drawing of an electron with $S = \frac{1}{2}$ interacting with one nucleus with $I = \frac{1}{2}$ in an applied magnetic field B_0. The bold arrows display the two spin states α and β along the magnetic field direction and the light arrows the nuclear spin components. The bold dotted lines display the splitting of the Zeeman interaction, caused by the hyperfine interaction. These lines are then further splitted by the nuclear Zeeman interaction (solid lines). Furthermore the allowed ESR transitions are shown (vertical lines)[30]

In ESR spectroscopy transitions between pairs of energy of different values of S_z and same I_z can be observed, leading to the following selection rules:

$$\Delta S_z = \pm 1 \quad \Delta I_z = 0$$

Besides the Zeeman and hyperfine interaction, there are multiple other interactions possible when looking at paramagnetic samples. Considering all possible interactions the Hamiltonian, which can be used to calculate the energy levels of the spin system, can be written as:[32,33]

$$\begin{aligned}\hat{H}_0 &= \hat{H}_{EZ} + \hat{H}_{NZ} + \hat{H}_{HFI} + \hat{H}_{ZFI} + \hat{H}_{EX} + \hat{H}_{DD} + \hat{H}_{NQI} \\ &= \frac{\mu B}{\hbar} \sum_k \vec{B_0}^T g_k \vec{\hat{S}} + \sum_i \omega_{I,i} \vec{\hat{I}}_{z,i} + \sum_k \sum_i \vec{\hat{S}}_k^T A_{ki} \vec{\hat{I}}_i + \sum_{S_k > 1/2} \vec{\hat{S}}_{k^T} D_k \vec{\hat{S}}_k \\ &+ \sum_k \sum_{l \neq k} J_{kl} \hat{S}_{z,k} \hat{S}_{z,l} + \sum_k \sum_{l \neq k} \vec{\hat{S}}_k^T D_{kl} \vec{\hat{S}}_l + \sum_{I_i > 1/2} \vec{\hat{I}}_i^T P_i \vec{\hat{I}}_i\end{aligned} \tag{3.7}$$

with the index i running over all nuclear spins, k and l over all eleectrons and $^{\mathrm{T}}$ denoting the response of a vector or vetor operator. $\hat{H}_{\mathrm{EZ}}$ being the Zeeman interaction, $\hat{H}_{\mathrm{NZ}}$ the nuclear Zeeman interaction, $\hat{H}_{\mathrm{ZFI}}$ the zero-field interaction, $\hat{H}_{\mathrm{FI}}$ the hyperfine interaction, $\hat{H}_{\mathrm{EX}}$ the exchange ineraction, $\hat{H}_{\mathrm{DD}}$ the dipole-dipole-intercation and $\hat{H}_{\mathrm{NQI}}$ the nuclear quadrupol interaction. Often times only one electron and one nuclear spin have to be considered, which simplifies the Hamiltonian.[33] The interactions provided here are for the sake of completeness. However, they are out of the scope of this thesis and therefore will not be discussed in further detail.

Electron spin resonance of doped polymers and organic devices

Because unpaired electrons in organic π-system-based materials and devices carry spin and charge, investigation via ESR spectroscopy is a widely used and important tool to gain deeper understanding of these devices. An insight into the relationship between charge motion and spin dynamics as well as a deeper understanding of spin-relaxation physics can be gained by using field-induced (FI) ESR. This allows for examination while the device is operating.[34–36] Unfortunately, this method could not be used in this thesis. However, there are a large number of studies in which the doping of polymers using additives such as F_4TCNQ has been investigated with the aid of ESR spectroscopy.[34,37–40]

3.4 Nuclear magnetic resonance

NMR spectroscopy is one of the most powerful techniques when it comes to the structure elucidation of molecules, either in solution or in solid-state. To detect an NMR signal, the sample needs to possess atoms with a nuclear spin that is unequal to zero. This can either for example be ^{1}H or ^{13}C nuclei (dipol) or ^{2}H (quadrupol). Most frequently detected are the ^{1}H-nucleus and the ^{13}C-nucleus. The nuclear magentic moment is given as:[41]

$$\mu = \frac{\gamma I h}{2\pi} \tag{3.8}$$

with Planck's constant h, the nuclear spin I, and the gyromagnetic ratio γ, which is a constant dependent on the nucleus. When placed in a magnetic field, the eigenstates of the nuclear spin will align themselves and according to quantum mechanics, there are $2I + 1$ possible orientations. This splitting of energy levels is referred to as the nuclear Zeeman splitting. When no external field is applied, no splitting is observed. This effect is analogous to the electron Zeeman effect (see ESR theory). The possible orientations are described by the magnetic quantum number m. The energy of the spin states can be written as:[41]

$$E = \frac{-\gamma h m B_0}{2\pi} \tag{3.9}$$

The magnetic quantum number m can only change by the selection rule $\Delta m = \pm 1$ and the transition energy is given by:

$$\Delta E = \frac{\gamma h B_0}{2\pi} \tag{3.10}$$

Such a transition can take place by inducing electromagnetic radiation, which can be described by:[41]

$$\nu = \frac{\gamma B_0}{2\pi} \tag{3.11}$$

When a spin is brought into a magnetic field it undergoes precessional motion. This precession frequency is referred to as the Larmor frequency. It is proportional to μ and B_0 and is equal to the frequency of the electromagnetic radiation μ that induces the transition within the nucleus. Normally, a nucleus is surrounded by electrons. These electrons induce a magnetic field, which is directed opposite to the external magnetic field. Because the magnetic field experienced by the nucleus varies from B_0, the frequency μ will change as well and 3.8 can be extended by a shielding constant σ:[41]

$$\mu = \frac{\gamma B_0(1-\sigma)}{2\pi} \tag{3.12}$$

Since the Larmor frequency may change depending on the spectrometer used, the chemical shift of references samples is used and normalized to a ppm-scale. The chemical shift is defined as the nuclear shielding divided by the applied field:

$$\delta = \frac{B_{\text{ref}} - B_{\text{sample}}}{B_{\text{ref}}} \tag{3.13}$$

where B_{ref} is the magnetic field at the reference nucleus and B_{sample} is the magnetic field at the sample nucleus. Accordingly, the chemical shift is a function of the nucleus and its environment. After a nucleus was excited it relaxes into the ground state. To do so there are two relaxation processes: spin-lattice relaxation or longitudinal relaxation and spin-spin relaxation or transverse relaxation. The first type is characterized by the spin-lattice relaxation time T_1 and the second by the spin-spin relaxation time T_2. Usually, the T_1 time is large for solid molecules, whereas the T_2 time is rather short.[41]
The first NMR experiments were carried out using continuous wave (CW) setups but were, later on, more and more replaced by the Fourier transformed (FT) NMR technique. Both of these types require a radio frequency source and a magnetic field.[41]

In the literature, there are only a few examples of the use of solid-state NMR spectroscopy for the investigation of polymer additive blends. This is probably related to the access to equipment as well as the long measurement times and relatively large amounts of material needed. Nevertheless, this is a promising method that can provide additional insight into molecular ordering.

3.5 Matrix-assisted laser desorption/ionization

Mass spectrometry (MS) allows the separation of analytes by their weight-to-charge ratio $\frac{m}{z}$, while providing information on the abundance of these molecules in the area of interest. In general, this technique can be applied to a wide range of samples. To detect the analyte, it must possess a charge. It does not matter if it is a positive or negative charge or even multiple charges. To avoid any kind of interference, the samples are handled in vacuum. Thus, the goal is to produce a charged analyte in the gas phase under vacuum conditions. In the gas phase, the analyte is transported to the mass detector by applying magnetic or electric fields. In a mass spectrum, the mass-to-charge ratio $\frac{m}{z}$ is plotted against the relative or absolute intensity. In general, a charge (or charges) can be introduced by either adding or removing electrons or protons from the molecule of interest. There are several ways to generate ions in mass spectrometry: chemical ionization, field ionization, and field desorption, fast atom bombardment, electron spray ionization, atmospheric pressure chemical ionization, and matrix-assisted laser desorption/ionization (MALDI).[42] Since only the MALDI method was used in this work, it is the only ionization method presented. In laser desorption ionization (LDI), photons are used to cause desorption and ionization of the analyte using a high-power UV or IR laser. It is essential that the wavelength of the laser is absorbed. Since photolytic decomposition of the analyte often occurs with this method, a matrix-assisted (MA) method is used as a much softer method. MADLI is referred to as a soft method because the analyte is embedded in a protective matrix, which

allows for soft ionization and in the best case little to no fragmentation of large molecules.[6] Here, the analyte is co-crystallized with a matrix that absorbs the laser wavelength well. Commonly used matrices are 2,5-dihydroxybenzoic acid (2,5-DHB) and 3,5-dimethoxy-4-hydroxycinnamic acid (sinapic acid, Figure 3.8) due to their conjugated system. The matrix molecules desorb and ionize themselves and can lead to signals in the low-mass region.[6,42] The choice of matrix depends strongly on the analyte.[42] One drawback of these matrices is that they are often applicable to either the positive or negative ion mode, but not both. Also, some of these low molecular weight matrices exhibit poor vacuum stability.[6] The spectrometer used in this work combines MALDI with time-of-flight (TOF) separation of the analyte. In this method, molecules are partitioned according to their weight: Since heavier particles move slower, they arrive later than lighter molecules, so the patrician weight can be extracted from the time it takes them to travel from the target to the detector.[42]

Horatz et al.[6] were the first to explore the use of conjugated polymers as MALDI matrices to overcome the problems described. Conjugated polymers are suitable MALDI matrices for several reasons: They contain large π systems and can absorb the laser wavelength well. They are also chemically stable and non-volatile, allowing spectra to be recorded without matrix peaks. Because these polymers often contain alkyl side-chains, they are soluble in organic solvents, allowing the coating of films without cleavage sites. These side chains, as well as the polymer backbone, allow specific chemical tailoring to any situation, leading to changes in solubility, analyte extraction, optical absorption, and vacuum stability. The polymers investigated were poly[*N*,*N'*-bis(2-octyldodecyl)-naphthalene-1,4,5,8-bis(dicarboximide)-2,5-diyl]-*alt*-5,5'-(2,2'bithiophene) (PNDI(T2)), poly(3-dodecylthiophene-2,5-diyl) (P3DDT), poly[2,3-bis(3-octyloxyphenyl)quinoxaline-5,8-diyl]-*alt*-(thiophene-2,5-diyl) (PTQ1), poly[*N*,*N'*-bis(2-octyldodecyl)-isoindigo-5,5'-diyl]-*alt*-5,5'-(2,2'-bithiophene) (PII(T2)), and poly(9,9-di-n-octylfluorenyl-2,7-diyl) (P9OFl) (Figure 3.8). Horatz et al. were able to show that these polymers can be used in both, positive and negative ion mode and are applicable to a variety of analytes. The performance of the polymers is comparable or better than well-established matrices.[6]

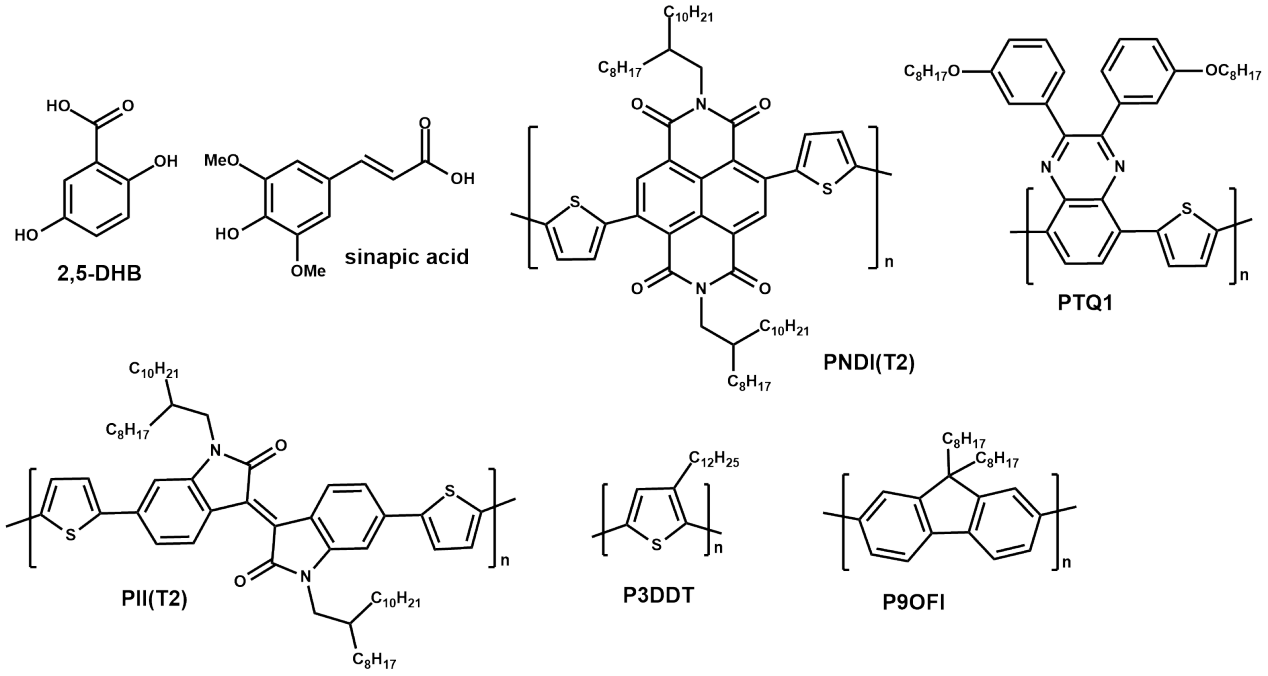

Figure 3.8: Commonly used MALDI matrices 2,5-DHB and sinapic acid[42] as well as recently study polymers as MALDI matrices PNDI(T2), PTQ1, PII(T2), P3DDT, P9OFI.[6]

4 Results and discussion

4.1 MALDI spectrometry

Originally, the aim of this thesis was to mainly perform MALDI measurements. However, due to the COVID-19 pandemic, access to the instrument was very limited and this was not possible.
As described earlier, OFET studies showed that the incorporation of molecular additives such as TCNQ lead to device improvements without doping the polymer. It is therefore assumed that these molecular additives passivate traps such as water and/or oxygen.[3–5] Since Horatz et al.[6] recently showed that polymers can be used as dual-mode MALDI matrices, the idea was to study polymer/additive blends, in which the polymers IDT-BT and F8BT would serve as MALDI matrices, allowing to study reaction products of the molecular additives. Therefore, it was first checked whether the polymers F8BT and IDT-BT could act as MALDI matrices. Accordingly, the next section is oriented on the recently published work by Horatz et al.[6]

4.1.1 IDT-BT and F8BT as MALDI matrices

To use the polymers IDT-BT and F8BT as MALDI matrices, they must absorb the light of the laser used. In the MALDI instrument used in this work, a Nd:YAG laser with a wavelength of 355 nm was used. Whether or not the wavelength is observed could be checked with the help of UV/vis spectra recorded by Sten Gebel, displayed in Figure 6.2, Appendix. For IDT-BT the absorption maximum is at 681.3 nm with a shoulder at 629.6 nm. An additional peak is at 418.9 nm. The relative absorption of the laser wavelength is rather low with $A_{\mathrm{Nd:YAg}}(\mathrm{IDT-BT}) = 10.6\ \%$ (setting the maximum to 100 %). The polymer F8BT shows an absorption maximum at 470 nm and two overlapping peaks at 323.1 nm and 337.8 nm. The relative absorption of the laser wavelength is $A_{\mathrm{Nd:YAg}}(\mathrm{FBT}) = 44.2\ \%$. From the relative absorbance, F8BT should work better as a MALDI matrix than IDT-BT. The recorded UV/vis spectra of the thin films are in good agreement with literature.[15,43]
The instrument used had a dual stage reflectron mode. This mode allows higher resolution but has a limited $\frac{m}{z}$ range. Alternatively, a linear mode could be used, which allows the measurement of high molecular weights but has a limited resolution.[6] Positive and negative ion mode spectra were recorded for the polymers without additional secondary matrix. The IDT-BT and F8BT polymers remain MALDI-still unless high laser intensity is used. Frequently found artefacts in positive reflectron mode are the alkali ions sodium Na^+ with $\frac{m}{z} = 23$ and potassium K^+ with $\frac{m}{z} = 29$. In the negative reflectron mode, the halides chloride Cl^- with $\frac{m}{z} = 39$ and bromine Br^- with $\frac{m}{z} = 79/81$ are often detected. These can also form clusters with the commonly used matrices 2,5-DHB and 9-aminoacridin.[6] However, these artefacts were not detected when IDT-BT and F8BT were used as matrices.
The samples were prepared using the thin layer method:[6] First, the analyte is applied onto the target and allowed to dry. Then the matrix is applied on top, also allowed to dry and thus coating the analyte. Compared to the often used preparation by cocrystallization, significantly less material is needed. To compare the matrix effect of the polymers, three measurements are compared in terms of their absolute intensity: matrix only, analyte only, and the combination of both (Figure 4.1 and Figure 4.2, from top to bottom). To find the best possible combination, matrix and analyte were

prepared in concentrations of 10, 1, and 0.1 $\frac{\text{mg}}{\text{mL}}$ and the respective concentrations were combined. The analyte tetra-*N*-butylammonium bromide (TBAB) was used to test the matrix properties in positive reflectron mode (see Appendix, Figure 6.1 for chemical structures). The spectra recorded in positive reflectron mode are shown in Figure 4.1a. Note that the results of all combinations can be found in Table 6.1 and Table 6.2, Appendix. The best combination found using IDT-BT as matrix was IDT-BT with a concentration of 0.1 $\frac{\text{mg}}{\text{mL}}$ and TBAB with a concentration of 10 $\frac{\text{mg}}{\text{mL}}$. The peaks are assigned to: $[\text{TBA}]^+$, $\frac{m}{z} = 245$ and $[\text{Bu}_3\text{N}]^+$, $\frac{m}{z} = 186$ (see Table 4.1 also). Since $[\text{TBA}]^+$ it is a precharged ion, it can be detected in positive ion mode without the use of a matrix. However, the analyte signal obtained when using IDT-BT as a matrix at the same laser intensity is significantly higher. When F8BT was used as matrix, the same combination of concentrations proved to be the best (F8BT with 0.1 $\frac{\text{mg}}{\text{mL}}$ and TBAB with 10 $\frac{\text{mg}}{\text{mL}}$). The detected signals are also identical. It is noteworthy that the spectra recorded with F8BT as a matrix in all combinations show very high intensities (see Table 6.2) and that the best combination shows intensities that are an order of magnitude higher than the best IDT-BT/TBAB combination. This is possibly because F8BT absorbs the laser wavelength better than IDT-BT. It was noted that when using the polymers in concentrations of 10 $\frac{\text{mg}}{\text{mL}}$ they seem to exhibit lacquer-like properties. These properties seem to suppress laser desorption and ionization. In summary, it was concluded, that both, IDT-BT and F8BT work as MALDI matrices in positive reflectron mode and that lower polymer concentrations yield better results.

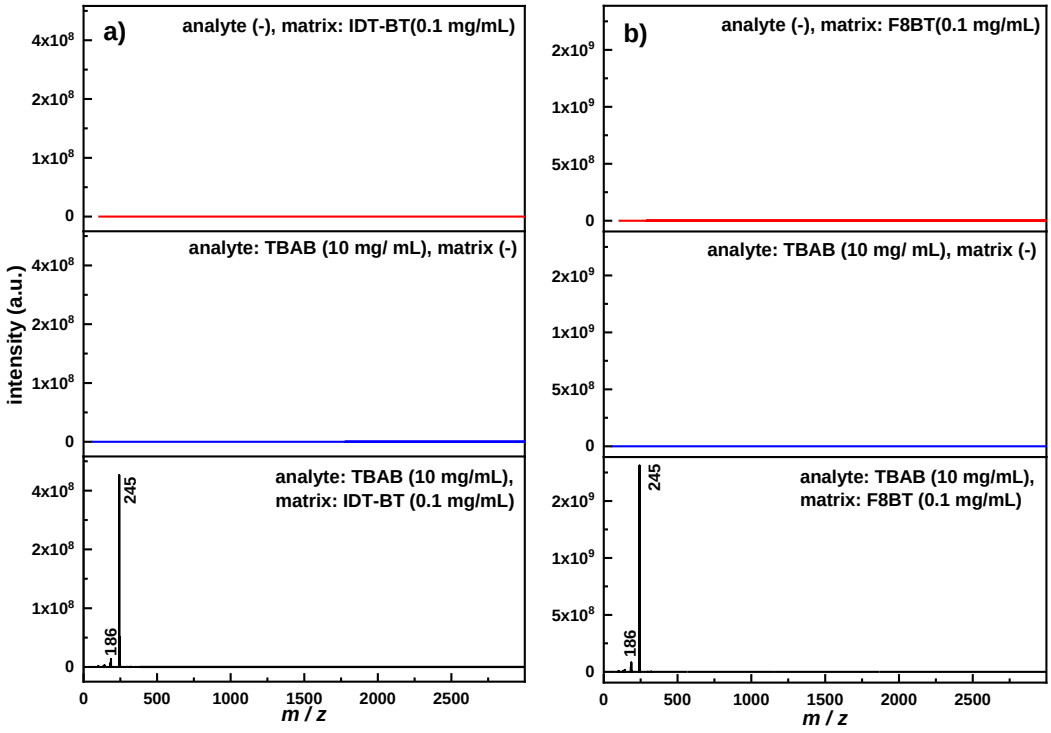

Figure 4.1: Refelectron positive mode MALDI-TOF spectra of **a)** IDT-BT and **b)** F8BT as matrix with the analyte TBAB. Red: matrix only, blue: analyte only and black: best combination of analyte and matrix found. Laser intensity = 70% for both.

In negative reflectron mode, the analytes citric acid and cholic acid were tested (see Appendix, Figure 6.1 for chemical structures). The recorded spectra are presented in Figure 4.2. Unfortunately, when IDT-BT is used as a matrix, no analyte corresponding signal can be detected for any of the analytes (see Table 6.1 for an overview). The addition of 25 mol% of sodium hydroxide (NaOH) to

deprotonate the citric acid also did not lead to an analyte-related signal being detected. The measurement was further complicated by the precipitation of the acid anion after deprotonation. When using cholic acid as an analyte, adding NaOH did not lead to any improvement either. These results are surprising since Hoartz et al. reported the detection of analyte signals in negative reflectron mode when using polymers as matrices and identical analytes without the addition of a base.[6] In the case of F8BT, the results are a little better: When F8BT (0.1 $\frac{\text{mg}}{\text{mL}}$) is combined with citric acid (10 $\frac{\text{mg}}{\text{mL}}$), the deprotonated acid can be detected with $\frac{m}{z} = 191$ (Figure 4.2a, origin: $[\text{CiA}-\text{H}^+]^-$). It is not clear where the other signals come from, they possibly are related to the use of F8BT as a matrix. For the F8BT/ citric acid combination, the analyte signal could only be detected in one other measurement and in none of the others. It was furthermore not beneficial to add 25 mol% NaOH to promote deprotonation of the acid. Since F8BT should absorb the laser wavelength well, better results would have been expected. When using cholic acid as an analyte, no analyte signal can be detected without the addition of NaOH. The combination F8BT (1 $\frac{\text{mg}}{\text{mL}}$) and cholic acid (1 $\frac{\text{mg}}{\text{mL}}$) in a qualitative study showed a cholic acid-related signal at $\frac{m}{z} = 407$ ($[\text{ChA}-\text{H}^+]^-$), see Figure 4.2b. However, there are also many signals in this spectrum that might be associated with F8BT. The absolute intensity in both, Figure 4.2a and Figure 4.2b is significantly lower than in positive reflectron mode.[6]
In summary, these measurements do not indicate that IDT-BT and F8BT can be used as MALDI matrices in negative reflectron mode, and thus they cannot be used as dual-mode matrices. As mentioned earlier, the access to the instrument was limited, so potentially further measurements can show that these polymers can be used in negative reflectron mode as well. It should also be mentioned that the approach of using conjugated polymers as MALDI matrices is fairly new and variations between instruments are possible when referencing this work to that of Horatz et al.

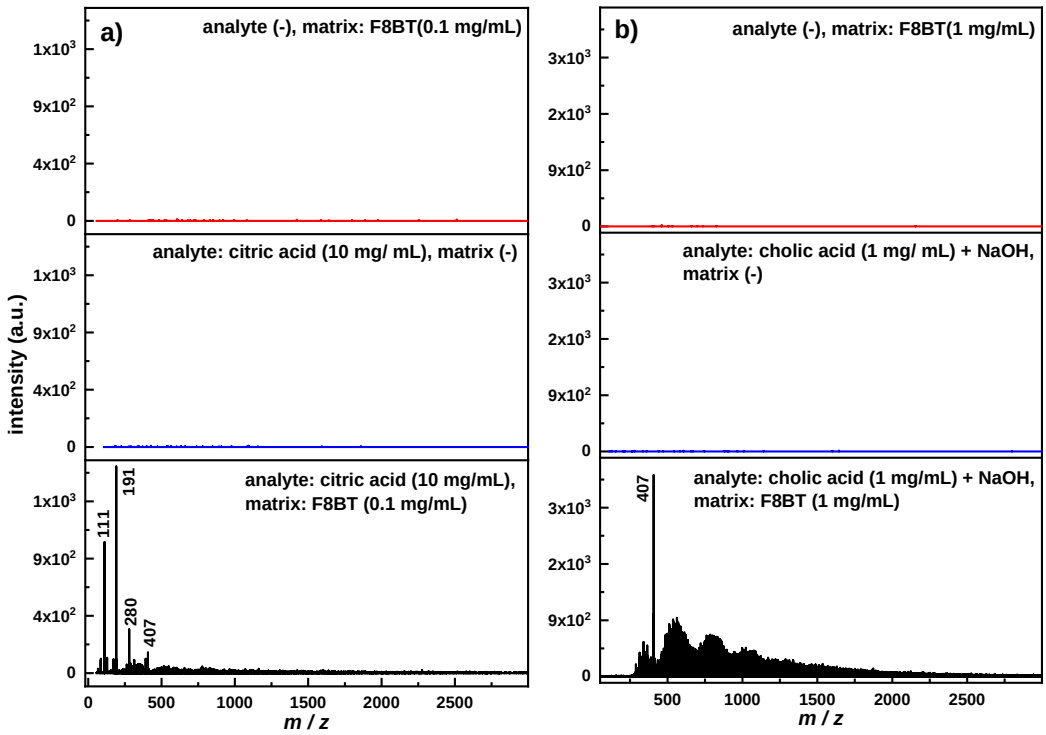

Figure 4.2: Reflectron negative mode MALDI-TOF spectra of F8BT as matrix with the analytes **a)** citric acid and **b)** cholic acid. To the cholic acid NaOH was added. Red: matrix only, blue: analyte only and black: best combination of analyte and matrix found. Laser intensity = 100% for a) and 50% for b).

Table 4.1: m/z and origin for IDT-BT and F8BT as MALDI matrices with TBAB, citric acid and cholic acid tested as analytes (see Figure 4.1 and Figure 4.2).

TBAB		citric acid		cholic acid	
$m\ /z$	origin	$m\ /z$	origin	$m\ /z$	origin
186	$[Bu_3N]^+$	111		407	$[ChA-H^+]^-$
245	$[TBA]^+$	191	$[CiA-H^+]^-$		
		280			
		407			

4.1.2 Pristine additives TCNQ and F_4TCNQ

To record MALDI-TOF spectra of TCNQ and F_4TCNQ, samples were prepared from chlorobenzene with concentrations of 1 $\frac{mg}{mL}$ under nitrogen atmosphere, similar to the solutions that were used in later on described experiments. As TCNQ[44,45] and F_4TCNQ probably as well can be used as MALDI matrices, no additional matrix was added. The spectra are presented in Figure 4.3a for TCNQ and Figure 4.3b for F_4TCNQ and the proposed origins of the peaks are summed in Table 4.2.

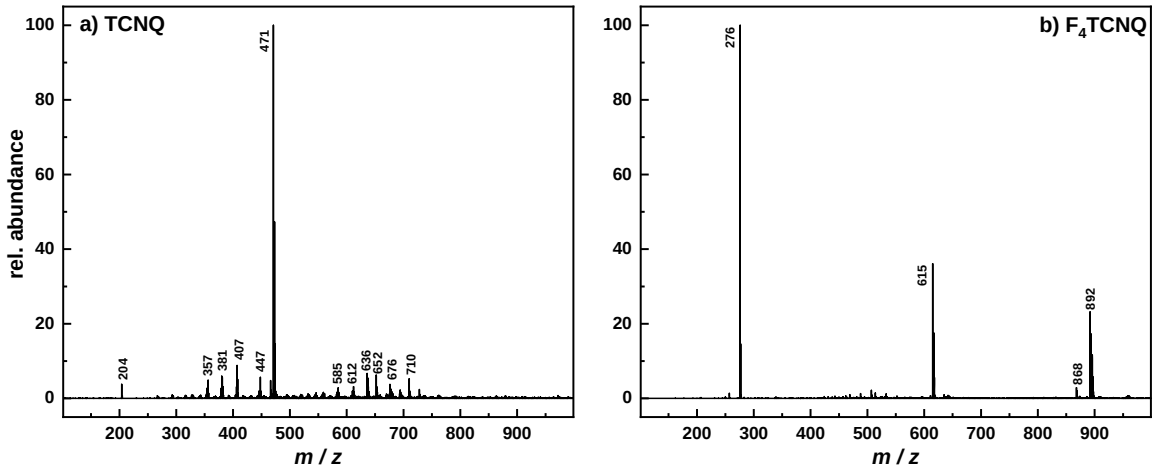

Figure 4.3: Reflectron negative reflectron mode MALDI-TOF spectra of pristine TCNQ and F_4TCNQ, dried from chlorobenzene under nitrogen atmosphere.

Using the positive electron impact ionization, Mermilliod et al.[46] presented a TCNQ mass spectrum. In the negative reflectron mode spectra presented here (Figure 4.3a), the highest signal shows at $\frac{m}{z} = 471$ and not at $\frac{m}{z} = 204$, which would be the $TCNQ^{\cdot -}$-related signal. There are no signals detected in the low mass regime, but only in the high mass regime, which are assigned to di- and trimers as well as their fragments, see Table 4.2. The spectrum shows a pattern with losses of CN and HCN. Another typical possible loss would be N_2. The peak with $\frac{m}{z} = 407$ can be assigned to the dimer $[TCNQ_2 - H]^-$. This dimer was found by Mermilliod et al. as well in small quantities.[46] The

dimer $[TCNQ_2]^{2-}$ also is known to form in solution.[26,27] It is unclear, whether those dimers form inside the sample or are generated through the measurement. It was not possible to record carbon NMR signals from analog prepared TCNQ samples, which might have provided further insight.
For F_4TCNQ the molecular peak with $\frac{m}{z} = 276$ can be assigned to the radical anion of F_4TCNQ (Figure 4.3b). As there are no peaks in the low mass regime, fragmentation did not seem to take place. In the high mass regime, three signals are detected. Those potentially originate from di- and trimers as well. A similarly prepared solid was studied using solid-state NMR spectroscopy, see Figure 8.11 for carbon NMR, in which no signals were detected that could not be assigned to the pristine F_4TCNQ. It is therefore concluded that those di- and trimers form due to the laser influence.

Table 4.2: *m /z* and relativ abundances (r. a.) of the observed peaks in the negative reflectron mode MALDI-TOF spectra of pristine TCNQ and F_4TCNQ (Figure 4.3) and proposed origins.

TCNQ			F_4TCNQ		
m /z	r. a.	origin	*m /z*	r. a.	origin
204	3.8	$[TCNQ]^{\cdot -}$	276	100	$[F_4TCNQ]^{\cdot -}$
356	4.9	$[TCNQ_2 - H - 2CN]^-$	615	36.6	$[2F_4TCNQ{+}C(CN)_2]^-$
380	6.0	$[TCNQ_2 - H - HCN]^-$	868	3.0	
407	8.8	$[TCNQ_2 - H]^-$	892	23.9	$[3F_4TCNQ{+}C(CN)_2]^-$
448	5.6				
471	100	$[2TCNQ{+}C(CN)_2{-}H^+]^-$			
559	1.6				
585	2.8	612-HCN			
612	3.2	636-2C			
636	6.1				
652	6.4	676-2C			
676	3.8	$[3TCNQ{+}C(CN)_2]^-$			
710	5.3				

4.1.3 Investigations on reactions with water in IDT-BT/TCNQ blends

As shown in a previous chapter, IDT-BT can be used as a MALDI matrix in positive ion mode. However, the results for negative reflectron mode were not satisfying. Moreover, TCNQ is a commonly used matrix in MALDI spectrometry.[44,46] It is also unclear whether the recorded signals originate from molecules or ions that were present in the sample before the measurement or from ions that were generated during the measurement. All of these factors complicate studies of polymer/additive thin films. It is also unclear what reaction products to expect from the possible reaction with water and what signal would be associated with those products since laser-induced reactions can occur. Because MALDI studies of polymer/additive mixtures have proven difficult, only a qualitative discussion will be presented here.
For these studies different samples were prepared: TCNQ in chlorobenzene with one equivalent water, TCNQ in chlorobenzene with an excess of water, and TCNQ with IDT-BT (10:1) in chlorobenzene with an excess of water. From those samples, drops of the organic phase were applied onto the MALDI target and one was allowed to dry at rt, while the other was annealed at 363 K for one hour. Of the samples, to which an excess of water was added, the same was repeated using the water phase. This entire setup was repeated using D_2O instead of H_2O as well. The idea was that peaks that are related to water would shift slightly and therefore would be identified more easily. The spectra recorded using H_2O are displayed in Figure 4.4, Figure 8.14 and Figure 8.15 and spectra recorded using D_2O

in Figure 8.16 and Figure 8.17. The peaks and relative abundances are listed in Table 8.1, Table 8.2 and Table 8.3 (Appendix). Due to the above-stated reasons, no origins of the peaks are proposed.

In general, the spectra all show similar signals within positive and negative refelctron ion mode with varying intensities. The different intensities may be related to the region under investigation, as MALDI does not examine the entire target at once. It should also be noted that non-ionized molecules cannot be detected. It is therefore likely that the MALDI measurement can only give an incomplete impression of the blends. Even though the assignment of the signals is challenging, it can be said that the addition of water does not clearly create a new signal or significantly change the intensity of specific signals (compare Figure 4.4, Figure 8.14 and Figure 8.15).

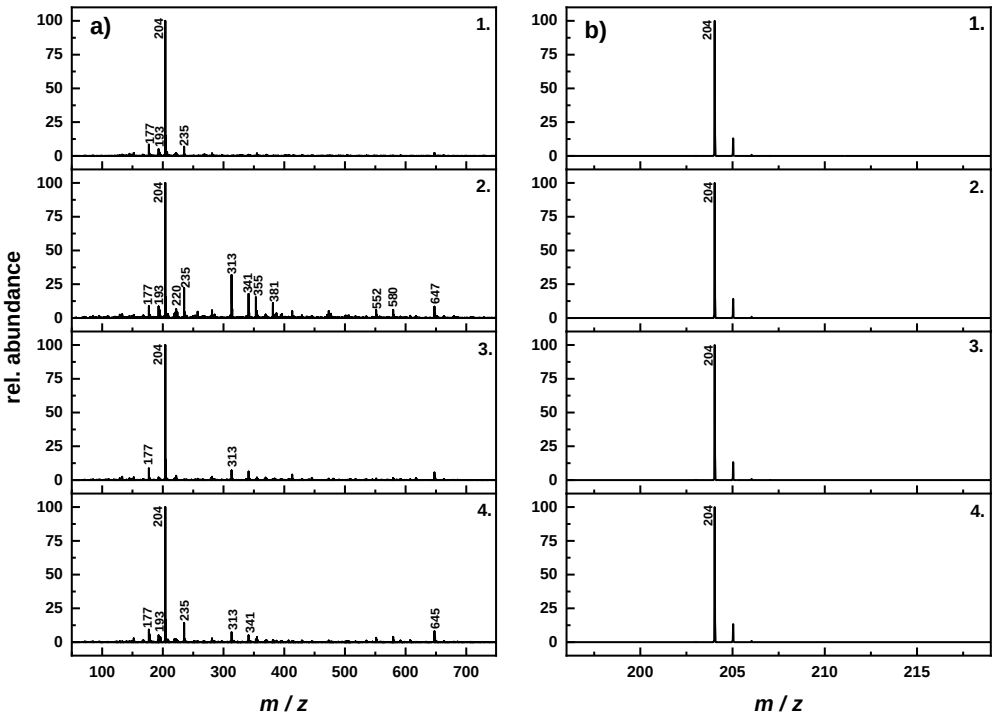

Figure 4.4: MALDI-TOF spectra in **a)** positive and **b)** negative reflectron mode. **1.** TCNQ in CB annealed at 363 K for 1 h, **2.** TCNQ in CB dried at rt, **3.** TCNQ and H_2O (1:1) in CB annealed at 363 K for 1 h and **4.** TCNQ and H_2O (1:1) in CB dried at rt.

In the course of these measurements, TCNQ from chlorobenzene was measured again, in both positive and negative mode (Figure 4.4a and Figure 4.4b; 1. and 2.). For the negative reflectron mode it is noticeable that only the signal of the pure TCNQ ($\frac{m}{z} = 204$) was detected in all samples (1.-4.). It should also be noted that the absolute intensity of the spectra recorded in the negative reflectron mode was significantly higher than that of the positive reflectron mode. This may be due to the chemical properties of TCNQ or the presence of pre-charged ions. The spectra recorded in positive reflectron mode (Figure 4.4a) do not show the 'typical' losses expected for TCNQ (CN, HCN, N_2[46]). It can furthermore be said that the annealed samples (1. and 3.) show mainly the TCNQ-related signal. This may be due to reactions taking place during the heating or the evaporation of the solvent and/ or water.

When considering reactions with water, from a chemical point of view, hydrolysis of the nitrile groups would be possible, as sketched in Figure 4.5. First, the imidocarboxylic acid is formed, which immediately changes to the acid amide. However, since the nitrile group has a low carbonyl activity, hydrolysis is only possible with strong acids in high concentrations (e.g. conc. HCl or 20-75% H_2SO_4) or 10-50 % alkaline solutions. Under these conditions, the nitrile would continue to react directly to the carboxylic acid. The ease of hydrolysis increases from the tertiary to the primary bonded nitrile group.[47] It can be assumed that these reaction conditions are not given when TCNQ is combined with water in a solvent with and without the addition of a polymer and therefore hydrolysis of the nitrile groups should not occur. The same can be assumed for the conditions under which the solutions are prepared for transistor fabrication.

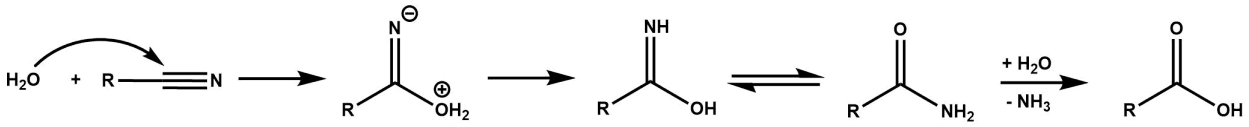

Figure 4.5: Nitrile hydrolysis. Note, that strongly acidic or baic conditions are required for this reaction to occur.[47]

As hydrolysis of the nitrile group is rather unlikely to happen (Figure 4.5[47]), another reaction product might be **A** (see Figure 3.4). This product could be identified by the $[TCNQOH]^-$ signal in negative mode or the protonated species $[HTCNQ]^+$ in positive mode. As already discussed, the first one was not found and the second is problematic to be verified. This is because the mass of this species is $\frac{m}{z} = 205$, which would overlap with the isotope pattern of non-protonated TCNQ. Even if the relative abundance detected for this $\frac{m}{z}$-ratio is larger than predicted, it could not be said whether this ion was present prior to the measurement, since protonation during the measurement is possible. When comparing these measurements with those in which D_2O was used instead of H_2O (Figure 8.16), again similar signals with varying intensities are found. This indicates that D_2O had evaporated and did not take place in a reaction with TCNQ. If a reaction would have occurred, a shift of specific peaks would have been expected, since deuterons are heavier than protons. The deuterated TCNQ however should be detectable more easily, since the mass of $[DTCNQ]^+$ is $\frac{m}{z} = 206$, which should be distinguishable from the isotope pattern of TCNQ. However, this signal was not observed in high intensities.
When additionally adding IDT-BT the same conclusions can be drawn. In the negative reflectron mode, the only peak detected can be assigned to the TCNQ radical anion or dianion, $\frac{m}{z} = 204$ (Figure 8.14b). In positive reflectron mode the same signals in varying intensities are observed (Figure 8.14a) as to when IDT-BT is not added. Again, the annealed samples (1. and 3.) show mainly the TCNQ-related signal. When comparing this to the measurements performed using D_2O instead of H_2O and the IDT-BT:TCNQ ratio being 1:1, the signals again are the same in varying intensities.

For the earlier discussed reasons, MALDI measurements did not generate the insight that was hoped for. However, as the access was limited and due to these unsatisfying results, ESR and NMR spectroscopy were used as well and the results are presented in the following chapters.

4.2 Electron spin resonance

4.2.1 Polymer and additive blends in ESR studies

As ESR spectroscopy detects unpaired electrons, this technique can generate a fundamental understanding of doping mechanisms between polymers and additives.[34,37–40] It is especially useful when studying systems involving molecular additives such as F_4TCNQ and TCNQ, because of their ability to form radical anions that are highly stable, even under ambient conditions.[23] In literature, different techniques are known to study doping of polymer/additive blends by ESR spectroscopy. One approach is to draw up the solution into the ESR-tube and let the solvent evaporate, either in vacuum[48] or at environmental pressure and rt.[49] Another one is to generate films on glass plates, scratch them off and transfer them into an ESR-tube.[50] In this thesis, the latter approach was chosen to be as close to the transistor fabrication as possible.[3] Note, that the ratios given in this section are molecular ratios, if not explicitly highlighted as weight percent. All experiments were conducted under nitrogen atmosphere. All polymer/additive combinations, reactions temperatures, and times as well as further experimental details can be found in Table 6.4, Experimental. The error given for all g-values is an assumed instrument-based error.

IDT-BT and F_4TCNQ

The first system investigated were IDT-BT/ F_4TCNQ blends. As follows from the HOMO energy of IDT-BT (-5.2 eV[3,15]) and LUMO energy of F_4TCNQ (-5.3 eV[17]), the transfer of one electron from the polymer to the molecular additive should occur, leading to the radical anion $F_4TCNQ^{\cdot -}$ and radical cation $IDT{-}BT^{\cdot +}$. These should then be detectable using ESR spectroscopy.

To generate thin films, IDT-BT and F_4TCNQ solutions in chlorobenzene were prepared with concentrations of 1 $\frac{\text{mg}}{\text{ml}}$. After dissolving of the solids, the IDT-BT/ F_4TCNQ solutions were prepared at ratios of 4:1 ($\hat{=}$ 5 wt%), 10:1 ($\hat{=}$ 2 wt%), and 20:1 ($\hat{=}$ 1 wt%). Of the at 333 K stirring IDT-BT/ F_4TCNQ solutions, liquid state samples were taken 5 and 30 min. after combining. Next, the solutions were drop-casted onto pre-heated glass plates and annealed for approx. 10 min. at 363 K. In case of the 4:1 and 10:1 ratios, solutions of pristine F_4TCNQ in chlorobenzene were prepared in the same composition as in the IDT-BT/F_4TCNQ blends to understand whether the radical content increased after polymer addition or not. Note, that the sample preparation was identical for all polymer/additive blends presented in this chapter. Furthermore, of both pristine polymers, IDT-BT and F8BT, ESR spectra were recorded in chlorobenzene as well as their films annealed from those solutions, showing no radical signal (see Figure 8.1, Appendix).

In Figure 4.6a-c the recorded spectra of the liquid and solid-state samples of the different IDT-BT/ F_4TCNQ ratios are displayed. The g-values were determined to be 2.0036 ± 0.0003 in all cases using a manganese standard. This is in agreement with the literature: Schott et al. determined the g-value of IDT-BT in a polystyrene matrix with incorporated F_4TCNQ to be 2.00243 and the g-value for F_4TCNQ in the same environment to be 2.00395.[34] For none of the recorded spectra hyperfine splitting is observed and the peak-to-peak width ΔH is 0.12 mT for a) and 0.18 mT for b) and c). Since F_4TCNQ and IDT-BT do not possess a symmetric paramagnetic center, more than one g-value would be expected. This, however, is not observed in solid state, because of all possible orientations contributing to the spectra and thereby broadening it. By using a spectrometer with a higher frequency they might be detectable. Furthermore, in organic radicals, the hyperfine splitting often dominates at X-band frequencies. In liquid state, the g-value often is averaged due to fast tumbling.[30,33] This applies to all presented ESR spectra.

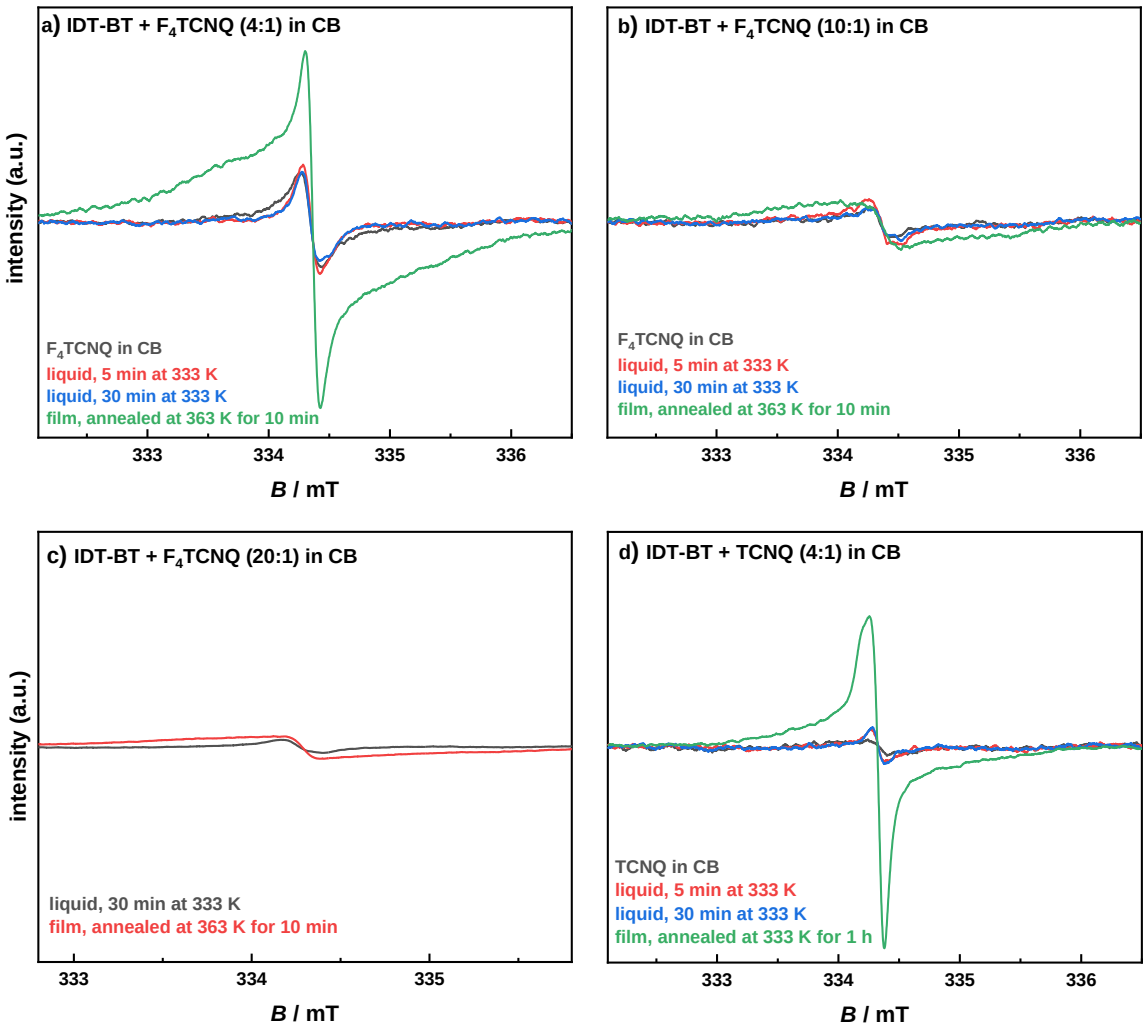

Figure 4.6: **a) - c)**: Liquid state ESR spectra of IDT-BT/ F_4TCNQ blends in CB 5 min and 30 min after combining as well as films prepared from these solutions. With molar ratios of polymer:dopant = **a)** 4:1 ($\hat{=}$ 5 wt %), **b)** 10:1 ($\hat{=}$ 2 wt %) and **c)** 20:1 ($\hat{=}$ 1 wt %). **a) - c)**: $g = 2.0036 \pm 0.0003$, measured at rt. **d)** Liquid state ESR spectra of IDT-BT/ TCNQ (4:1) in CB 5 min. and 30 min. after combining as well as the film (molar ratio = 4:1, $g = 2.0034 \pm 0.0003$, measured at rt).

In the spectra displayed in Figure 4.6a (ratio 4:1) and Figure 4.6b (ratio 10:1) there is no difference in signal intensity between samples containing F_4TCNQ in chlorobenzene only and samples containing a polymer/additive blend. This is surprising, as doping of the polymer should occur and radicals should be generated as a result. However, since the total amount of F_4TCNQ itself is small and then even smaller in the sample that is raised into the ESR-tube, this could be the reason for the detection of such a small signal. It is further possible that the reaction time for the doping process was too short at only 30 min. or that the temperature was not high enough. The signal of the IDT-BT:F_4TCNQ film with a ratio of 4:1 (Figure 4.6a) seems to consist of a narrow and a broad signal that overlap. This may be explained by the fact that two radicals should form: $F_4TCNQ^{\cdot -}$ and $IDT{-}BT^{\cdot +}$. However, Tati et al.[48] did not observe this type of shape when studying P3HT/F_4TCNQ blends, for which doping should occur. Another conclusion that can be drawn from the ESR spectrum of the thin film, is that heating might be crucial for the redox reaction to take place, which is also supported by the results presented in the NMR section (see Figure 4.22 and following results).

For ratios of IDT-BT:F_4TCNQ = 10:1 (Figure 4.6b) and 20:1 (Figure 4.6c), the signal intensities of liquid and solid samples are identical. Similar to the results presented in Figure 4.6a, an increase in signal intensity from liquid to solid was expected. The absolute amount of F_4TCNQ inside the films should have been high enough to detect a signal. It is therefore assumed that this is not an instrument-based effect, but rather due to no radical anions being present. Other or further reactions of the radical anions cannot be excluded. These experiments were carried out twice, showing the same results.

It is noteworthy that when F_4TCNQ is used as a dopant in organic devices the presence of radical anions does not seem to have a negative effect on the performance.[3,34] This is important to consider when discussing the results below.

IDT-BT and TCNQ

As a next step, IDT-BT/TCNQ blends were studied using ESR spectroscopy. For this, the same procedure was followed as described for IDT-BT/F_4TCNQ blends, using a polymer:dopant ratio of 4:1. This ratio was chosen, as it was shown in transistor studies that below 5 wt% no device improvement occurs, which corresponds to a molar ratio of approx. 4:1.[3] Note, that doping should not occur as the LUMO energy of TCNQ is approx. -4.7 eV.[1] The recorded spectra are displayed in Figure 4.6d, where $g = 2.0034 \pm 0.0003$ and the peak-to-peak width ΔH is 0.13 mT. In the liquid state ESR spectra, there is no increase in signal between the sample containing TCNQ in chlorobenzene only and the sample containing the IDT-BT/ TCNQ blend. This observation is similar to the one made for the IDT-BT/F_4TCNQ blends (Figure 4.6a and Figure 4.6b) and might be explained by the same arguments or that no redox reaction took place. In the solid-state ESR spectra of the IDT-BT/ TCNQ film a large, asymmetric signal is detected. As there are no two overlapping signals as in Figure 4.6a and doping should not occur, the signal most likely is due to the radical anion $TCNQ^{\bullet -}$, the origin, however, is unclear. The asymmetry may be attributed to $TCNQ^{\bullet -}$ in varying environments and therefore resulting in different signals. This experiment was the only one in which such an asymmetry was observed.

When searching literature on the subject of radical anion formation of TCNQ in combination with donors, there are a couple of papers that might be of interest. For example, Stößer et al.[51] report the formation of TCNQ radical anions in the unpolar solvent dichloromethane when adding *N*-heterocycles such as 1,10-phenanthroline by recording ESR spectra. They attribute this to the formation of complexes, the donicity of the *N*-heterocyles, and the stabilization of the radical anion through the *N*-heterocyle. Additional irradiation leads to an increase in intensity of the radical signal. Furthermore, Kim et al.[52] report the formation of charge-transfer complexes (CTC) when combining TCNQ with 4-aminobiphenyl, benzidine, or 2-aminobiphenyl in acetonitrile. This was concluded from recording UV/ vis spectra and π-π interactions between donor and acceptor were found to be essential for the formation of these complexes. Upon irradiation, the formation of these CTCs takes place more quickly, since the non-irradiated samples were stored in the dark for six days before recording spectra. To conclude, the additive TCNQ in combination with heterocycles possesses the ability to form radical anions. Possibly, with the help of IDT-BT, complexes are formed as well, in which the polymer contributes to the stabilization of the radical anion. Another, remotely related report of Qi et al.[53] describes the deposition of TCNQ onto graphene. After being exposed to air, $DCTC^-$ was observed using Raman scattering. The authors interpret this as a sign of doping and that $DCTC^-$ is the reaction product of the radical anion $TCNQ^{\bullet -}$ with oxygen. With respect to the results presented in here, it could also be an analogous phenomenon in which radical anions (and dianions) are formed and stabilized due to the spatial proximity to the graphene (polymer).
Another approach to explaining the observance of radicals is to consider the temperature dependence

of redox reactions. This follows from the Nernst equation ($E = E^0 + \frac{RT}{zF} ln(\frac{c_{ox}}{c_{red}})$). Since the HOMO and LUMO energies of the polymer and additive are furthermore dependent on the solvent and potential interactions between the both of them, the values given in Figure 3.3 might not be accurate. The spreading of energy sites originating from non-uniform polymers needs to be considered as well.[2] It has also been shown in literature, that despite negative energy differences between the HOMO of the polymer and the LUMO of the molecular additive (approx. –0.1 eV), doping can take place.[17,54] It is difficult to retrace what happens between the polymer and the additive during the heating at 363 K, as this is a rather high temperature. However, despite the above-presented arguments, it cannot be concluded that doping took place.

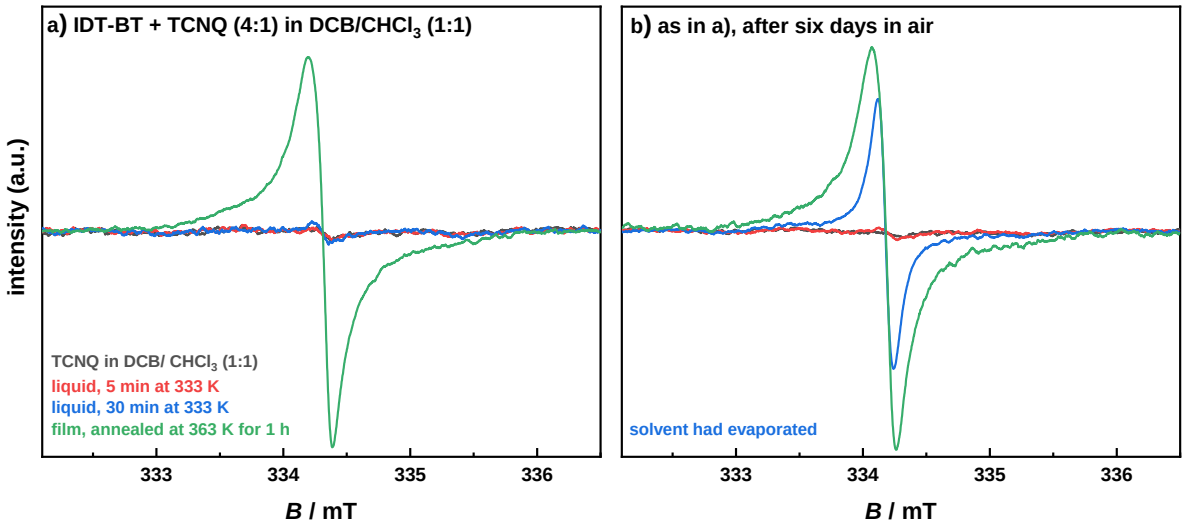

Figure 4.7: Liquid state ESR spectra of IDT-BT and TCNQ in DCB/$CHCl_3$ = 1:1 and films annealed from these solutions at 363 K for 1 h. Molar ratio of polymer:dopant = 4:1, measured at rt and $g = 2.0034 \pm 0.0003$. **a)** shows the spectra measured right after the sample preperation and **b)** the same samples after six days in air.

To further understand the potential interactions between IDT-BT and TCNQ, the solvent was changed from chlorobenzene to a one-to-one mixture of chloroform and *ortho*-dichlorobenzene, similar to [3]. Again, the same sample preparation procedure as before was followed and the IDT-BT:TCNQ ratio was 4:1. However, the annealing time has been increased to one hour for this and all other following annealed films. The spectra recorded on the same day as setup are displayed in Figure 4.7a and the re-recorded spectra after the samples were allowed to rest in air for six days in Figure 4.7b. The g-values are 2.0034 ± 0.0003 and $\Delta H = 0.2$ mT for Figure 4.7a, 0.19 mT for Figure 4.7b, green curve, and 0.11 mT for Figure 4.7b, blue curve. Again, there is only a small signal detectable in the liquid state ESR samples and a large signal in the solid-state sample. Under these changed conditions the radicals still form. It is noteworthy that from the re-measured liquid sample, which was taken 30 min. after combining IDT-BT and TCNQ, the solvent had evaporated (Figure 4.7b, blue curve). As the radical signal increased drastically, it could be concluded that not the temperature is responsible for the formation of radicals, but rather the aggregation condition. Maybe the radical formation is supported by molecular ordering. This further shows that even in the liquid state ESR samples with small volumes there is enough material present to obtain a good detectable radical signal. In solid-

state there might be improved interactions due to close spatial proximity between ID-BT and TCNQ, allowing for π-π stacking and potentially leading to CTCs. Of course, the radical formation can also be connected to the time the sample sat in air. However, in that case, a change in the signal would have been expected for the other samples as well.

As a next parameter, the annealing temperature was investigated, again with the ratio of IDT-BT:TCNQ being 4:1. As the redox potential is temperature-dependent and only in solid-state radicals are detected, two solid-state samples were prepared from the same stock solution: One was annealed at 363 K for 1 h and one dried at rt for 24 h. The spectra are displayed in Figure 4.8, where $g = 2.0034 \pm 0.0003$ and $\Delta H = 0.14$ mT. Interestingly, the signal detected for the sample dried at rt is larger than the one for the sample that was annealed. This suggests that heating is not beneficial for the formation of radicals and further supports the hypothesis, that the aggregation condition plays a crucial role. Another possible explanation is that the radicals are less stable at higher temperatures and decay via reaction channels that are not accessible at lower temperatures.

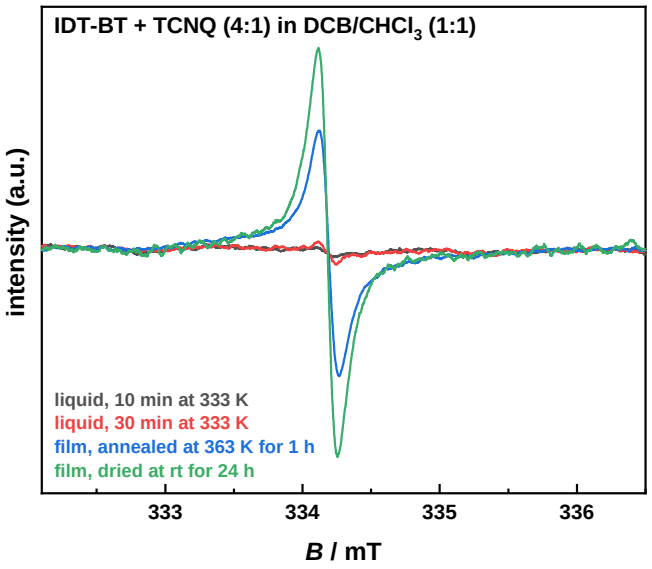

Figure 4.8: Liquid state ESR spectra of IDT-BT and TCNQ in DCB/$CHCl_3$ = 1:1 and films annealed from these solutions at 363 K for 1 h with molar ratios of polymer:dopant = 4:1. Measured at rt and $g = 2.0034 \pm 0.0003$.

Further experiments were carried out on the IDT-BT/TCNQ films, but in these samples, only low radical signals were detected. It is worth mentioning that all samples that showed high radical signals were prepared in a row and then all samples that showed small radical signals only were prepared in a row as well. General contaminants such as glovebox conditions or chemical cleanliness were considered, but no clear correlation was found. One experiment in which only low radical signals could be detected was the comparison of an annealed film, which was under nitrogen atmosphere during the whole process, with an annealed film, which was allowed to sit in air for one to two hours prior to the measurement (Figure 8.2, ratio 4:1 and Figure 8.3, ratio 4:1). In addition, the comparison of annealed and non-annealed films was repeated (Figure 8.4, ratio 2:1, Appendix).
No radical signal does not necessarily mean no reaction took place, as can be seen in some of the IDT-BT/F_4TCNQ blends: Although doping should occur, no signal is observed for the ratios 10:1

and 20:1 (Figure 4.6). It must also be emphasized that the ESR spectroscopy itself, since it only detects radicals, most likely cannot give a complete insight into this process. Other reaction products, for example, dianions, cannot be detected.

F8BT and TCNQ

Next, the combination of the polymer F8BT with the molecular additive TCNQ was studied. Initially, the idea was to show that this combination would not result in a radical signal, since at this point the electron transfer between IDT-BT and TCNQ still was considered. The HOMO energy of F8BT is at about -5.9 eV[16] and therefore doping should theoretically be ruled out. The earlier described procedure was followed, using a polymer:dopant ratio of 4:1. For both spectra (Figure 4.9a and Figure 4.9b) the g-values are 2.0032 ± 0.0003 and $\Delta H = 0.09$ mT. In Figure 4.9a, two solid-state samples from the same stock solution were investigated: One was annealed at 363 K for one hour, and one dried at rt for two hours. As observed previously, the liquid state samples showed very small radical signals only. Here the same arguments as before apply. The film that was annealed shows a higher signal than the film dried at rt, which is the reverse result to that obtained when using the polymer IDT-BT (Figure 4.8). This may be attributed to the different chemical structures of F8BT and IDT-BT.

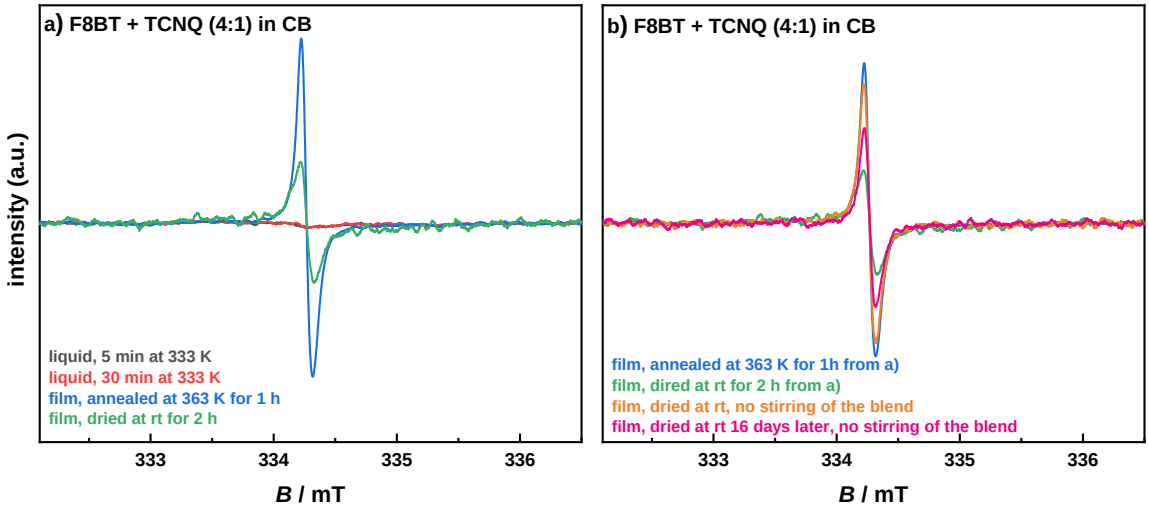

Figure 4.9: **a)** Liquid state ESR spectra of F8BT and TCNQ in CB and films prepared from this solution at 363 K for 1 h and rt with molar ratios of polymer:dopant = 4:1. **b)** Combination of solid-state samples from **a)** and two newly prepared solids. Measured at rt and $g = 2.0032 \pm 0.0003$.

Figure 4.9b shows a combination of two different setups, all in solid-state. The blue and green curves are the solid-state samples from Figure 4.9a. As it was noted that heating had an influence, the joint stirring at 333 K was investigated. To do so, there was no joint stirring after combining the solutions in the appropriate ratios, but rather a quick mix. The solution was drop cast onto a glass plate immediately and allowed to dry at rt (orange curve, Figure 4.9b). From this solution, a part was held back and after remaining in nitrogen atmosphere for 16 days it was drop-cast onto a glass plate

and dried at rt as well. Since the signal for the orange curve is almost as high as for the blue curve, it may be concluded that the radicals form instantly and that this is a heat- and time-independent but an aggregate-dependent process. From the pink curve, it furthermore appears that with time fewer radicals are present, which may be due to dimerizations/diproptionations,[19,23,25–27] acid-base-chemistry[19,23] and redox-chemistry.[19,23]

In all investigated mixtures of F8BT and TCNQ there were radicals present (see Appendix Figure 8.5 also). There were also samples prepared in air, showing the same result. It seems that the polymer plays a crucial role in the formation of radicals, even though no redox reaction between polymer and additive may be taking place. Here the same arguments apply as before. It is also concluded that F8BT seems to support the radical anion formation better than IDT-BT, since there were no F8BT/TCNQ blends that did not show radical signal. After this series of experiments, a doping reaction between the polymer and additive was ruled out (except for the IDT-BT/ F_4TCNQ blends). This is because the energy gap between F8BT and TCNQ simply should be too large for a doping reaction to occur. Therefore, other origins of radical anions were investigated next.
For samples with polymer-additive combinations of IDT-BT/F_4TCNQ (Figure 4.6), IDT-BT/TCNQ (Figure 4.6, Figure 4.7 and Figure 4.8) and F8BT/TCNQ (Figure 4.9) radical signal could still be detected two months after sample preparation. Since the samples were in air for this long period of time and the signal was almost unchanged, this is seen as an indication that the very stable TCNQ and F_4TCNQ radical anions were formed, since polymer radicals should be much more unstable. However, as discussed earlier, their origin remains unclear.

F8BT and F_4TCNQ

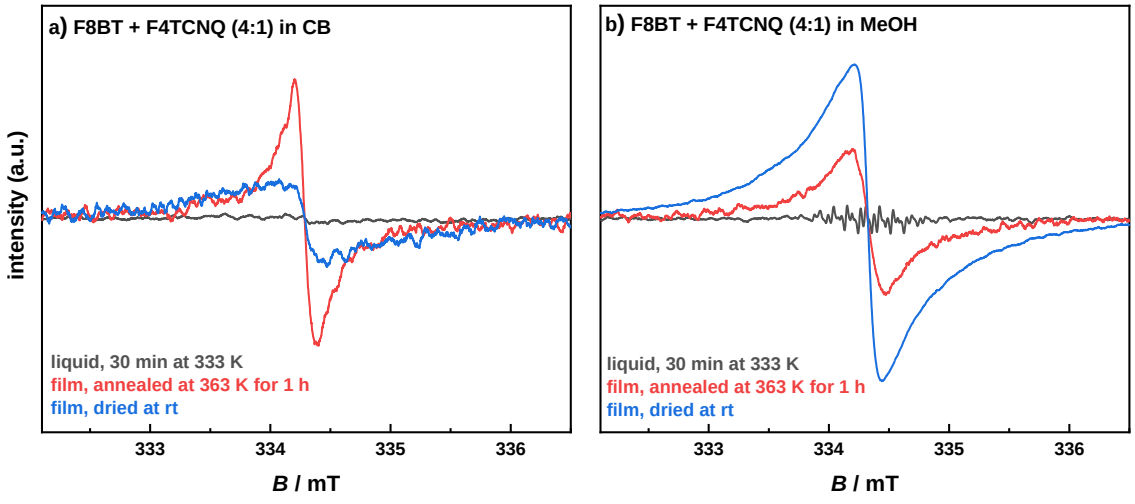

Figure 4.10: Liquid state ESR spectra of F8BT and F_4TCNQ in **a)** CB and **b)** MeOH and films prepared from these solutions at 363 K for 1 h and rt with molar ratios of polymer:dopant = 4:1. Measured at rt and $g = 2.0032 \pm 0.0003$.

Since the detection of radicals (in higher or lower concentrations) was permanent, it was hypothesized that they always form in a certain percentage regardless of the HOMO and LUMO energies of polymer and additive. This formation of radical anions should also influence the OFET performance and might even be beneficial. From Figure 3.4 it can be seen that the reduced additives can be protonated and by this may be passivating traps. To investigate this hypothesis, further polymer/additive combinations were examined, in which the transfer of an electron should also not occur.
Therefore, the next investigated combination was the polymer F8BT with the additive F_4TCNQ (see Figure 3.3 for HOMO and LUMO energies). For this series, the solvents chlorobenzene (Figure 4.10a) and methanol (Figure 4.10b) were chosen. Methanol was chosen because it was shown that F_4TCNQ forms radicals when being annealed from it (see next chapter, Figure 4.16c) and it should be checked whether the same effect can be observed in the presence of polymers or not. Again, one film was allowed to dry at rt and one was annealed at 363 K for 1 h. For both plots $g = 2.0032 \pm 0.0003$ and $\Delta H = 0.2$ mT for Figure 4.10a and 0.22 mT for Figure 4.10b applies. The detection of radicals in liquid state samples is as expected with regard to the later on presented results (see Figure 4.16a). In all solid-state samples radicals were present, however, in Figure 4.10a the annealed film shows a higher signal than the one dried at rt whereas in Figure 4.10b it is the exact opposite. Potentially, this is a solvent-related effect, but it might also be caused by inconsistent reactions taking place. This being a solvent-related effect seems reasonable as in methanol a lot more radical anions $F_4TCNQ^{\cdot -}$ are present before being added to the polymer solution than in chlorobenzene. Due to this fact, there might be other reaction pathways than when neutral F_4TCNQ is added. What exactly happens, however, remains unclear. As discussed earlier a redox reaction can not be entirely ruled out but is expected to be unlikely. It can be concluded that for this polymer/additive combination, radical anions form, although there most likely has not been an electron transfer from the polymer to the additive and thereby supporting the earlier stated hypothesis.

F8BT and DDQ

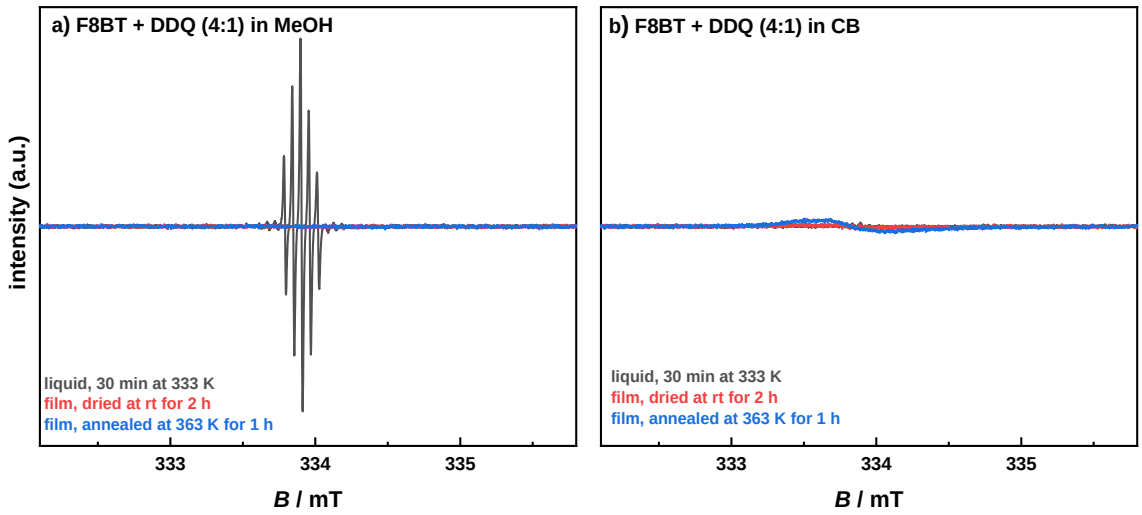

Figure 4.11: Liquid state ESR spectra of F8BT and DDQ in **a)** MeOH and **b)** CB and films prepared from these solutions at 363 K for 1 h and rt with molar ratios of polymer:dopant = 4:1. Measured at rt and $g = 2.0056 \pm 0.0003$.

Finally, the above hypothesis should be tested for the combination of the polymer F8BT with the additive DDQ. Again, no doping should occur (see Figure 3.3). The solvents methanol and chlorobenzene were used, for the reasons described above, and again, two films were prepared. The recorded spectra are displayed in Figure 4.11 and $g = 2.0056 \pm 0.0003$. The g-value is in agreement with literature values for the DDQ radical anion.[55] A large radical signal with hyperfine coupling from the two equivalent nitrogen atoms of DDQ shows for the liquid sample in methanol and no radical signal is detected in chlorobenzene. There were two films prepared from the same stock solution: One was annealed at 363 K for 1 h and one was allowed to dry in air, which took two hours for both samples. In all solid-state samples, except for the one annealed from chlorobenzene, no radical signal is detected, and even in that one a small signal only. This stands in contrast to the theory that the additives, even though if not reduced by the polymer, form radicals. Especially because in methanol there were radicals present, surprisingly, none are detected inside the film. It appears that the radicals engaged in further reactions. However, it cannot be concluded what those reactions might be. The different chemical structures of DDQ, TCNQ, and F_4TCNQ need to be considered as well and might be related to no radical anions being observed inside the films.

Temperature-dependent ESR studies

As it remained unclear, how the radicals form in samples where no electron transfer from polymer to additive should occur, temperature-dependent ESR spectra were recorded. As spin saturation occurs more easily with decreasing temperature,[56] the microwave power was chosen very low to avoid this effect. The idea was that thermally activated diradicals could form as the solution is annealed and thus enabling reactions of different kinds to occur. Diradicals are molecules carrying two unpaired spins with an interaction large enough to produce two spin states: singlet ($S = 0$, spin multiplicity $= 1$) or triplet ($S = 1$, spin multiplicity $= 3$). Whether a singlet or triplet state is present depends on the distance between the two spins. Small distances often lead to singlet and large distances to triplet states.[56] The temperature-dependent ESR signal intensity for the thermally excited triplet state can be described by:[31]

$$I \; \alpha \; T^{-1} \left[3 + exp\left(\frac{J}{k_{\mathrm{B}} T} \right) \right] \tag{4.1}$$

with the intensity I, the temperature T, the singlet-triplet exchange coupling constant J and the Boltzmann constant k_{B}. The F_4TCNQ/F8BT film, dried at rt from methanol, prepared for the spectra displayed in Figure 4.10b was studied. Before measuring, the sample remained in air for one day. In this sample, a signal was detected already and the film was not heated before. Therefore, an increase in signal would suggest the temperature-induced forming of diradicals. Note, that a redox reaction between the polymer and the additive should not take place, according to the HOMO and LUMO energies. In Figure 4.12a the temperature-dependent ESR spectra are displayed with T ranging from 128 K - 378 K. In Figure 4.12b the normalized spectra are displayed, to understand if the line shape is temperature-dependent. For all temperatures, almost identical Lorentzian line shapes are observed. Increased narrowing with increased temperature would suggest motional and/or exchange narrowing.[48] In Figure 4.12c the double integral (normalized to the rt intensity) is plotted against $\frac{1}{T}$. Here, Curie law-according behaviour for isolated spins centers ($S = 1/2$) is observed ($I \; \alpha \; T^{-1}$), suggesting the absence of spin-spin-interactions.[31,48] The double integrals determined for higher temperatures shift from the linear trend, however, this is seen to be within the error of the integration and may also be attributed to the signal-to-noise ratio.
It was very recently shown by Tati et al. that F_4TCNQ doped P3HT films show temperature-dependent behavior deviating from the Curie-law and suggesting thermally accessible triplet states using Equation 4.1 in the range of 100 K to rt.[48] However, no clear relation to the doping ratio was found and the singlet-triplet exchange coupling constant J is small compared for example to studies

of TMPD-TCNQ charge transfer salts.[57] This may be due to the F_4TCNQ being placed within the P3HT side chains,[58,59] leading to a decrease in exchange coupling.[48]

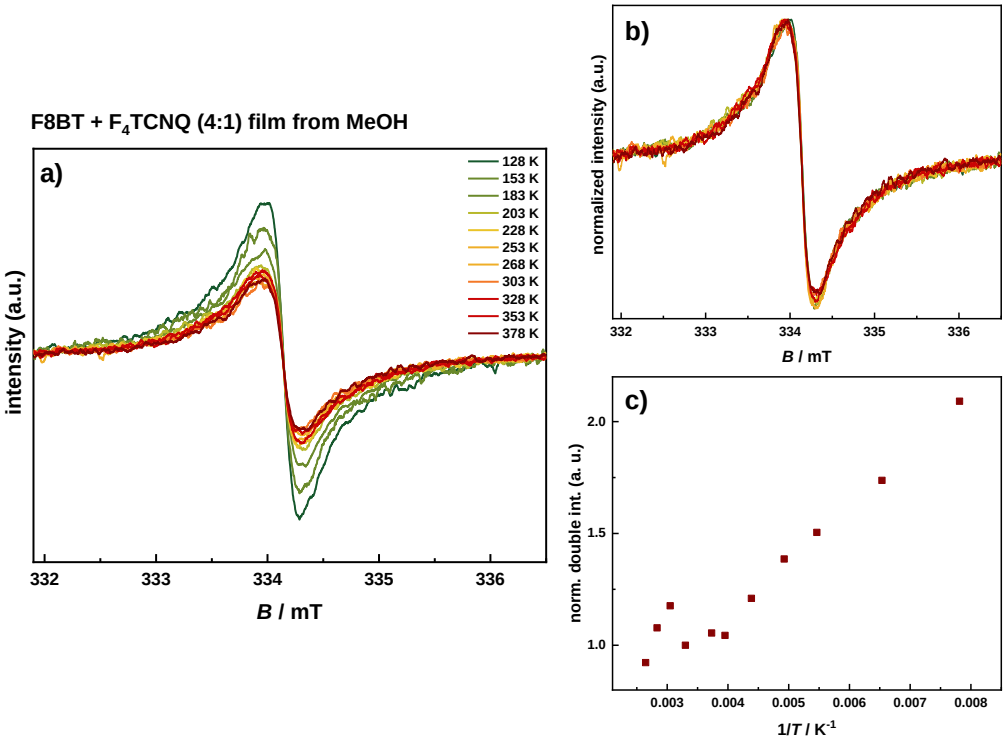

Figure 4.12: Temperature dependent ESR spectra of F8BT/F_4TCNQ film, dried from MeOH at rt with molar ratio of polymer:dopant = 4:1. The same sample as prepared for Figure 4.10b was used, after it remained in air for one day. **a)** recorded spectra, intensity not normalized, **b)** recorded spectra, intensity normalized and **c)** double integral normalized to rt value plotted against T^{-1}.

A second sample examined was the F8BT/TCNQ film (4:1) annealed at 363 K for 1 h (see Figure 4.9a). This sample was actually studied before the F_4TCNQ/F8BT film. The spectra are shown in Figure 4.13. It appears that the microwave power was chosen too high in this measurement, resulting in spin saturation at lower temperatures. This is evident from the broadening of the peak-to-peak width ΔH with decreasing temperature. In addition, the sample sat in air for two months before the temperature-dependent ESR spectra were recorded. During this time further reactions could have occurred. Clearly, the ambient conditions had no effect on the radical, which is another indicator that the very stable radical anion $TCNQ^{\cdot -}$ had formed. However, this plot is interesting because of the spectra recorded at 328 K, 303 K, and 253 K. An increase in intensity is seen at the higher temperatures, which is the opposite behavior to that expected from Curie's law. Also, no peak-to-peak broadening is observed in these spectra. This suggests that possibly the triplet state is thermally accessible and plays a role in the formation of radical anions. Although this result is interesting, it is not discussed further and should be viewed with caution for the reasons stated above. Unfortunately, further measurements were not possible due to time constraints. However, this result should be considered for further experiments.

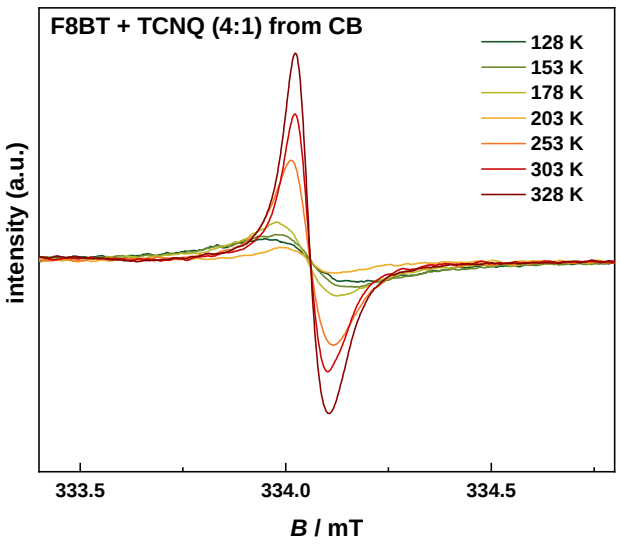

Figure 4.13: Temperature dependent ESR spectra of F8BT/TCNQ film, annealed from CB with molar ratio of polymer:dopant = 4:1. The same sample as prepared for Figure 4.9a was used, after it remained in air for two months.

4.2.2 Pristine additives and polymers in ESR studies

Due to the permanent detection of radicals in polymer/additive blends without a clearly identifiable origin of the same, the pure additives were examined more closely next. In fact, literature shows that the molecules TCNQ and F_4TCNQ can form radical anions in solutions depending on the solvent used.[26,28,51,60,61] This effect is accompanied by solvatochromism (see Figure 4.14 for TCNQ and F_4TCNQ in methanol, acetonitrile, chlorobenzene, and chloroform). As already highlighted, the radical anions are stable, even under ambient conditions.[23] To understand the formation of radicals better, ESR measurements of TCNQ and F_4TCNQ in methanol, chlorobenzene, chloroform, and acetonitrile were performed. The chemicals were used as received from the supplier, who purified them by sublimation. The solutions were prepared under nitrogen atmosphere with concentrations of 1 $\frac{\text{mg}}{\text{mL}}$. This concentration was chosen to be as close as possible to the transistor fabrication[3] and the earlier conducted experiments. After setup, the solutions were allowed to stir at 313 K for 30 min. to ensure dissolving. The samples then were measured immediately. Additionally, the same solutions were re-measured after sitting in nitrogen atmosphere for nine days. Furthermore, solid-state samples were generated from drop-casting the solutions onto pre-heated glass substrates (363 K), where they were annealed for one hour. The solid-state samples were prepared this way to recreate the transistor fabrication but without the normally added polymer. These experiments were conducted to gain a deeper understanding of the TCNQ and F_4TCNQ molecules that might be present in the transistor film. The recorded spectra are displayed in Figure 4.15 and Figure 4.16. Note that both, TCNQ and F_4TCNQ, were additionally measured in solid-state as received from the supplier, showing no radical signal.

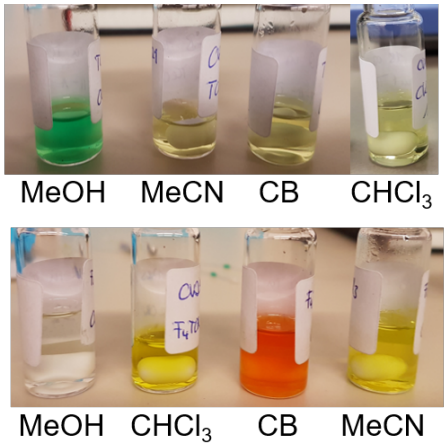

Figure 4.14: Solvatchromism of TCNQ and F_4TCNQ, nine days after setup under nitrogen atomsphere using anhydrous solvents.

Additionally, an ESR calibration was performed using 2,2,6,6-tetra-methylpiperidonyloxyl (TEMPO), which is a stable radical, in the according solvent.[38] From double integrating the signals and plotting them against the concentration, a linear dependence between double integral and concentration is found. Using this dependence, in a sample of unknown radical concentration, the radical amount present can be determined by double integrating the signal. The determined calibration fits are displayed in Figure 6.3, Appendix. From these fits the radical concentrations of TCNQ, F_4TCNQ and DDQ in the different solvents were extracted, the values are summed up in Table 4.4. The errors were calculated using the Gaussian error propagation and the error from the linear regression. To provide insight into the amount of radical signal detected, within one plot similar scales were chosen. For detailed ESR parameters see Experimental.

TCNQ

As expected from literature, TCNQ shows large radical signals in methanol[26,51] and acetonitrile,[60] but none in chloroform and chlorobenzene (Figure 4.15). The g-values were determined to be 2.0033 $\pm$ 0.0003, which is in the range of the reported literature value.[62] Interestingly, Stößer et al. detected no radical signal while measuring ESR spectra of TCNQ in acetonitrile, which is in direct contrast with the herein presented results.[51] For TCNQ in methanol there is furthermore hyperfine splitting visible, arising from the hyperfine coupling to the four equivalent hydrogen and four equivalent nitrogen atoms. From performing simulations using *EasySpin*, isotropic hyperfine coupling constants of $a_{\mathrm{iso}}(^{14}\mathrm{N})$= 1.31 MHz and $a_{\mathrm{iso}}(^{1}\mathrm{H})$= 0.78 MHz were determined (see Appendix, Figure 8.6 for plots). For TCNQ in acetonitrile, the hyperfine splittingis not resolved, which might be caused by a too high free radical concentration or it is averaged out due to fast molecular tumbling.[30] Another explanation for the missing hyperfine splitting may be the polarizability of the solvent.[51] The percentage of radicals present, determined using the calibration, shows that in general only a small amount of free radicals was present (see Table 4.4). The highest value was determined for acetonitrile, which still is less than 1 %. It should also be noted that the percentage decreased in all cases over the course of nine days. Follow-up reactions may have occurred here. The calculated percentages are in the same range as literature values for other solvents and are very similar for methanol.[51]

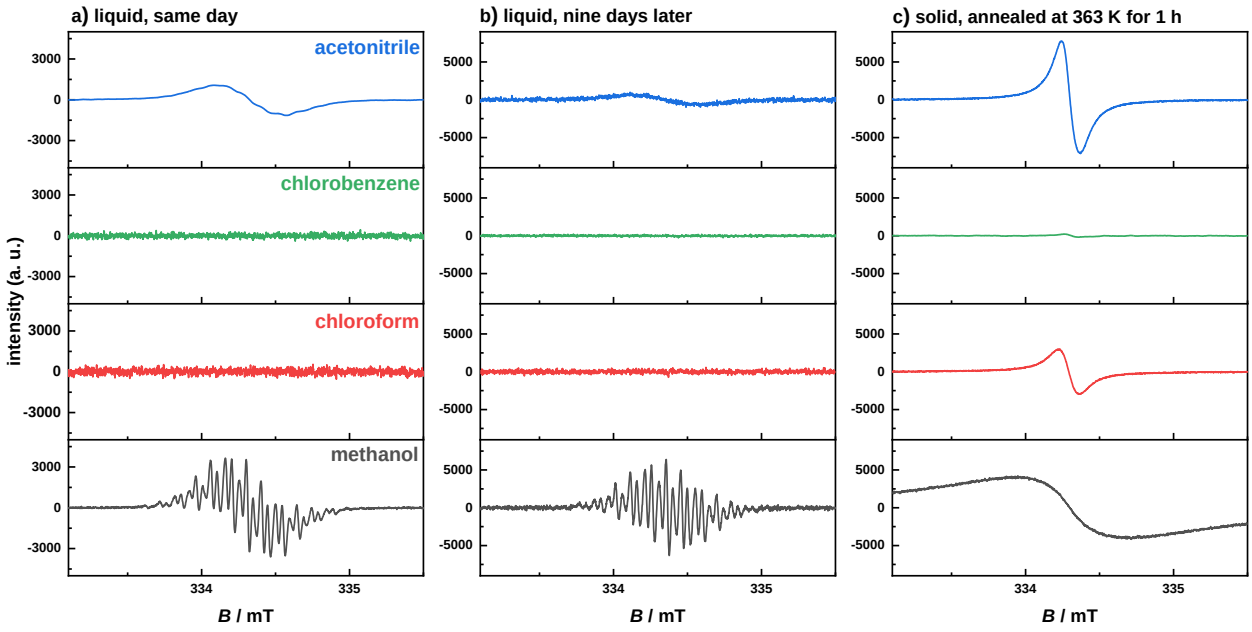

Figure 4.15: For all spectra applies: blue = in MeCN, green = in chlorobenzene, red = in chloroform, black = in MeOH. **a)** liquid state ESR spectra of **TCNQ** in colour-according solvents, **b)** liquid state ESR spectra of TCNQ in colour-according solvents, nine days after setup, **c)** solid-state ESR of TCNQ dried from colour-according solvents at 363 K for 1 h. For all plot applies: g = 2.0033 $\pm$ 0.0003, c = 1 $\frac{\mathrm{mg}}{\mathrm{mL}}$ and measured at rt.

The solid-state ESR spectra of TCNQ annealed from different solvents, displayed in Figure 4.15c, show a similar trend as the liquid state samples: The samples annealed from methanol and acetonitrile show large radical signals, TCNQ dried from chlorobenzene shows a very small signal only, and from chlo-

roform a large signal in comparison to the liquid sample, suggesting there were radicals generated during the heating process. A possible reaction is furthermore supported by the colour change: the previously orange/ pink powder had turned greenish-yellow in cases of acetonitrile, chloroform, and chlorobenzene and dark green in case of methanol. Note, that this colour change could not be observed when studying polymer/additive blends involving IDT-BT, due to the dark colour of the polymer. For films involving F8BT, which itself is orange in solid-state and yellow in solution, green discolorations in some regions of the films were observed. In none of the spectra, hyperfine coupling with the nitrogen and hydrogen atoms could be resolved. Because the electron Zeeman interaction is anisotropic, each molecule orientation contributes to the spectra, making hyperfine splitting unresolvable and leading to line broadening.[33] It is important to mention that in solid-state the number of analyte molecules is larger than in liquid samples. Therefore, in liquid samples, radicals might be present in concentrations too low to detect them. Furthermore, in the sample prepared from methanol the peak-to-peak width ΔH is significantly larger than in all the other samples (see Table 4.3 also). This might be due to unsuitable ESR parameters during the measurement or be related to the different environments of the radicals, which is supported by the colour difference.
These measurements confirm two observations already discussed for polymer/TCNQ blends: First, that TCNQ can form radical anions without an obvious reducing partner, and second, that more radicals are formed when polymer is present and nonpolar solvents such as chlorobenzene are used.

In literature, there are different theories concerning the formation of TCNQ radical anions and the TCNQ solvatchromsim. Tamaya et al.[21] have proposed that the TCNQ solvatochromism is due to the formation of the uncharged benzenoid diradicals, but could not observe them using Raman spectroscopy. It is also discussed that the colour change is due to anion radical forming or the formation of CT-complexes.[60] One proposed mechanism that leads to the formation of radical anions is that the electron is transferred from the solvent to the TCNQ and the solvent subsequently acts as a (positively charged) counterion in the case of ethanol and acetonitrile.[60] For the chemically related TCNE thermal or light-induced formation of radical anions is discussed, also.[51] In a publication from Ma et al.[63] from 2015 the formation of anions and dianions in TCNQ and F_4TCNQ crystals is described. These are expected to form upon charge transfer between excited donor and neutral acceptor molecules after absorbing one photon. The excitation wavelength in this study was $\lambda_{exc} = 475$ nm.[63] If this kind of reaction takes place in solution as well, it would leave positively charged ions. These ions in the transistor film could then take up an electron from the polymer, as the energy levels now would match and this way lead to doping. In general, positively charged TCNQ ions should be highly reactive and could potentially engage in all kinds of reactions. It furthermore appears that a high solvent pK_a is beneficial for the radical formation, as methanol has a pK_a of 16 and acetonitrile and chloroform of 25. Stößer et al. also discuss the radical anion stabilization by the solvent as well as the formation of a solvent cage.[51]

Table 4.3: Peak-to-peak width ΔH for TCNQ and F_4TCNQ annealed from in methanol, chloroform, chlorobenzene and acetonitrile at 363 K for 1 h (see Figure 4.16c and Figure 4.15c).

solvent	TCNQ	F_4TCNQ
methanol	0.63 mT	0.16 mT
chloroform	0.14 mT	0.09 mT
chlorobenzene	0.14 mT	0.10 mT
acetonitrile	0.31 mT	0.12 mT

F_4TCNQ

The solvent dependence of F_4TCNQ appears to be similar to TCNQ: Large amounts of radicals are detected in methanol and acetonitrile and very small amounts in chloroform and chlorobenzene (see Figure 4.16a). All g-values were determined to be 2.0032 $\pm$ 0.0003, which is in the range of the literature value.[62] For the same reasons discussed above, only one g-value is observed. Again, hyperfine coupling with four equivalent fluorine atoms and four equivalent nitrogen atoms could be resolved for F_4TCNQ in methanol and only partially for F_4TCNQ in acetonitrile. The isotropic hyperfine coupling constants in both, methanol and acetonitrile, were determined to be $a_{iso}(^{14}N) = 1.19$ G and $a_{iso}(^{19}F) = 1.67$ G using *EasySpin* (see Appendix, Figure 8.6 for plots). Note, that in acetonitrile there is Lorentzian and Gaussian line broadening. Interestingly, after letting the solutions sit for nine days in nitrogen atmosphere, the radical signal in methanol is almost vanished (see Figure 4.16b). This is accompanied by a colour change: The previously greenish solution had turned colourless. The colour change could indicate that a chemical reaction took place, potentially acid-base-chemistry or disproportion reactions.[19] The percentages of radicals present calculated using the calibration, show that the highest amount of radical is present in acetonitrile with 7.2 %. In general, the percentages for F_4TCNQ are higher than for TCNQ in all cases, which may be attributed to the higher electron affinity of F_4TCNQ.[1,17] Furthermore, the percentages increased over the course of nine days, except for methanol.

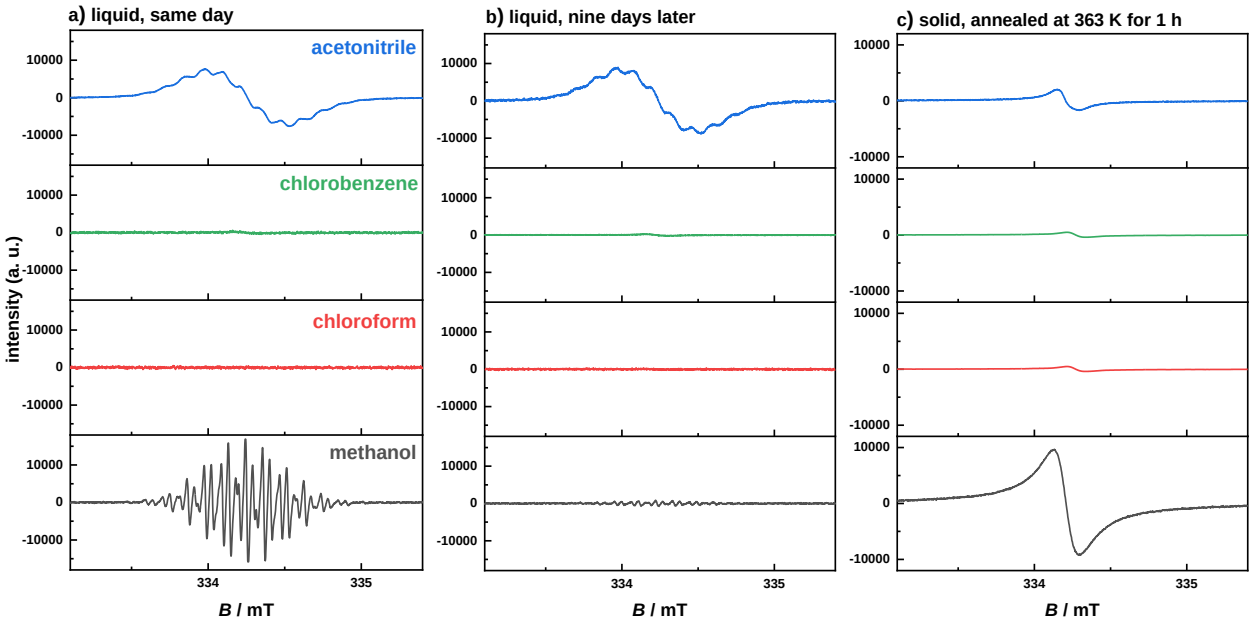

Figure 4.16: For all spectra applies: blue = in MeCN, green = in chlorobenzene, red = in chloroform, black = in MeOH. **a)** liquid state ESR spectra of **F_4TCNQ** in colour-according solvents, **b)** liquid state ESR spectra of F_4TCNQ in colour-according solvents, nine days after setup, **c)** solid-state ESR of F_4TCNQ dried from colour-according solvents at 363 K for 1 h. For all plot applies: $g = 2.0032 \pm 0.0003$, $c = 1 \frac{mg}{mL}$ and measured at rt.

In the solid-state spectra (Figure 4.16c) there is radical signal detected for every sample: The largest amount of radicals is detected when F_4TCNQ in annealed from methanol and acetonitrile and only

small signals when F_4TCNQ is annealed from chloroform and chlorobenzene. Note, that the solids of F_4TCNQ annealed from acetonitrile, chloroform and chlorobenzene appeared greenish-yellow and from methanol dark green to dark blue. The powder received from the supplier had an orange/ pink colour. These results indicate that regardless of whether doping is expected or not when using F_4TCNQ as an additive in OSCs there probably is some amount of F_4TCNQ that is present as a radical anion and thus supporting the hypothesis stated earlier.

To my knowledge, only little research on the solvent dependence of F_4TCNQ is available. Arvind et al.[38] showed that radical anions form by dissolving F_4TCNQ in THF. They attribute this effect to adventitious H_2O or OH^-. For the experiments conducted in this project these reactions are expected to be ruled out as they were conducted under nitrogen atmosphere and in anhydrous solvents. Since all samples were prepared at the same time, the glovebox conditions were identical and should have resulted in an identical amount of radical anion, which was not the case. Furthermore, the underlying mechanism of an electron transfer, which is necessary for the formation of radical anions, including water or hydroxide anions remains unclear. It has also been shown that under light illumination of 405 nm F_4TCNQ in acetonitrile can react with THF.[22] Misseeuw et al.[61] studied the solvent-dependence of F_4TCNQ in methyl ethyl ketone (MEK) via UV/vis spectroscopy and report the instant formation of radical anions, which is attributed to an electron transfer from MEK to F_4TCNQ. The authors also report the formation of radical anions in acetonitrile.[61]
Polarization of F_4TCNQ (and TCNQ) may be supported in polar solvents (analogous to ionic structure in Figure 3.4), allowing for reactions with the solvent. Alternatively, optical or thermal excitation could be the starting point for further reactions.

Table 4.4: Double integral, corresponding radical concentration and radical percentage of TCNQ, F_4TCNQ and DDQ in methanol (black plots), chloroform (red plots), chlorobenzene (green plots) and MeCN (blue plots, see Figure 4.15, Figure 4.16, Figure 4.17, and Figure 6.3 for calibration). The errors were determined using the Gaussian error propagation.

sample	double intergral [a.u.]		radical conc. [µM]		radical percentage [%]	
	same day	9 days later	same day	9 days later	same day	9 days later
TCNQ in MeOH	338.9	292.3	43 ± 2	37 ± 1	0.89 ± 0.04	0.77 ± 0.02
TCNQ in $CHCl_3$	0	55.3	0	7.2 ± 0.4	0	0.15 ± 0.01
TCNQ in CB	0	0	0	0	0	0
TCNQ in MeCN	280.0	143.0	35 ± 9	18.6 ± 0.4	0.73 ± 0.02	0.38 ± 0.01
F_4TCNQ in MeOH	196.5	9.4	24.9 ± 0.9	1.2 ± 0.5	0.69 ± 0.03	0.033 ± 0.001
F_4TCNQ in $CHCl_3$	21.5	99.1	2.7 ± 0.1	12.9 ± 0.7	0.076 ± 0.003	0.36 ± 0.02
F_4TCNQ in CB	0	38.2	0	6.9 ± 0.4	0	0.19 ± 0.01
F_4TCNQin MeCN	2070.1	2354.3	259 ± 6	294 ± 7	7.2 ± 0.2	8.1 ± 0.2
DDQ in MeOH	14.4	-	1.8 ± 0.1	-	0.041 ± 0.002	-
DDQ in $CHCl_3$	23.4	-	3.2 ± 0.2	-	0.072 ± 0.005	-
DDQ in CB	28.5	-	5 ± 2	-	0.118 ± 0.005	-
DDQ in MeCN	139.0	-	17.4 ± 0.4	-	0.395 ± 0.009	-

DDQ

Additionally to TCNQ and F_4TCNQ, the molecular additive DDQ was investigated. The liquid state ESR spectra of DDQ in acetonitrile, chloroform, chlorobenzene, and methanol are displayed in Figure 4.17. Similar to the other additives, there are radicals present in methanol and acetonitrile. Again, the hyperfine splitting arising from the coupling to the two equivalent nitrogen atoms is fully resolved in methanol and only partially in acetonitrile. The g-values were determined to be 2.0056 $\pm$ 0.0003 and the hyperfine coupling constant $a_{\mathrm{iso}}(^{14}\mathrm{N})$= 0.8 G (see Figure 8.7 for plots). The g- values are in agreement with the literature (2.0052)[55] and notably larger than the ones of TCNQ and F_4TCNQ. It is noteworthy, that to detect a spectrum at concentrations of 1 $\frac{\mathrm{mg}}{\mathrm{mL}}$ in methanol the Gain had to be adjusted drastically and therefore leading to manipulation of the area under the curve and also in the determined concentration. Interestingly, all these additives appear to form radical anions under the appropriate conditions, although radical anions are not necessarily expected to form.

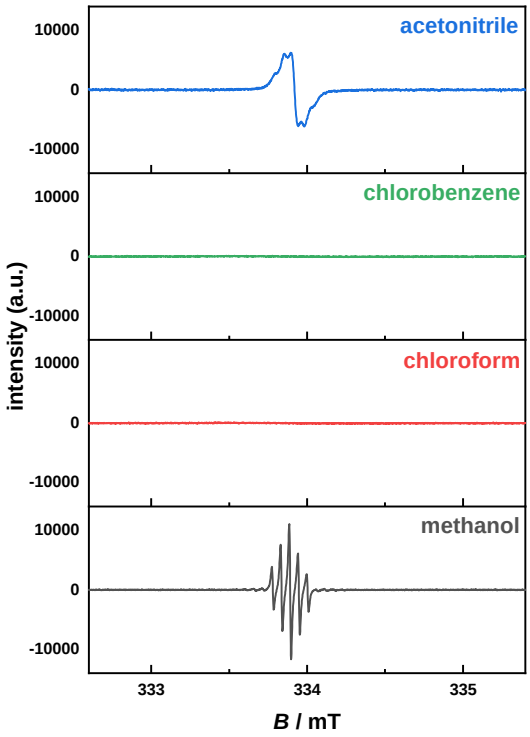

Figure 4.17: Liquid state ESR of **DDQ** in blue = MeCN, green = chlorobenzene, red = chloroform, black = MeOH. For DDQ in MeCN (blue) and MeOH (black) g = 2.005 6 $\pm$ 0.0003 applies. The concentrations of the liquid samples were 1 $\frac{\mathrm{mg}}{\mathrm{mL}}$, measured at rt.

4.3 Nuclear magnetic resonance

As already discussed, NMR spectroscopy is one of the most important analytical methods in both, nuclear and solid-state samples. In this chapter pristine IDT-BT and F_4TCNQ as well as blends of both of them will be examined using solid-state NMR spectroscopy. Furthermore, potential reactions between the molecular additive TCNQ and water will be investigated.

4.3.1 Structure determination of IDT-BT

To the best of my knowledge, no solid-state NMR spectra of IDT-BT have been reported yet. ^{1}H MAS, $\{^1H\}$-^{13}C CP MAS at 0.3, 1 and 3 ms CP contact time and ^{1}H-^{13}C-HETCOR spectra were recorded (see Appendix, Figure 8.9 and Figure 8.10 for latter spectra). In the ^{1}H MAS spectrum, Figure 4.18a, there are two regions: An aliphatic peak with a chemical shift of 0.9 ppm and an aromatic peak with a chemical shift of 7.5 ppm. The aliphatic peak originates from the protons of the side chains and the aromatic region from protons of the polymer backbone. The $\{^1H\}$-^{13}C CP MAS spectrum, Figure 4.18b at 1 ms CP contact time, shows peaks in the aromatic and aliphatic region as well. In the aromatic region they have been assigned the following way: 157.4 ppm (C^e), 154.3 ppm (C^c), 142.3 ppm ($C^{f,k}$), 137.2 ppm (C^g), 125.7 ppm (C^b) and 113.8 ppm ($C^{a,h,i,j}$). The assignment follows the fact that multiple overlaps are present and the respective peaks can not be assigned with their exact values. These overlaps may furthermore be due to amorphous regions in the polymer. For the aliphatic signals the assignment is as follows: 54.9 ppm (C^d) and the side chain signals from 40.7 - 14.6 ppm. As there are in total sixteen carbon atoms in each of the side chains and the peaks overlap, distinct assignment is difficult. It is however concluded, that the signal with the lowest chemical shift of 14.6 ppm can be assigned to the $-CH_3$ groups. The signal at 23.3 ppm is assigned to the $-CH_2-$ groups right next to the $-CH_3$ groups. Since this chain end can move more isotropically than on the other side, the signal is weaker. Following the same argument, the signal at 24.7 ppm is assigned second $-CH_2-$ groups. The other, overlapping signals at 32.4 ppm and 30.2 ppm are assigned to $-CH_2-$ groups that lie in between the to side-chain ends. Lastly, the signal at 40.7 ppm is assigned to the $-CH_2-$ groups located right next to the polymer backbone. These assignments are furthermore supported by DFT calculations (functional B3LYP, 6-31+ (d,p)).
Structure determination of F8BT by solid-state NMR has been presented elsewhere.[64]

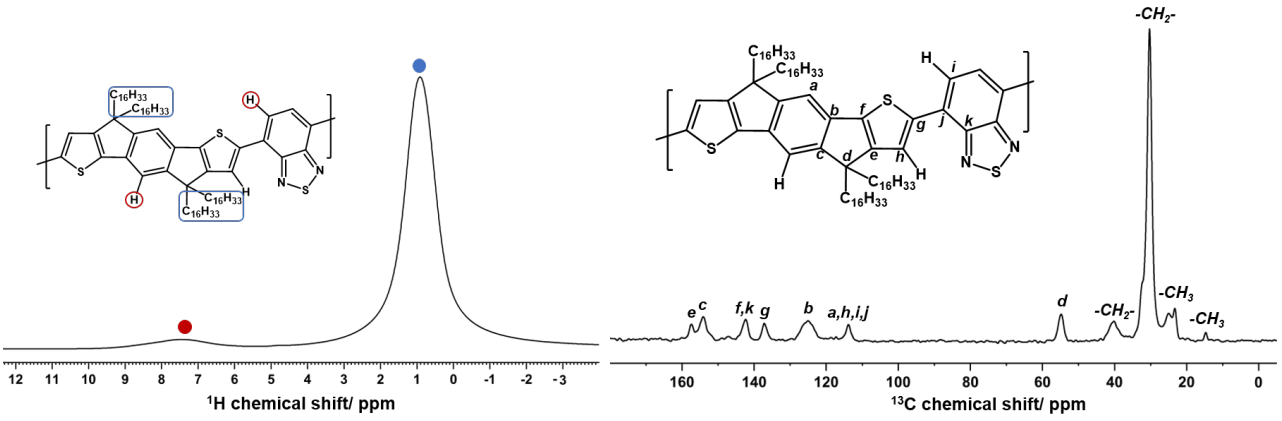

Figure 4.18: **a)** ^{1}H MAS and **b)**$\{^1H\}$-^{13}C CP MAS spectra of pristine IDT-BT.

4.3.2 Solid-state NMR of pristine F_4TCNQ, annealed from different solvents

ESR measurements showed that F_4TCNQ can form radicals when being annealed from different solvents (Figure 4.16). Therefore, F_4TCNQ annealed from chlorobenzene and acetonitrile were further analyzed using solid-state NMR spectroscopy. To probe electron transfer reactions, ^{19} F-based NMR experiments can lead to a detailed insight into the molecular transformations. Both, ^{1}H MAS and ^{19}F MAS spectra are presented in Figure 4.19, ^{19}F-^{19}F DQ-SQ correlation spectra in Figure 4.20, ^{1}H-^{19}F HETCOR MAS spectra with 1 ms contact time in Figure 4.21 and $\{^{19}F\}$-^{13}C CP MAS spectra in Figure 8.11, Appendix.
Figure 4.19a shows the pristine F_4TCNQ. It is directly noticeable, that for the pristine F_4TCNQ, as received from the supplier, there are signals in the ^{1}H MAS spectra where there should be none. There is a broad peak in the aromatic region at 6.9 pm and a small one in the aliphatic region at 1.0 ppm. The latter peak may be assigned to leftover grease. It is unclear where the other signal arises from. Potentially, there are impurities left from the chemical synthesis or sample preparation or the signal is related to the rotor cap. The ^{19}F MAS spectra however shows the expected signals at -129.0 ppm and -132.2 ppm (marked by the blue lines throughout a) - d)). Although the fluorine atoms are chemically equivalent, they experience different environments in the crystal lattice due to the herringbone structure. Literature shows that one fluorine atom coordinates to the nitrogen of a cyano group and the other to the π-system of the neighboring molecule.[65]

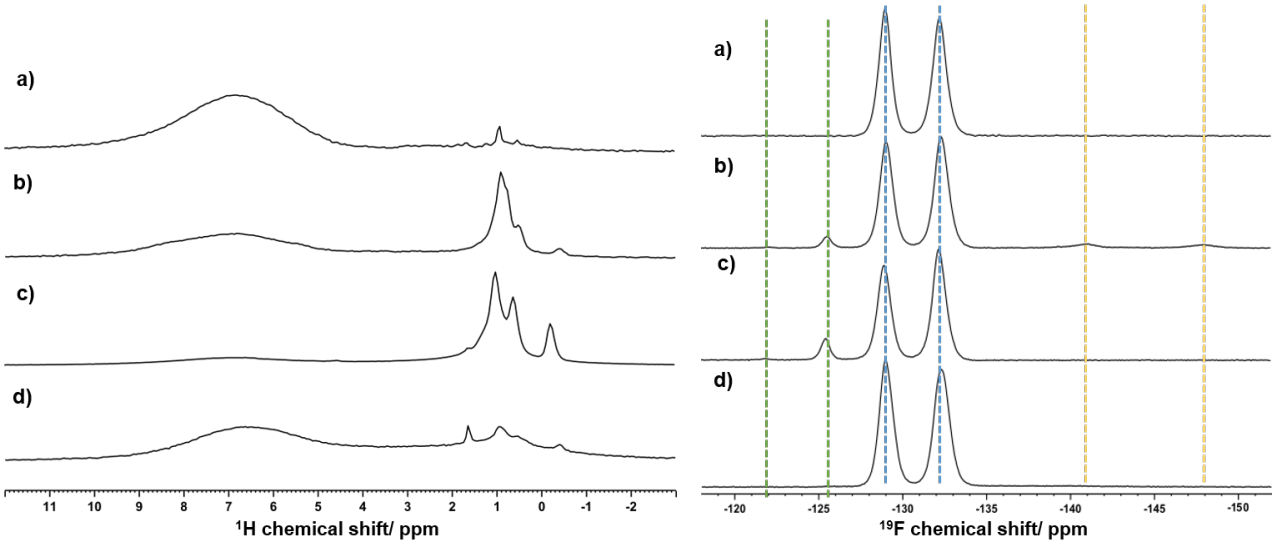

Figure 4.19: Left: ^{1}H MAS and right: ^{19}F MAS spectrum of F_4TCNQ: **a)** pristine, **b)** annealed from chlorobenzene using a glass syringe, **c)** annealed from chlorobenzene using a plastic syringe and **d)** annealed from acetonitrile (annealed at 363 K for one hour, applies for **b)-d)**).

In Figure 4.19b and Figure 4.19c both, ^{1}H and ^{19}F MAS, show the respective resonances for F_4TCNQ annealed from chlorobenzene. To test impurities that may be introduced by the syringes, in Figure 4.19b a glass syringe and in Figure 4.19c a plastic syringe was used. The chemical shifts of the peaks in the ^{1}H MAS spectra are for Figure 4.19b 6.8 ppm, 0.9 ppm and 0.4 ppm and for Figure 4.19c 7.0 ppm, 4.6 ppm, 1.6 ppm (shoulder), 1.0 ppm, 0.6 ppm and 0.2 ppm. As none of these peaks were expected and they furthermore differ from one another, it is unclear where they originate from. One possible origin of the aromatic signals might be leftover chlorobenzene. However, due to the annealing time of one hour at 363 K, chlorobenzene was expected to be evaporated. Because the $\{^{19}F\}$-^{13}C CP

MAS spectrum shows F_4TCNQ-related signals only (see Appendix, Figure 8.11), it is concluded that the signals in the ^1H MAS spectra are related to some F_4TCNQ species. The ^{13}C chemical shifts and assignments are: 143.2 ppm (C^a), 142.4 ppm ($C^{a'}$), 137.3 ppm (C^b), 113.5 ppm (C^d), 112.1 ppm ($C^{d'}$) and 85.9 ppm (C^c). The values are in good agreement with the calculated chemical shifts, see Table 4.5, first column. The ^{13}C chemical shifts for the radical anion and dianion have been calculated as well, however, neither of them was observed in carbon NMR spectra. Unfortunately, the recording of ^1H-^{13}C HETCOR spectra was not possible for either of the samples.

Table 4.5: ^{13}C chemical shifts for F_4TCNQ, $F_4TCNQ^{\cdot -}$, F_4TCNQ^{2-} using th DFT functional B3LYP, 6-31G+ (d,p).

carbon atom	F_4TCNQ	$F_4TCNQ^{\cdot -}$	F_4TCNQ^{2-}
a / a'	132.2 ppm	131.0 ppm	132.2 ppm
b	125.0 ppm	110.0 ppm	114.0 ppm
d / d'	96.6 ppm	103.8 ppm	102.5 ppm
c	77.0 ppm	45.0 ppm	10.1 ppm

The recorded ^{19}F MAS spectra displayed in Figure 4.19b and Figure 4.19c show unexpected results: Not only the expected two F_4TCNQ signals appear (blue lines), but also two more at – 122.1 ppm and – 125.6 ppm (green lines) and in Figure 4.19c there are two additional peaks at –141.1 ppm and – 148.0 ppm (yellow lines). As these chemical shifts in Figure 4.19c (–141.1 ppm and – 148.0 ppm) vary significantly from the pristine F_4TCNQ, this suggests a redistribution of electron density, and the latter peaks might potentially be assigned to the crystallized dianion F_4TCNQ^{2-}. This is supported by the fact that the peaks are narrow and not broad, as would be expected for either radicals or amorphous regions. Furthermore, the adding of electrons leads to increased electronic shielding of the fluorine atoms and therefore a shift to higher fields. The obtained chemical shifts are in agreement with the ones previously observed for the dianion (–144 ppm and –149 ppm), which was concluded from a personal conversation with C. Haese.

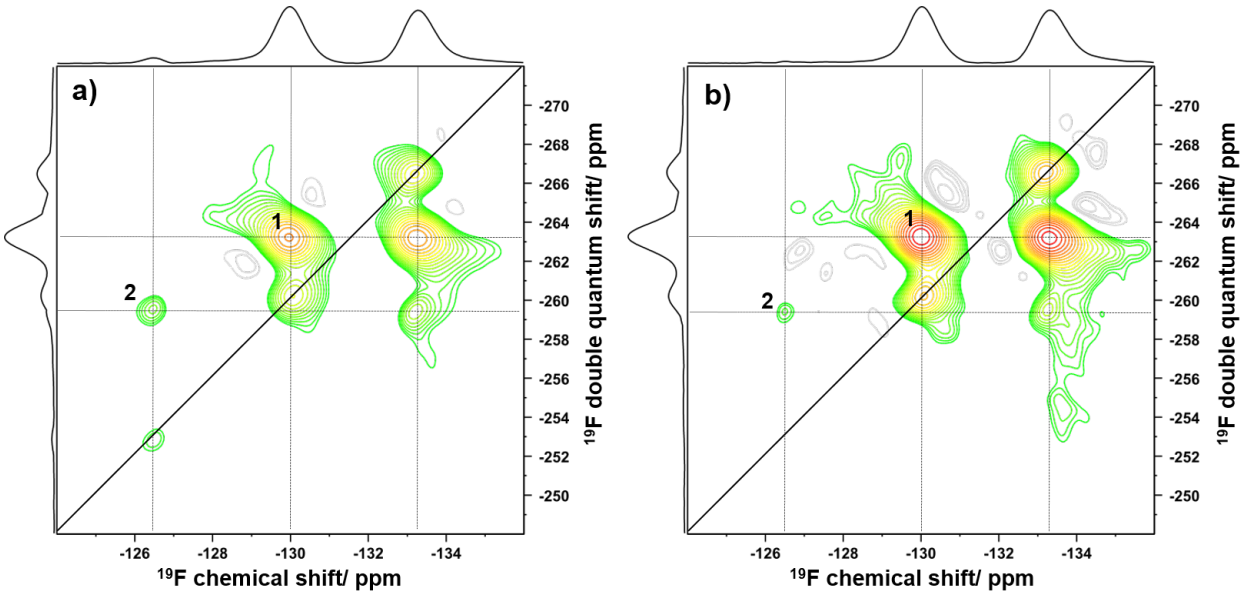

Figure 4.20: ^{19}F-^{19}F DQ-SQ correlation spectra with a recoupling time of 4τ of F_4TCNQ annealed from chlorobenzene using **a)** a plastic syringe and **b)** a glass syringe.

For F_4TCNQ annealed from chlorobenzene using a plastic or glass syringe, ^{19}F-^{19}F DQ-SQ correlation spectra were recorded to gain further insight into the newly formed signals. They are displayed in Figure 4.20. Along the straight black line are correlations between nuclear spins of the same chemical shifts. Correlations between different spins are observed as cross-peaks with equal patterns on both sides. As described earlier, F_4TCNQ shows two signals due to its crystal structure.[65] Therefore, in the ^{19}F-^{19}F DQ-SQ correlation spectra there is an additional signal for pristine F_4TCNQ, labeled **1** in both spectra. In the spectrum shown in Figure 4.20a (plastic syringe used), there is an additional coherence between the newly appeared peak at –125.6 ppm and the peak of pristine F_4TCNQ at –132.2 ppm, which is labeled **2**. This correlation can be observed in Figure 4.20b as well (glass syringe used). It is therefore concluded, that by annealing F_4TCNQ from chlorobenzene, a new F_4TCNQ-related species forms. There are no correlations found for the new signals marked by the yellow lines in Figure 4.19b nor the self-correlation of the newly occurred peak at –125.6 ppm. This may be due to their low intensity or that crystals of the dianion have a very long relaxation time (> 1000 s), as has been told in a personal conversation with R. Graf and thus they have not been detected.

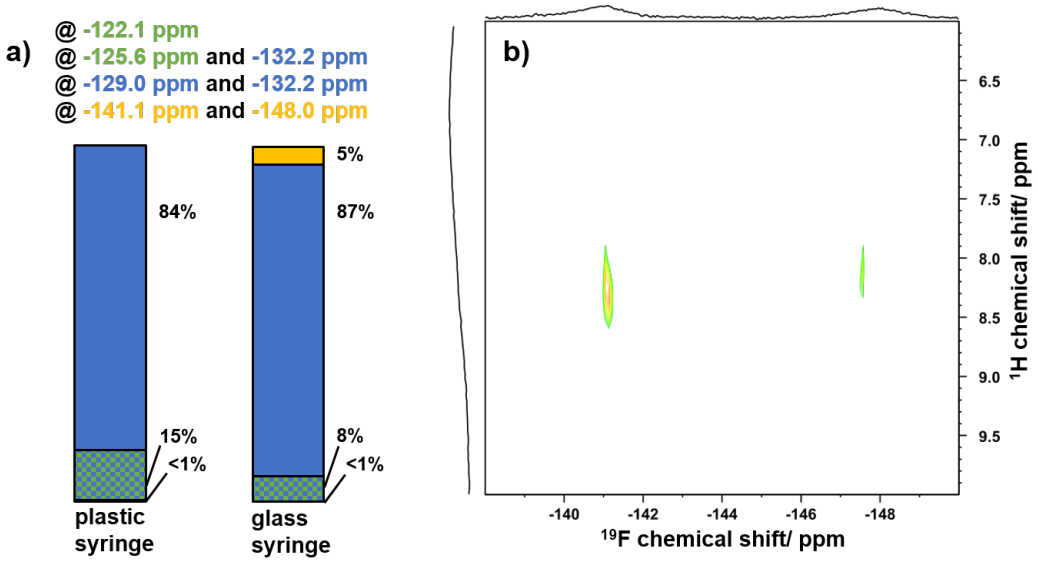

Figure 4.21: **a)** Graphical illustration of the different species present when annealing F_4TCNQ from CB using either a plastic or glass syringe and **b)** ^{1}H-^{19}F HETCOR spectrum of F_4TCNQ annealed from chlorobenzene using a glass syringe.

Since it could be concluded from the ^{19}F-^{19}F DQ-SQ correlation spectra that there the signals at –125.6 ppm and –132.2 ppm are correlated (see Figure 4.19b and Figure 4.19c, correlation labeled **2**), the signals were integrated using this background knowledge to determine the proportions of the different signals. For F_4TCNQ annealed from chlorobenzene using a glass syringe (Figure 4.19b and Figure 4.20b), the following amounts were determined: <1% for green line at –122.1 ppm, 8% for the correlation between the green and blue line at –125.6 ppm and –132.2 ppm, 87% for the pristine F_4TCNQ (–129.0 ppm and –132.2 ppm) and 5 % for the signals at –141.1 ppm and –148.0 ppm (yellow lines). For F_4TCNQ annealed from chlorobenzene using a plastic syringe (Figure 4.19c and Figure 4.20a), the amounts are as follows: <1% for green line at –122.1 ppm, 15% for the correlation between the green and blue line at –125.6 ppm and –132.2 ppm and 84% for the pristine F_4TCNQ (–129.0 ppm and –132.2 ppm). See Figure 4.21a for graphical illustration.
The ^{1}H-^{19}F HETCOR spectrum of F_4TCNQ annealed from chlorobenzene using a glass syringe with a contact time of 1 ms (Figure 4.21b) shows that there is a correlation between an aromatic signal

at 8.28 ppm and the newly formed species with ^{19}F chemical shifts of –141.1 ppm and –148.0 ppm (yellow lines in Figure 4.19b). Since the chemical shift of the proton signal does not exactly match the aromatic signal at 6.81 ppm obtained in the ^{1}H MAS spectra, it is assumed that there is an underlying signal that could not be distinguished. One explanation is chlorobenzene being incorporated into the crystal structure since there is no other known source of aromatic protons. Chlorobenzene and F_4TCNQ (or its respective salts) could form charge-transfer complexes. If these were present in the transistor film, they could potentially affect the charge transport and molecular ordering. The overall low intensity in Figure 4.21b indicates a low concentration of this new species inside the sample.

Overall, the results, are unexpected. It is unclear, why there seem to be different results when using either a glass or a plastic syringe. Potentially, this difference is due to uncontrolled and therefore non-uniform reactions taking place. Of course, this effect may also be related to the proton signals obtained for the samples and the impurities potentially present in the chemical received from the supplier. Because the samples were prepared and handled under nitrogen atmosphere, the proton signals should most likely be related to F_4TCNQ reacting with the solvent. Reactions with remaining water, as some amount of it is always present, are considered as well. However, the obtained signals show an intensity too high for the amount of water expected to be present under these conditions. If the radical anion formation is accompanied by the formation of a radical cation, it is conceivable that this could be related to unexpected signals. A positively charged F_4TCNQ ion should be very reactive due to very high electron affinity.

Lastly, F_4TCNQ was annealed from acetonitrile. As it was known that F_4TCNQ forms radicals in acetonitrile and when being annealed from it, it should be checked whether there are additional forms of F_4TCNQ present or not (see Figure 4.16 for ESR spectra). The spectra are presented in Figure 4.19d. Again, proton signals are obtained, their chemical shifts are 6.8 ppm, 0.9 ppm, 0.5 ppm, and 0.4 ppm. Surprisingly, these are the same chemical shifts as obtained in Figure 4.19b. Therefore, the allocation to solvent-related signals seems to be unlikely. The peak at 6.8 ppm might be rotor cap-related. In the ^{19}F MAS there are mainly the two signals arising from pristine F_4TCNQ. Additionally, when increasing the signal intensity, the radical anion can be obtained in very small quantities at approx. –140 ppm. As radicals do not result in distinct peaks, this value can not be given in higher accuracy. This result is in agreement with the results from solid-state ESR measurements (Figure 4.16). It is not surprising that the amount $F_4TCNQ^{\bullet -}$ is so low as ESR spectroscopy is more sensitive than NMR spectroscopy and is, therefore, able to record even such small amounts.[32]

Because it was not clear, whether this formation of new F_4TCNQ species is heat or solvent related, pristine F_4TCNQ was successively heated inside the NMR spectrometer to 313 K, 333 K and 353 K. Each of these temperatures were held for 30 min. before recording ^{1}H and ^{19}F MAS spectra. However, in none the spectra a change compared to the unheated F_4TCNQ was observed. It is therefore concluded, that the solvent and following annealing are essential for the formation of these new species and not just the heating itself.

4.3.3 Solid-state NMR studies of IDT-BT/F_4TCNQ blends

For this study, an IDT-BT/F_4TCNQ-film was prepared as described in the Experimental section. The ratio of polymer:dopant was 2:1. Note, that for this combination of polymer and additive the transfer of one electron is expected, leading to the radical anion $F_4TCNQ^{\cdot -}$ and radical cation $IDT{-}BT^{\cdot +}$ (see Figure 3.3 for HOMO and LUMO energies). This combination is convenient due to the reaction being traceable by measuring ^{19}F NMR. The studied film was prepared at rt under nitrogen atmosphere and measured for the first time in this state. Next, the rotor containing the sample was heated at 373 K for one hour and then re-measured at rt. This procedure was repeated at 383 K, 393 K, and 403 K. Because in ESR studies the films were annealed before the measurements, the measurements are not fully comparable. Also the chosen polymer:dopant-ratios were different. Before the first heating and after the last ^{1}H, ^{19}F and $\{^1H\}$-^{13}C CP MAS spectra were recorded. For the other heat treatments only ^{19}F MAS spectra were recorded. All recorded ^{19}F MAS spectra are summarized in Figure 4.22. The blue lines indicate the pristine, crystalized F_4TCNQ with chemical shifts of –129.0 ppm and –132.2 ppm, the red line indicates the radical anion $F_4TCNQ^{\cdot -}$ with a chemical shift of approx. –139 ppm and the grey lines the (not present) dianion F_4TCNQ^{2-} with expected chemical shifts of –144 ppm and –149 ppm. From a personal conversation with C. Haese the chemical shifts of F_4TCNQ^{2-} are known. The green line indicates a with annealing temperature increasing signal at approx. –125 ppm. Note, that the glass transition temperature T_g of IDT-BT using dynamic mechanical analysis performed on IDT-BT drop-casted onto a polyimide substrate, was determined to be 185.15 K for the alkyl side chains and 343.55 K for the backbone.[66]

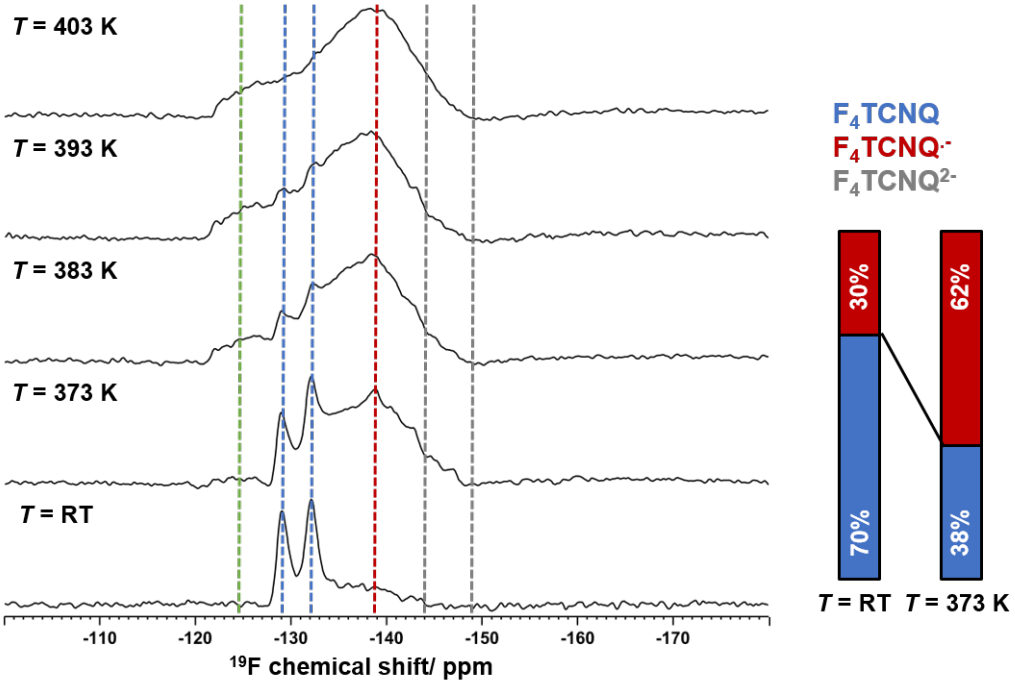

Figure 4.22: ^{19}F MAS spectra of IDT-BT/ F_4TCNQ blends (molar ratio = 2:1) prepared at rt and then heated at 373 K, 383 K, 393 K and 403 K for one hour each and distribution of F_4TCNQ redox states at rt and after annealing at 373 K for 1 h.

From the two ^{19}F signals of crystalline F_4TCNQ it can be concluded that after the film was prepared at rt, the majority of the F_4TCNQ molecules were unreacted and crystalized phase-separated (spectrum at the bottom in Figure 4.22). Either only small amounts of radical anion were present, as indicated

by the emerging broad signal, marked by the red line, or some part of the F_4TCNQ is present in amorphous IDT-BT domains. As doping is expected and IDT-BT is known to be a near amorphous polymer,[67,68] it might also be a combination of both. However, mainly crystalline F_4TCNQ was present. Potentially a high temperature is needed for the redox reaction to take place, or the degree of doping is inefficient and low in general. The amount of unreacted F_4TCNQ was determined to be 70% and either radical anion $F_4TCNQ^{\cdot -}$ or F_4TCNQ in the amorphous phase to be 30% by integrating the signals using *DM fit*. Because the mixture was stirred at 333 K for 60 min. and the energy levels match, the redox reaction was expected to take place. After heating at 373 K for one hour, either the amorphous or radical anion-containing domain grew. There still was crystalline F_4TCNQ present in the film. Fitting the signals revealed that approx. 38% were present as crystalline, unreacted F_4TCNQ and 62 % as either the radical anion or F_4TCNQ in the amorphous phase. Since the $T_g(\mathrm{IDT-BT})$ was exceeded upon the first heating cycle, a rearrangement of the polymer chains might have occurred, leading to the F_4TCNQ being placed within the side chains. From comparing the spectra before and after the first heating cycle it might be concluded that in an analogous transistor fabrication process a relatively high amount of F_4TCNQ does not take part in the doping process. However, the crystalline F_4TCNQ does not seem to negatively influence the transistor performance. With increasing annealing temperature, the crystalline domaine decreased and disappeared after annealing at 403 K. Interestingly, the signal at –125 ppm grew with increasing annealing temperature. Maybe this signal represents the same F_4TCNQ species present in Figure 4.19b (green line). The signal shape may again be attributed to the incorporation into amorphous regions. It is unclear what structure stands behind this signal. For 383 K, 393 K, and 403 K no integrations were performed due to the undefined signal structure, leading to unreliable results.
From these measurements, it cannot be concluded whether all the F_4TCNQ molecules took up an electron or the molecular ordering was changed. A combination of both is suspected. In none of the spectra, the dianion F_4TCNQ^{2-} was obtained. This is in agreement with the second ionization energy (–4.7 eV[17]).

From the ^{1}H MAS and {^{1}H}-^{13}C CP MAS spectra (Figure 8.12 and Figure 8.13) no difference can be seen between the pristine polymer, the blend prior to heating and the blend after heating. When comparing the ^{1}H MAS of the blend with the one recorded of F_4TCNQ annealed from chlorobenzene, it is obvious that the unexplained signals for drop cast and annealed F_4TCNQ are not obtained in the blend. Two explanations are thought of: Either the signals overlap and therefore are not resolved or the signals in the drop cast and annealed F_4TCNQ are due to reactions with the solvent. Because the blend is dried at rt and then measured for the first time, the potential reaction with the solvent may be caused by the annealing at 363 K. As there are no additional signals observed after heating the blend, it is concluded that no protonation of the F_4TCNQ takes place. This is in agreement with the literature: By performing detailed electrochemical analysis of F_4TCNQ in acetonitrile, Le et al.[23] found the equilibrium constant K_{eq} for the protonation of the radical anion $F_4TCNQ^{\cdot -}$ to be $3.9 \cdot 10^{-6}$. Obviously, the conditions for the experiment presented here are different, however, the general trend of a reaction being likely or unlikely to occur should be similar. Another publication from Watts et al.[69] from 2020 showed that for the F_4TCNQ/P3HT system protonation of the additive takes place. Without going into further detail, it can be stated that the proton is thought to be transferred from the α-carbon of the hexylic side-chains of the P3HT to the F_4TCNQ. These side-chains are located in 3-position on the thiophene unit. The polymer structure of IDT-BT is fundamentally different (see Figure 3.3 for chemical structure) and no side-chain is located in 3-position on the thiophene unit. It, therefore, seems plausible that no additional signal is observed in the ^{1}H MAS spectra.

4.3.4 ^{2}H NMR studies to investigate reactions between TCNQ and water

Solid-state NMR studies

In literature, it is discussed that TCNQ is removing traps like water inside the transistor films by either replacing it or passivating it through chemical reactions[3–5] As mentioned earlier, these reactions are difficult to show inside the films as the total concentration of additives is low and signal detection is furthermore complicated by signals arising from the polymer. Because of these reasons, it was decided to investigate possible reactions by using D_2O instead of H_2O and thereby be able to detect newly formed species by recording ^{2}H NMR spectra. Using IR spectroscopy, the amount of H_2O in D_2O was determined to be <1%. As a first step solid-state ^{2}H MAS spectra were recorded, because in previous experiments solvent dependence was observed and if reactions take place inside the transistor film those products ought to be in solid state. Potential reaction products are shown in Figure 3.4. Note, that any protonated (deuterated) species as well as potentially forming carboxylic acids[28] (if protonated/ deuterated) should be detectable. Species like $DCTC^-$, as not containing protons, would not be observed. The presented experiments were conducted at air and rt. Three different solvents were chosen: chlorobenzene, acetonitrile, and dichloromethane. TCNQ was dissolved in those with a concentration of 1 $\frac{mg}{mL}$ and an excess of D_2O was added. The solutions then were allowed to stir for 48 h. Afterwards, the entire solvent was removed in vacuum, the remaining solid dried in vacuum as well, and then transferred into a zirconium rotor. D_2O does not dissolve in chlorobenzene and dichloromethane. Due to this fact, the complete mixture was dried, to also obtain any molecules that may have dissolved in the water phase (possibly ions). These very simple reaction conditions were chosen because no precautions are taken during transistor preparation to favor possible reactions between TCNQ and water.[3]

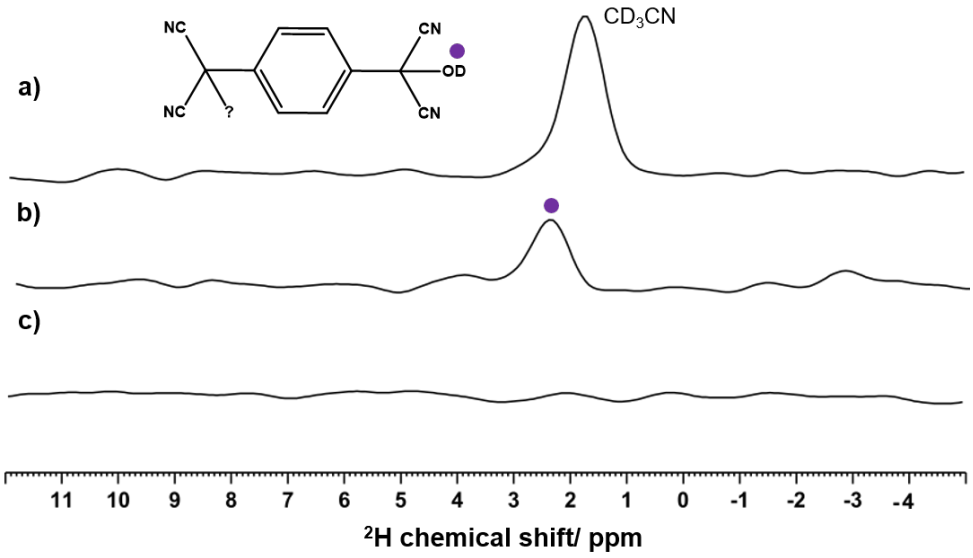

Figure 4.23: ^{2}H MAS spectra of solids obtained from stirring TCNQ in **a)** MeCN, **b)** DCM and **c)** CB with an excess of D_2O for 48 h in air.

The recorded ^{2}H MAS spectra are displayed in Figure 4.23. The signal detected in Figure 4.23a is attributed to residual acetonitrile with a chemical shift of 2.09 ppm. It was not expected to find deuterated solvent in the spectra, because the solid was dried properly and the probability of finding not the protonated, but deuterated solvent is thought to be rather low. Because there are no other signals detected, no reaction products including deuterons appear to have formed. This is surprising as

literature suggests the formation of different products in acetonitrile. The authors did not isolate the product, so potentially it forms in solution only.[28] As already mentioned in a previous chapter, the hydrolysis of the nitrile groups is theoretically conceivable (see Figure 4.5). The conditions given in this study, however, should not allow such a reaction, which is why it is excluded as a reaction product. Another point to consider is the formation of radicals anions in acetonitrile. These can then dimerize to neutral TCNQ and the dianion $TCNQ^{2-}$,[26,27] which in the next step could be either protonated or react to $DCTC^{-}$.[19,29] Maybe the protonation (deuteration) took place in too low quantities to be detected. Although radical anions are detected using ESR spectroscopy, the quantity may be low as this method is highly sensitive.[32]
Figure 4.23b shows the solid gained from stirring TCNQ in dichloromethane with an excess of D_2O. A signal is detected with a chemical shift of 2.49 ppm. Because this peak cannot be assigned to the solvent (chemical shift = 5.32 ppm) or residual D_2O (chemical shift = 1.52 ppm), it was concluded that it somehow had to be TCNQ-related. The most likely structure is proposed in Figure 4.23. However, the chemical shift does not fit well: Because of the electron-withdrawing effect of the cyanide groups and the oxygen, a chemical shift at higher ppm-values is expected. Furthermore, if one side does carry an alcohol group (-OD, respectively), it is unclear what chemically happened to the other side (therefore marked with a question mark). These results have to be evaluated with care and therefore are neither interpreted as evidence or counter-evidence for a reaction with water.
Lastly, in Figure 4.23c the remaining solid from stirring TCNQ in chlorobenzene with an excess of D_2O is displayed. There are no signals detected. Is therefore concluded, that no reaction product including deuterons was formed.

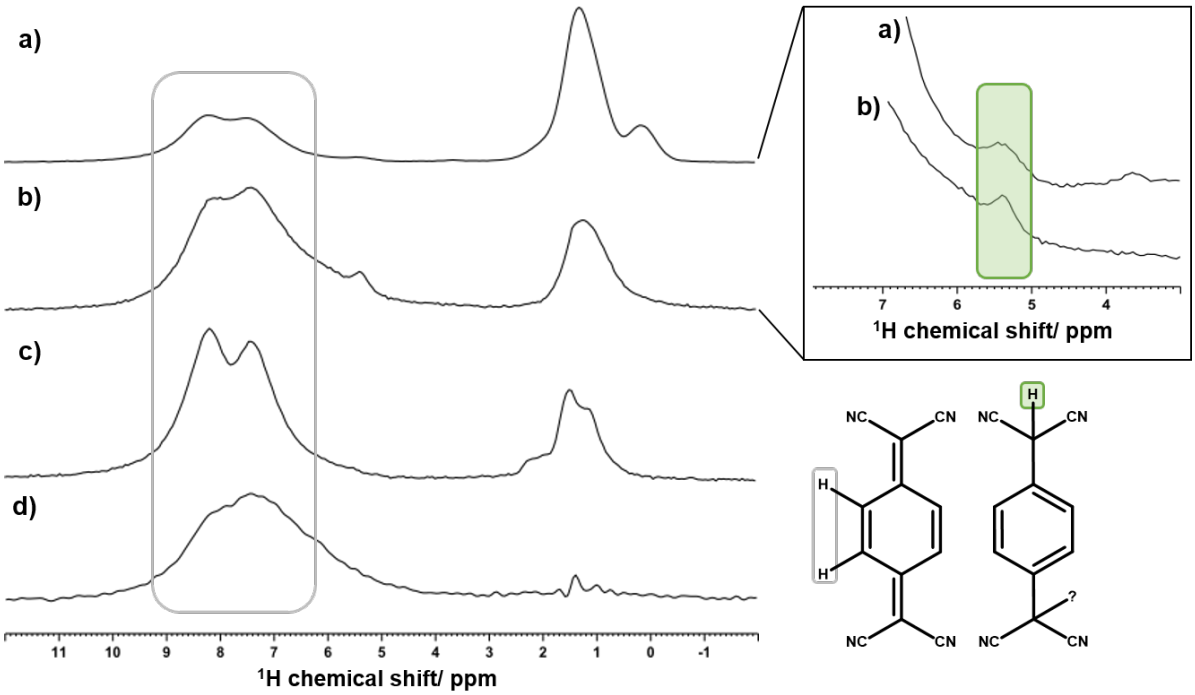

Figure 4.24: ^1H MAS spectra of solids obtained from stirring TCNQ in **a)** chlorobenzene, **b)** dichloromethane and **c)** acetonitrile with an excess of D_2O for 48 h in air and **d)** pristine TCNQ, packed and handled under nitrogren atmosphere.

Of the prepared solids ^1H MAS spectra were recorded as well. The spectra are displayed in Figure 4.24 and Figure 4.24d shows the pristine TCNQ. As for F_4TCNQ, the protons in TCNQ are chemically equivalent but not crystallographically, resulting in two signals.[70] Because the spinning rate with

25 kHz was not high enough, the peaks could not be fully resolved. The chemical shifts have been determined to be 8.08 ppm and 7.44 ppm, which is in good agreement with the literature (8.06 ppm and 7.44 ppm,[70] see chemical structure in Figure 4.24 also). These signals can be found in the solids prepared from chlorobenzene, dichloromethane, and acetonitrile as well. In the solids prepared from chlorobenzene and dichloromethane there is an additional peak at 5.42 ppm (Figure 4.24a and Figure 4.24b), zoomed-in area and highlighted in green). Since the chemical shift is very similar to that of dichloromethane (5.32 ppm), the solid in the rotor was heated to 423 K for two hours. This was to ensure that the remaining solvent evaporated. The spectra before and after heating are identical, so a solvent-related signal is ruled out. The signals might potentially be assigned to a protonated TCNQ species, as proposed graphically. The chemical shift for a related structure is 5.07 ppm (recorded in $CDCl_3$).[71] As already discussed, protonation may have occurred after the reduction of TCNQ. If such a reaction took place, the protons most likely were transferred from the solvent, because D_2O was added instead of H_2O and neither of them dissolves well in chlorobenzene or dichloromethane. Just like for the F_4TCNQ samples dried from different solvents (Figure 4.19), there are peaks in the aliphatic region for the TCNQ samples as well. The chemical shifts are: 1.30 pmm and 0.16 ppm for Figure 4.24a, 1.24 ppm for Figure 4.24b, 2.27 ppm (shoulder), 1.49 ppm and 1.17 ppm (shoulder) for Figure 4.24c and 1.42 ppm for Figure 4.24d. Since in the pristine TCNQ there is only a small impurity in the aliphatic region, the signals in spectra a)-c) must have been introduced at some point during the sample preparation. In addition to their origin being unclear, the signals vary for the different samples, making assignment even harder. Potentially, impurities were introduced during the sample preparation or were present in the zirconia rotor used to record solid-state NMR spectra.

Unfortunately, it was not possible to detect carbon signals with either cross-polarization or one pulse measurements. Those would potentially generate further insight. It is unclear, why the measurements failed. Solid-state ESR and MALDI-TOF spectra were recorded also. The ESR spectra can be found in Figure 8.8, Appendix. Since the set parameters varied strongly between the measurements, which has a big influence on the signal intensity and peak-to-peak width, it can only be said qualitatively that radicals were present. It furthermore appears that ambient conditions and the presence of (deuterated) water do not prevent radical formation.

Solution NMR studies

To gain further insight into potential reactions, solution NMR studies were performed. For that, the mixtures were set up in undeuterated chlorobenzene and D_2O was added. The goal was, again, to record ^{2}H-signals. Because the polymer-additive mixture is stirred at 333 K and a temperature influence was suspected, the (polymer-)additive-D_2O mixture was heated inside the NMR spectrometer and re-measured at that temperature. In Figure 4.25 the NMR spectra of TCNQ with D_2O (1:3) in chlorobenzene at rt (approx. 298 K) and 333 K are displayed. The peaks labeled with CB are assigned to the solvent chlorobenzene and referenced to literature values. The aliphatic signal (marked in grey) could not be assigned at first, therefore D_2O was measured in chlorobenzene, resulting in the same signal (1.01 ppm). It was concluded that the signal is not TCNQ-related. Note, that D_2O does not dissolve in chlorobenzene and TCNQ has a quite low solubility in chlorobenzene at rt. The total amount is therefore low, which also makes detection more difficult. Nevertheless, work was carried out with this solvent to be closer to transistor fabrication. It should be noted that the reaction of TCNQ with water in the transistor film, or during preparation, becomes less likely due to the poor solubility of H_2O.
At 5.00 ppm D_2O is detected with a shoulder at 5.08 ppm. As displayed in Figure 4.25, this peak may be assigned to deuterated TCNQ. As suggested in literature on the other side of the molecule there might be an alcohol group (-OD, respectively)[28] or simply an additional deuteron, meaning D_2TCNQ

was present in solution. Watts et al. showed that the dianion F_4TCNQ^{2-} can be protonated by weak acid H_2O.[24] Because $TCNQ^{2-}$ is a stronger base than F_4TCNQ^{2-},[19] it can be suspected that acid-base-chemistry involving water should be possible as well. The remaining OH^- (OD^-) might then lead to further reaction products. In the spectrum recorded at 333 K the signals for some reason vanished. The measurements were performed right after one another so it is unclear what happened in between. Because of this unexpected result, the signals were integrated, normalizing the chlorobenzene signal to one. The integral of the aliphatic signal at 333 K is 4.93 and the two signals at rt are 4.74 (aliphatic: 3.64, @ 5.00 ppm = 1.10). It seems as if the signals were shifted toward the aliphatic region upon heating. The aliphatic signal itself shifts from 1.01 ppm to 0.94 ppm upon heating. Heating might affect the solubility of D_2O in chlorobenzene and shift the reaction equilibrium toward unprotonated species, according to the Gibbs-Helmholtz equation ($\Delta G = \Delta H - T\Delta S$, with the Gibbs energy ΔG, the enthalpy ΔH, the temperature T, and the entropy ΔS) which states that the reaction with increasing temperature is entropy controlled. This experimental setup was repeated with the addition of potassium iodide, to ensure the reduction of TCNQ. The dianion $TCNQ^{2-}$ then ought to be able to be deuterated. In fact, signals of the same chemical shift were observed, supporting the hypothesis that deuterated TCNQ had formed.

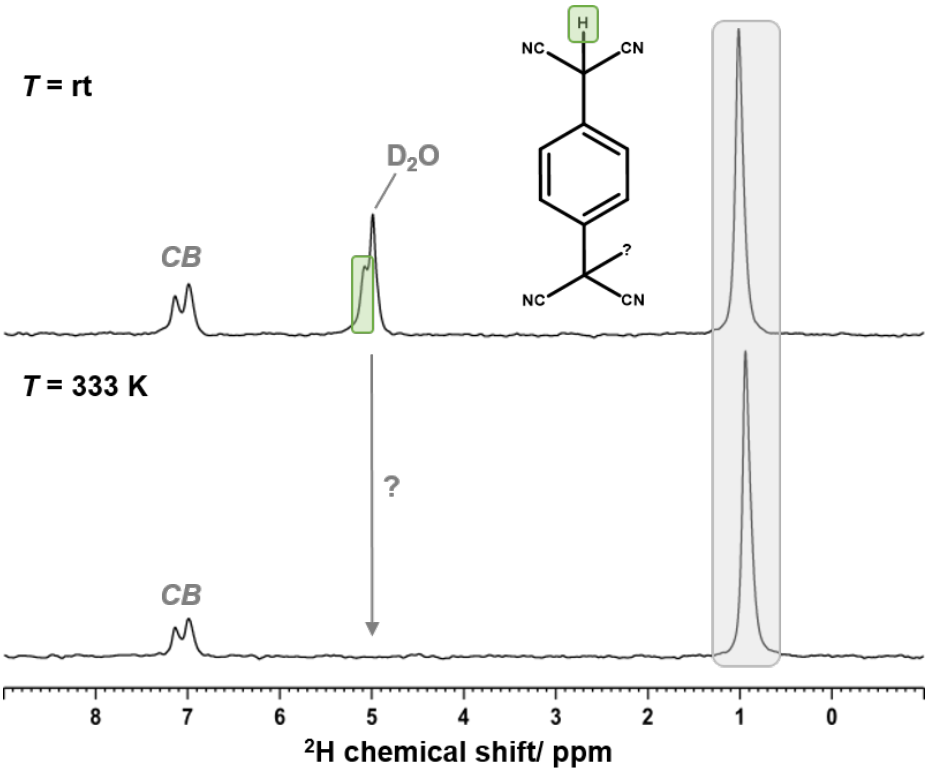

Figure 4.25: ^2H NMR spectra of TCNQ with D_2O (1:3) in chlorobenzene at rt and 333 K; setup and measured in air.

The same experiments were repeated with the adding of the respective polymers (IDTBT and F8BT). The ^2H NMR spectra at rt and 333 K are displayed in Figure 4.26. Similar to Figure 4.25 the chlorobenzene signals and the aliphatic signals are detected. In both experiments, the aliphatic signals shift upon heating from 1.00 ppm at rt to 0.93 ppm at 333 K. Surprisingly, no D_2O signals are detected and only the aliphatic signals. No signal was detected that could be related to TCNQ.
For the F8BT-TCNQ blend, an additional experiment was carried out under nitrogen atmosphere. For this purpose, F8BT, TCNQ, and D2O (ratio 1:1:3) were added together in chlorobenzene. A

solution ^{2}H NMR at 333 K was recorded, which, however, showed no signal analogous to the other experiments. Next, the mixture was annealed at 363 K for 60 min., the solid was transferred into a zirconia rotor and a ^{2}H MAS spectra were recorded. Unfortunately, no signal could be detected in this measurement, leading to the conclusion that no deuterium-containing compound was formed. Additional ESR spectra were recorded from the solid, in which a radical signal can be seen. The presence of D_2O does not seem to inhibit the formation. Furthermore, the radical anion $TCNQ^{\cdot -}$ does not appear to pick up a proton (deuteron), which is consistent with the literature (equilibrium constant K_{eq} for the protonation is $4 \cdot 10^{-2}$, determined using steady-state voltammetric methods in acetonitrile[19]).

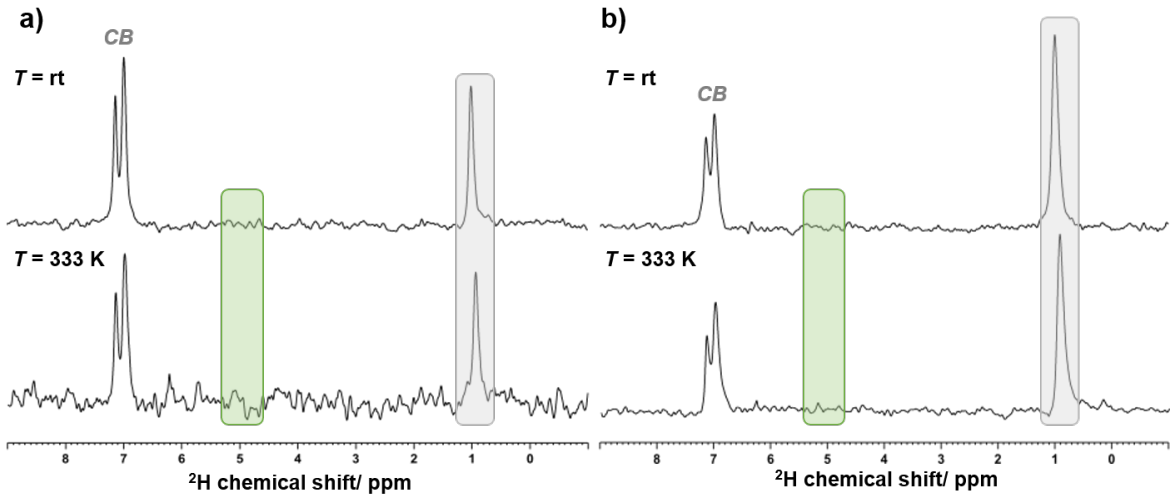

Figure 4.26: ^{2}H NMR spectra of TCNQ in chlorobenzene with D_2O and **a)** IDT-BT and **b)** F8BT at rt and 333 K; setup and measured in air. The ratio of additive:polymer:D_2O was 1:1:3.

5 Summary and outlook

In summary, MALDI spectrometry, ESR spectroscopy, and NMR spectroscopy were used to study the pristine polymers IDT-BT and F8BT and pristine additives TCNQ, F_4TCNQ and DDQ, as well as combinations of both. The molecular additives were previously reported to enhance the performance and operational stability of polymer thin-film transistors[3] and this work aimed to identify the mechanisms and potential chemical reactions of the additives (e.g. with water and/ or oxygen) that cause these effects.

MALDI spectrometry showed that the polymers IDT-BT and F8BT cannot be used as dual, but only as MALDI matrices in positive reflectron mode. The investigation of polymer/additive/water mixtures was further obstructed by the fact that TCNQ can serve as a MALDI matrix.[44,45] In conclusion, no potential reaction products of TCNQ with water and/or oxygen could be detected using mass spectrometry. As mentioned earlier, access to the instrument was limited due to the COVID-19 pandemic. Further studies might give additional insight.

ESR spectroscopy was used to investigate the formation of radicals in polymer/additive blends as well as in the pristine additives in solid and liquid state. ESR studies of the polymer/additive blends showed that radicals, most likely the additive radical anion, oftentimes are present in polymer/additive films, although no doping reaction should occur. Only small radical signals were detected in liquid state samples of the polymer/additive blends, which may be related to the low amount of radicals present due to the small sample volume. In summary, the following was observed for the different polymer/additive films: IDT-BT/F_4TCNQ only partially showed the formation of radicals (doping expected), IDT-BT/TCNQ showed a large radical signal in some samples and only a small one in others (doping not expected), F8BT/TCNQ always shows a radical signal, as does F8BT/F_4TCNQ (doping not expected in both cases) and F8BT/DDQ shows no radical signal (doping not expected). For this unexpected formation of radical anions, the temperature dependence of the redox potential as well as inaccurate HOMO and LUMO energies were discussed. However, the energy gap in some cases simply should be too large for a doping reaction to take place. Therefore, other sources of radical forming were considered as well. Potentially, the polymers as being heterocycles benefit the formation as in they stabilize the radical anion. The formation of CTCs was considered as well. Furthermore, spatial distance seems to influence the formation of radicals, since large radical signals were only obtained for the films. In addition, temperature-dependent ESR spectra were recorded to check for thermally accessible triplet states of the additives that might be involved in the formation of radical anions. The F8BT/ F_4TCNQ films however showed Curie-like behavior. At this point, there is potential for further research, since, despite attempts of the literature to explain the formation of radical anions, it is (for almost all experiments presented here) unclear how they are generated and literature encourages these considerations.[48]
The solvent-dependent formation of radical anions of TCNQ, F4TCNQ, and DDQ in methanol, chloroform, chlorobenzene, and acetonitrile in solid and liquid state was investigated. They form radical anions in methanol and acetonitrile and little to none in chlorobenzene and chloroform. It was further observed that the radical amounts of TCNQ in these solvents decreased over the course of nine days, but increased for F_4TCNQ (with the exception of methanol). In addition, in the solids obtained by annealing the solutions, radical signals were obtained in all samples in amounts analogous to the liquid state samples. These results support the hypothesis that no redox reaction took place between

the polymers and additives. It was furthermore concluded, that the aggregation state, as well as the presence of polymers, is crucial for the formation of radical anions in unpolar solvents. It is hypothesized that it may be the radical anions of the molecular additives that lead to improved transistor performance. These radical anions could react to TCNQ and $TCNQ^{2-}$ [26,27] and the dianion could chemically bind oxygen[29] and water.

Lastly, NMR spectroscopy was used to study the pristine IDT-BT, the drop cast and annealed F_4TCNQ, IDT-BT/ F_4TCNQ blends, and potential reactions of TCNQ with water. Studies of the drop cast and annealed F_4TCNQ were conducted to gain further inside into the chemical reactions that might be involved in the formation of radical anions observed using ESR spectroscopy. It was shown that when annealing the same from chlorobenzene, novel F_4TCNQ species form. It is not entirely clear, what those species are. The influence of the solvent is suspected, as furthermore in the ^1H MAS spectra signals were observed, where none were expected. This finding in combination with the permanent observance of radical anions using ESR spectroscopy raises the question of the stability of these molecular additives and if they really just engage in doping reactions as often intended.
Studies of IDT-BT/ F_4TCNQ blends using solid-state NMR spectroscopy revealed that annealing of the film most likely leads to reorientation of the molecular ordering as well as doping of the polymer. However, even after the film is annealed, approx. one-third of the F_4TCNQ molecules do not seem to take part in a redox reaction.
To investigate the potentially happening reactions between water and TCNQ, D_2O was used instead of H_2O, and thus ^2H NMR spectra in solid-state and solutions could be acquired. Recording solid-state ^2H MAS spectra of the solids obtained from stirring of TCNQ in different solvents with an excess of D_2O, did not show a clear indication of a reaction product. Only one solid showed a signal that may be TCNQ-related. Additionally recorded ^1H MAS spectra showed not assignable signals in the aliphatic region. In the aromatic region signals that could be related to the protonated TCNQ were observed. The recording of $\{^1H\}$-^{13}C MAS as well as ^1H-^{13}C HETCOR spectra failed, through which more insight could have been generated. Solution ^2H NMR spectra of TCNQ in chlorobenzene with D_2O at rt showed a peak that was assigned to the protonated (deuterated) TCNQ. The signal vanished at 333 K, which might be due to a temperature-dependent equilibrium. In blends of F8BT (or IDT-BT) and TCNQ with D_2O no such signal was observed, which lead to the conclusion that no reaction product including deuterons was formed. These results overall do not suggest that TCNQ takes part in a reaction with H_2O or D_2O, respectively.

As discussed above, further research on temperature-dependent ESR studies seems promising.[48] This might provide information about the formation of radical anions of the molecular additive. Based on the results presented here, it may be interesting to further investigate OFETs with organic semiconductors and molecular additives for which doping is not expected. Processing them from different solvents could directly test the influence of radical anion on the device performance. Finally, studying polymer/ additive blends via UV/vis spectroscopy might be interesting due to the clear footprint of neutral molecules, radical anions, and dianions.[23,72]

6 Experimental

6.1 Methods and materials

Chemicals and solvents

All purchased chemicals were used without any further purification. TCNQ and F_4TCNQ (purified by sublimation, pruity >98 %) were purchased from TCI, F8BT from *Sigma Aldrich* and IDT-BT was provided by the group of Iain McCulloch at the King Abdullah Universtiy of Science and Technology. Used solvents were chlorobenzene (CB), *ortho*-dichlorobenzene (DCB), $CHCl_3$, *iso*-propanol, aceton, methanol and acetonitrile and purchased from *Sigma Aldrich*. Deuterised solvents (d_4-*ortho*$-$dichlorobenzene, CD_3CN, CD_2Cl_2, $CDCl_3$ and D_2O) were purchased from *Deutero* and *Sigma Aldrich*.
If not noted otherwise, all sample preperations and measurements have been conducted under nitrogen atmosphere. For that a Glovebox from *MBraun*, type *UniLab* was used with oxygen and water values of: $O_2 = < 1 - 15$ ppm and $H_2O < 1$ ppm.

ESR

To record ESR-spectra the *MiniScope MS 200* from *Magnettech* was used. The samples were introduced into the sample holder, which is placed in a homogenous B-field. The samples were irradiated with a constant frequency of about 9.4 GHz (X-Band). This could be read via a *5340 A Frequency Counter* from the company *Hewlett Packard*. As a standard Mn^+-ions with reported g-values of 2.188, 2.066, 2.0267, 1.9858, 1.946 and 1.906 were used. Samples were prepared in 50 µL micropipette capillaries from *BLAUBRAND* and sealed using *Critoseal*. Spectra were recorded at rt (298 K) and processed using *EasySpin* in *Matlab* as well as *Origin 2019b*. All displayed spectra of polymer-additive blends have been smoothed using the Savitzky-Golay filter in *EasySpin*. The parameters used can be found in the respective experiment description. They were carefully evaluated to avoid spin saturation and broadening to the peak-to-peak width.
Solid-state samples were produced by drop-casting the solution on to clean glass substrates (25 mm x 85 mm). Their cleaning procedure was analogous to the cleaning procedure of MALDI targets and is described in the mass spectrometry section.

NMR

Solid-state NMR spectra were recorded using a Bruker Avance III 500 MHz wide bore system equipped with double resonance probehead (^{1}H MAS, ^{19}F MAS, $\{^1H\}^{13}C$ CP MAS as well as HETCOR spectra) and a Bruker Avance III 700 MHz standard bore system equipped with a tripple resonance probehead (^{2}H MAS) at 25 - 50 kHz MAS spinining frequency. Zirconia rotors with an other diameter of 2.5 mm were used. ^{1}H MAS spectra were aquired with 32-64 scans and relaxation delay of 2 s, ^{19}F MAS spectra were aquired with 64 scans and relaxation delay of 10-1000 s, ^{2}H MAS spectra were aquired with 1024 scans and a relaxation delay of 5 s and $\{^1H\}^{13}C$ CP MAS spectra were aquired with 8192

scans, relaxation delay of 3 s and CP contact times of 0.1, 1 and 3 ms.
Solution NMR measurements were recorded on a Bruker Avance III console for 700 MHz, equipped with a QXI probehead with z-gradient. ^{2}H spectra were recorded with 256 scans and relaxation delay of 1 s. All spectra were processed using *TopSpin* and for fitting *DM fit*.

Mass Spectrometry

A MALDI target from *Waters* was used for all measurements. Prior to usage, the substrate was cleaned in the clean room. In an ultra sound bath at 40 °C the traget was firstly cleaned in water for five minutes, then in acetone for ten minutes and lastly in *iso*-propanol for ten minutes. Next, the target was dried in an oven at 140 °C for ten minutes and then treated in an UV-ozone oven for additional 20 minutes.
All measurements were performed using the *Waters Synapt G2Si*. Processing of the data was performed using *mMass* and *Origin 2019b*.

6.2 MALDI studies

Unless otherwise indicated, all samples were prepared and handled in air.

IDT-BT and F8BT as MALDI matrices

This sections is orientated on the recently publish paper from Horatz et al., [6]. Accordingly, polymer and analyte (see Figure 6.1) solutions with concentrations of 10 $\frac{mg}{ml}$, 1 $\frac{mg}{ml}$ and 0.1 $\frac{mg}{ml}$ were prepared. The polymers IDT-BT and F8BT were dissolved in chlorobenzene, TBAB in acetonitrile and citric acid and cholic acid in aceton. The target was cleaned as discribed in methods and materials, mass spectrometry part. The solutions were applied via the thin layer method: First, the analyte was applied via drop-casting (2 µL) and allowed to dry for approx. 1 - 2 min. Next, the polymer solution (2 µL) was applied on top of the analyte via the drop-casting method, also, and allowed to dry for approx. 5 min. In order to examine the best analyte-polymer combination, each analyte concentration was combined with each polymer concentration. The results are listed in Table 6.2 and Table 6.1. In Figure 4.2 the addition of NaOH to cholic acid are presented as well. Since this was only a test run, without exact measurement of concentrations or volumes, these are not to be indicated. The combinations IDT-BT (1 $\frac{mg}{ml}$) and F8BT (1 $\frac{mg}{ml}$) with cholic acid (10 $\frac{mg}{ml}$ and 1 $\frac{mg}{ml}$ + NaOH) were tested.

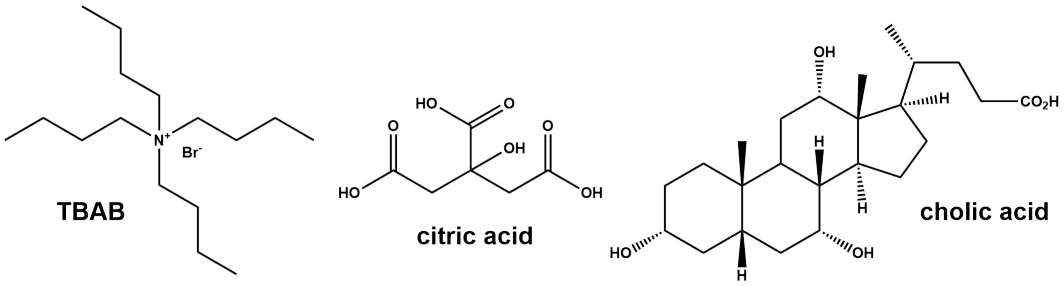

Figure 6.1: Chemical structures of TBAB, citric acid and cholic acid used as analytes to investigate the possible use of IDT-BT and F8BT polymers as MALDI matrices.

Table 6.1: Tested concentration combinations for IDT-BT as MALDI matrix with the analytes TBAB, citic acid, citric acid with NaOH and cholic acid. With "p" for positive and "n" for negative ion mode.

analyte	ion mode	IDT-BT 10 mg/ml	IDT-BT 1 mg/ml	IDT-BT 0.1 mg/ml	no matrix
TBAB 10 mg/ml	p	bad	bad	very good	ok
TBAB 1 mg/ml	p	ok	good	very good	ok
TBAB 0.1 mg/ml	p	good	very good	good	ok
citric acid 10 mg/ml	n	-	-	-	-
citric acid 1 mg/ml	n	-	-	-	-
citric acid 0.1 mg/ml	n	-	-	-	-
citric acid 10 mg/ml+NaOH 25 mol%	n	-	-	-	-
citric acid 1 mg/ml+NaOH 25 mol%	n	-	-	-	-
citric acid 0.1 mg/ml+NaOH 25 mol%	n	-	-	-	-
cholic acid 10 mg/ml	n	-	-	-	-
cholic acid 1 mg/ml	n	-	-	-	-
cholic acid 0.1 mg/ml	n	-	-	-	-

Table 6.2: Tested concentration combinations for F8BT as MALDI matrix with the analytes TBAB, citic acid, citric acid with NaOH, cholic acid and cholic acid with NaOH.

analyte	ion mode	F8BT 10 mg/ml	F8BT 1 mg/ml	F8BT 0.1 mg/ml	no matrix
TBAB 10 mg/ml	p	very good	very good	very good	ok - bad
TBAB 1 mg/ml	p	very good	very good	very good	ok
TBAB 0.1 mg/ml	p	very good	very good	very good	ok - bad
citric acid 10 mg/ml	n	-	-	-	-
citric acid 1 mg/ml	n	bad	-	-	-
citric acid 0.1 mg/ml	n	bad	-	-	-
citric acid 10 mg/ml + NaOH 25 mol%	n	-	-	-	-
citric acid 1 mg/ml + NaOH 25 mol%	n	-	-	-	-
citric acid 0.1 mg/ml + NaOH 25 mol%	n	-	-	-	-
cholic acid 10 mg/ml	n	-	-	-	-
cholic acid 1 mg/ml	n	-	-	-	-
cholic acid 0.1 mg/ml	n	-	-	-	-

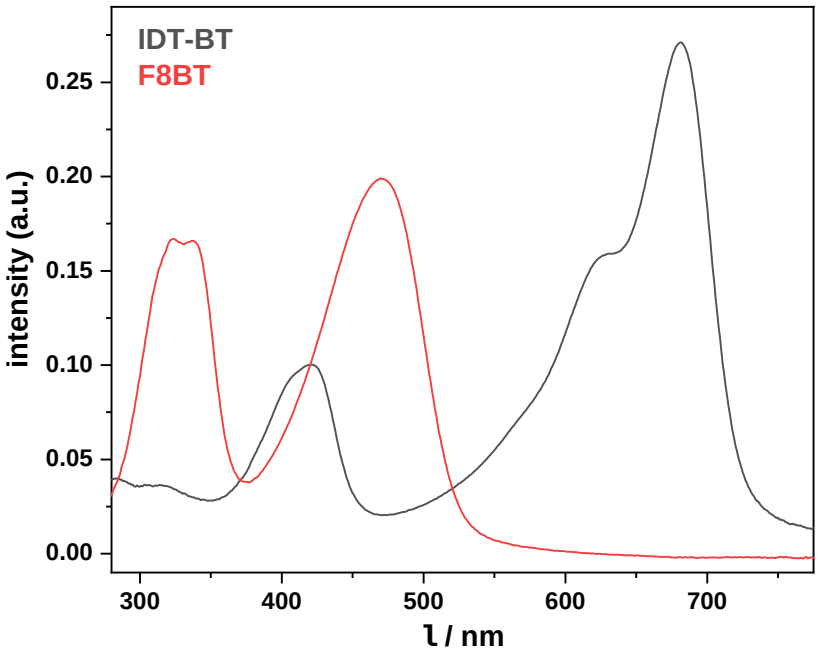

Figure 6.2: UV/vis spectra of IDT-BT and F8BT thin films.

Pristine additives

These samples were prepared under nitrogen atmosphere. The only time the samples were in air was to transfer them in to the MALDI instrument. Solutions of TCNQ and F_4TCNQ in chlorobenzene with concentrations of 1 $\frac{\text{mg}}{\text{ml}}$ were prepared, stirred for one hour at 333 K and then applied onto a glass substrate. The substrate was cleaned similary to the target.

Polymer and additive combinations

For these measurements, samples were prepared by combining TCNQ in chlorobenzene with either H_2O or D_2O and for some samples IDT-BT in chlorobenzene, also. The amounts and combinations are listed in Table 6.3. In samples where an excess of H_2O or D_2O was added, the water phase also was investigated. Furthermore, from all these solutions there was one set dried at rt and one annealed at 363 K for one hour.

Table 6.3: Equilavents and combinations of TCNQ, D_2O or H_2O and IDT-BT used for MALDI studies.

	TCNQ	H2O	D2O	IDT-BT
I	1	2	-	-
II	1	excess	-	-
III	10	excess	-	1
IV	1	-	2	-
V	1	-	excess	-
VI	1	-	excess	1

6.3 ESR studies

Polymer and additive blends

All reaction parameters are summarized in Table 6.4. It has to be noted that both additive and polymer solutions always have a concentration of 1 $\frac{\text{mg}}{\text{mL}}$. The following procedure applies to all experiments. First, the polymer and additive solutions were prepared. The seperate solutions were allowed to stirr for approx. 30 min. at 333 K (sometimes longer if there were parts undissolved). The solutions were then combined in the indicated volumes and stirred for additional 30 min. at 333 K. In most cases, liquid state ESR samples were taken from this solution 5 min. after combining and 30 min. after combining. Simultaneously, the heating plate was set to 363 K with the cleaned glass substrates on top (see MALDI methods for cleaning procedure). Then, the solution was deposited by the drop-casting method and set to dry for the amount of time given in Table 6.4. In cases of solids prepared at rt the liquid was simply drop-casted on to the cold glass substrate. After drying, the solid was collected and transferred into the sample tube and sealed. After preperation, the samples were measured immediately. The following ESR settings were selected (depending on the sample): field = 3342 G, sweep = 50 G, sweep time = 60 - 200 s, modulation = 200 - 400 mG, microwave power = 1 - 50.12 mW and number of passes = 3 - 10.

Table 6.4: Reaction parameters for ESR studies of polymer-additive blends. All used polymer and additive concentrations c_{polymer} and c_{additive} were 1 $\frac{\text{mg}}{\text{mL}}$. Reaction parameters of ESR studies of pristine TCNQ and F_4TCNQ can be found in Table 6.5. P:A gives the polymer-to-additive molecular ratio.

figure no.	poylmer	V_{polymer}	additive	V_{additive}	P:A	wt%	solvent	T_{reaction}	t_{reaction}	$T_{\text{annealing}}$	$t_{\text{annealing}}$
Figure 4.6	IDT-BT	1.1 mL	F_4TCNQ	55 µL	4: 1	5	CB	333 K	30 min.	363 K	10 min
Figure 4.6	IDT-BT	1.0 mL	F_4TCNQ	20 µL	10:1	2	CB	333 K	30 min.	363 K	10 min
Figure 4.6	IDT-BT	1.1 mL	F_4TCNQ	11 µL	20:1	1	CB	333 K	30 min.	363 K	10 min
Figure 4.6	IDT-BT	1.2 mL	TCNQ	48.2 µL	4:1	5	CB	333 K	30 min.	368 K	10 min
Figure 4.7	IDT-BT	1.2 mL	TCNQ	48.2 µL	4:1	5	DCB/ $CHCl_3$	333 K	30 min.	363 K	1 h
Figure 4.8	IDT-BT	1.3 mL	TCNQ	52.2 µL	4:1	5	DCB/$CHCl_3$	333 K	30 min.	rt	22 h
Figure 8.2	IDT-BT	1.0 mL	TCNQ	40.1 µL	4:1	5	CB	333 K	30 min.	363 K	1 h
Figure 8.3	IDT-BT	2.0 mL	TCNQ	160.5 µL	2:1	10	CB	333 K	30 min.	363 K and rt	1 and 2 h
Figure 8.4	IDT-BT	1.2 mL	TCNQ	48.2 µL	4:1	5	CB	333 K	30 min.	363 K and rt	1 h (both)
Figure 4.9	F8BT	1.2 mL	TCNQ	117.2 µL	4 :1	5	CB	333 K	30 min.	363 K and rt	1 and 2 h
Figure 4.9	F8BT	1.3 mL	TCNQ	126.9 µL	4:1	5	CB	-	-	rt	2 h
Figure 4.10	F8BT	1.35 mL	F_4TCNQ	127.7 µL	-	-	CB	333 K	30 min.	363 K and rt	1 h
Figure 4.10	F8BT	1.35 mL	F_4TCNQ	127.7 µL	-	-	CB a. MeOH	333 K	30 min.	363 K and rt	1 h
Figure 4.11	F8BT	1.35 mL	DDQ	146.5 µL	-	-	CB a. MeOH	333 K	30 min.	363 K and rt	1 h
Figure 8.1	IDT-BT	0.5 mL	-	-	-	-	CB	-	-	363 K	1 h
Figure 8.1	F8BT	0.5 mL	-	-	-	-	CB	-	-	363 K	1 h

ESR calibration using TEMPO

To determine the radical concentration present in solution, a calibration using TEMPO was performed. For that, concentrations of 1.5, 1.0, 0.5 and 0.1 mM in chlorobenzene, MeCN, MeOH and chloroform were prepared and measured. Then the double integrals were calculated using *MatLab* and plotted against the concentration. The resulting fits performed using *Origin 2019b* are shown in Figure 6.3 with the slopes being $7900 \pm 300\ \frac{1}{\text{mM}}$ for TEMPO in MeOH, $8000 \pm 200\ \frac{1}{\text{mM}}$ for TEMPO in MeCN, $5500 \pm 200\ \frac{1}{\text{mM}}$ for TEMPO in CB and $7700 \pm 400\ \frac{1}{\text{mM}}$ for TEMPO in MeOH. For the calibration the following settings were selected: field = 3337 G, sweep = 60 G, sweep time = 100 s, modulation = 400 mG, microwave power = 15.85 mW and number of passes = 3.

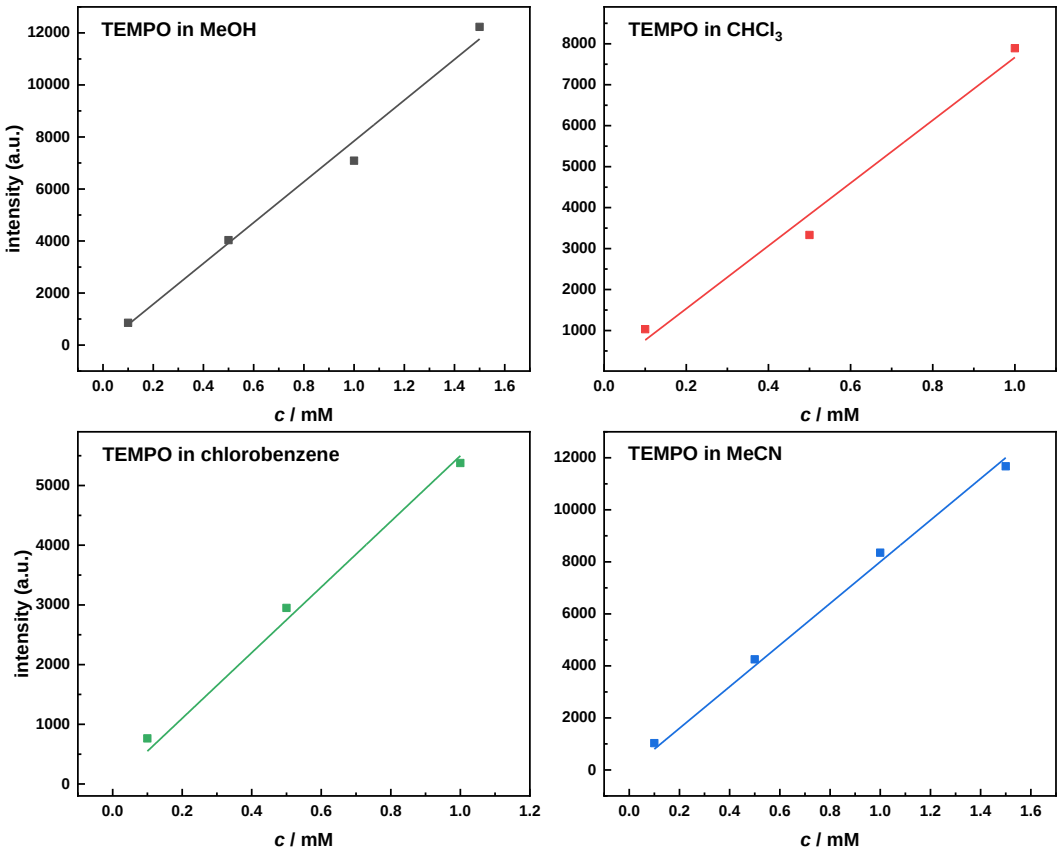

Figure 6.3: Calibrations performed to determine the radical concentration in solution using TEMPO in methanol, chloroform, chlorobenzene and acetonitrile.

Pristine TCNQ and F_4TCNQ studies

To investigate the solvent dependence of the additives, they were dissolved in the appropriate unhydrous solvent under inert gas conditions (see Table 6.5), then stirred at 40 °C for 30 min., transferred into the ESR tubes and measured directly. For the spectra recorded nine days later, the solutions were kept inside the glovebox at rt. Samples were taken without re-heating the solutions.
For the solid-state ESR spectra, new solutions with concentrations of 1 $\frac{\text{mg}}{\text{ml}}$ were prepared and after stirring for 30 min. at 313 K they were drop-casted onto pre-heated glass sides and then annealed at 363 K for one hour. The solids then were scratched off, transferred into the ESR tubes and measured directly.
The following ESR settings were selected (depending on the sample): field = 3339 - 3342 G, sweep = 50 G, sweep time = 60 s, modulation = 1000 - 100 mG, microwave power = 1 - 50.12 mW and number of passes = 10.

Table 6.5: Parameters to perform solvent dependent ESR measurements for the additives TCNQ, F_4TCNQ and DDQ.

	F4TCNQ				TCNQ				DDQ			
solvent	MeOH	MeCN	CB	CHCl3	MeOH	MeCN	CB	CHCl3	MeOH	MeCN	CB	CHCl3
m/mg	1.7	1.3	1.3	1.3	1.3	1.1	1.4	0.9	0.9	1.1	0.9	1.2
c/ $\frac{\text{mg}}{\text{mL}}$	1	1	1	1	1	1	1	1	1	1	1	1
c/ $\frac{\text{mmol}}{\text{mL}}$	3.6	3.6	3.6	3.6	4.8	4.8	4.8	4.8	4.4	4.4	4.4	4.4
colour	pale green	yellow	orange/red	yellow	green	pale yellow	pale yellow	yellow				
colour (solid)	dark green	green	green	green	dark green	green	green	green	-	-	-	-

6.4 NMR studies

Solid-state NMR of IDT-BT and F_4TCNQ (2:1) films

This series of experiments was performed under nitrogen atmosphere. Separately prepared solutions of IDT-BT (10 $\frac{mg}{ml}$, dark green solution) and F_4TCNQ (1 $\frac{mg}{ml}$, orange/pink solution) in chlorobenzene were kept overnight at 333 K. After combining the solutions in the appropriate molar ratio (2:1), they were stirred for an additional 30 min. at 333 K. The solution was then drop-casted onto a pre-cleaned glass plate (20 x 17 cm) at rt. A manual bar coating system was used to prepare the films. After evaporation of the solvent (approx. 3 h), the film was scraped off and placed in a 2.5 mm diameter zirconia rotor. The films first were measured at rt, then heated at 373 K, allowed to cool down and heated again. This was repeated at 383 K, 393 K and 403 K.

Solid-state NMR of TCNQ and D_2O in varying solvents

These experiments were conducted at rt and in air. Solutions of TCNQ in CH_2Cl_2, CB and MeCN (1 $\frac{mg}{ml}$) were prepared. An excess of D_2O was added. In case of CH_2Cl_2 and CB phase separation took place. The mixtures were allowed to stirr for 48 h. Then the entire solvent was removed in vacuum and the resudial solid was inserted into a zirconia rotor. Solid-state NMR as well as solid-state ESR and MALDI-TOF measurements were performed.

Liquid state NMR of TCNQ and D_2O (and IDT-BT or F8BT)

TCNQ was dissolved in chlorobenzene with a concentration of 1 $\frac{mg}{ml}$, then D_2O (and IDT-BT or F8B) were added in the appropriate amounts and NMR measurements performed. The ratios were TCNQ:D_2O = 1:3 and TCNQ:polymer:D_2O = 1:1:3.

7 Danksagung

An erster Stelle bedanken möchte ich mich bei Dr. Ulrike Kraft, für die tolle Betreuung und Unterstützung während meiner gesamten Arbeit, so wie auch Sten Gebel, für die gute Gruppendynamik und Einblicke in fremde Fachgebiete. Außerdem sind zu nennen Prof. Pol Besenius für das Zweitgutachten meiner Arbeit und Prof. Paul Blom für das Ermöglichen der Durchführung meiner Arbeit in seinem Arbeitskreis. Mein weiterer Dank gilt Constantin Haese, für Unterstützung, gute Ideen, viel Messzeit am Spektrometer und die netten Gesprächen. Außerdem möchte ich mich bei Dr. Robert Graf und Prof. Martin Baumgarten bedanken, für die Hilfe und Zeit, die sie mir haben zukommen lassen. Abschließend zu nennen ist der gesamte Arbeitskreis Blom, der mich trotz Kontaktbeschränkung sehr nett aufgenommen hat, wodurch ich mich sehr wohl gefühlt habe.

Zuletzt danke ich meiner Familie und meinen Freunden für die gesamte Unterstützung während meines Studiums.

Bibliography

[1] I. E. Jacobs, A. J. Moulé, *Adv. Mater.* **2017**, *29*.
[2] P. W. M. Blom, *Adv. Mater. Technol.* **2020**, *5*, 2000144.
[3] M. Nikolka, I. Nasrallah, B. Rose, M. K. Ravva, K. Broch, A. Sadhanala, D. Harkin, J. Charmet, M. Hurhangee, A. Brown, S. Illig, P. Too, J. Jongman, I. McCulloch, J.-L. Bredas, H. Sirringhaus, *Nat. Mater.* **2017**, *16*, 356–362.
[4] M. Nikolka, G. Schweicher, J. Armitage, I. Nasrallah, C. Jellett, Z. Guo, M. Hurhangee, A. Sadhanala, I. McCulloch, C. B. Nielsen, H. Sirringhaus, *Adv. Mater.* **2018**, 1801874–1801878.
[5] J. Armitage, L. J. Spalek, M. Nguyen, M. Nikolka, I. E. Jacobs, L. Marañón, I.Nasrallah, G. Schweicher, I. Dimov, D. Simatos, I. McCulloch, C. B. Nielsen, G. Conduit, H. Sirringhaus, **2019**, 1–10, online: https://arxiv.org/pdf/1910.13325.
[6] K. Horatz, M. Giampà, Y. Karpov, K. Sahre, H. Bednarz, A. Kiriy, B. Voit, K. Niehaus, N. Hadjichristidis, D. L. Michels, F. Lissel, *J. Am. Chem. Soc.* **2018**, *140*, 11416–11423.
[7] I. Salzmann, G. Heimel, M. Oehzelt, S. Winkler, N. Koch, *Acc. Chem. Res.* **2016**, *49*, 370–378.
[8] D. A. Stanfield, Y. Wu, S. H. Tolbert, B. J. Schwartz, *Chem. Mater.* **2021**, *33*, 2343–2356.
[9] K. Müllen, W. Pisula, *J. Am. Chem. Soc.* **2015**, *137*, 9503–9505.
[10] H. Sirringhaus, *Adv. Mater.* **2014**, *26*, 1319–1335.
[11] S. Fratini, M. Nikolka, A. Salleo, G. Schweicher, H. Sirringhaus, *Nat. Mater.* **2020**, *19*, 491–502.
[12] H. T. Nicolai, M. Kuik, G. A. H. Wetzelaer, B. de Boer, C. Campbell, C. Risko, J. L. Brédas, P. W. M. Blom, *Nat. Mater.* **2012**, *11*, 882–887.
[13] I. E. Jacobs, F. Wang, N. Hafezi, C. Medina-Plaza, T. F. Harrelson, J. Li, M. P. Augustine, M. Mascal, A. J. Moulé, *Chem. Mater.* **2017**, *29*, 832–841.
[14] Z. Liang, A. Nardes, D. Wang, J. J. Berry, B. A. Gregg, *Chem. Mater.* **2009**, *21*, 4914–4919.
[15] R. S. Ashraf, B. C. Schroeder, H. A. Bronstein, Z. Huang, S. Thomas, R. J. Kline, C. J. Brabec, P. Rannou, T. D. Anthopoulos, J. R. Durrant, I. McCulloch, *Adv. Mater.* **2013**, *25*, 2029–2034.
[16] Q. Zhang, Q. Wei, X. Guo, G. Hai, H. Sun, J. Li, R. Xia, Y. Qian, S. Casado, J. R. Castro-Smirnov, J. Cabanillas-Gonzalez, *Adv. Sci.* **2019**, *6*, 1801455.
[17] D. Kiefer, R. Kroon, A. I. Hofmann, H. Sun, X. Liu, A. Giovannitti, D. Stegerer, A. Cano, J. Hynynen, L. Yu, Y. Zhang, D. Nai, T. F. Harrelson, M. Sommer, A. J. Moulé, M. Kemerink, S. R. Marder, I. McCulloch, M. Fahlman, S. Fabiano, C. Müller, *Nat. Mater.* **2019**, *18*, 149–155.
[18] G. A. E. Mostafa, A. Bakheit, N. AlMasoud, H. AlRabiah, *Molecules* **2021**, *26*.
[19] T. H. Le, A. Nafady, X. Qu, A. M. Bond, L. L. Martin, *Anal. Chem.* **2012**, *84*, 2343–2350.
[20] P. Skurski, M. Gutowski, *J. Mol. Structure* **2000**, *531*, 339–348.
[21] H. Tamaya, Y. Torii, T. Ishikawa, H. Nakano, T. Iimori, *ChemPhysChem* **2019**, *20*, 2531–2538.
[22] C. Enengl, S. Enengl, S. Pluczyk, M. Havlicek, M. Lapkowski, H. Neugebauer, E. Ehrenfreund, *ChemPhysChem* **2016**, *17*, 3836–3844.
[23] T. H. Le, A. Nafady, X. Qu, L. L. Martin, A. M. Bond, *Anal. Chem.* **2011**, *83*, 6731–6737.
[24] K. E. Watts, K. E. Clary, D. L. Lichtenberger, J. E. Pemberton, *Anal. Chem.* **2020**, *92*, 7154–7161.
[25] A. Yamagishi, M. Sakamoto, *Bull. Chem. Soc. Jpn.* **1974**, *47*, 2152–2157.
[26] S. Hashimoto, A. Yabushita, T. Kobayashi, I. Iwakura, *Chem. Phys. Lett.* **2016**, *650*, 47–51.
[27] R. H. Boyd, W. D. Phillips, *J. Chem. Phys.* **1965**, *43*, 2927–2929.
[28] A. Cehak, A. Cwal, M. Radomska, R. Radohski, *Mol. Cryst. Liq. Cryst.* **1985**, 327–331.

[29] H. Karimi, J. Q. Chambers, *J. Electroanal. Chem. Interf. Electrochem.* **1987**, *217*, 313–329.
[30] M. Brustolon, *Principles and applications of electron paramagnetic spectroscopy*, Wiley, Hoboken, N.J., **2009**.
[31] J. A. Weil, J. R. Bolton, *Electron paramagnetic resonance, Elementary theory and practical applications*, Wiley-Interscience, Hoboken, N.J., **2007**.
[32] M. M. Roessler, E. Salvadori, *Chem. Soc. Rev.* **2018**, *47*, 2534–2553.
[33] G. Jeschke, *Lecture Notes Physical Chemstriy IV Part 2: Electron Paramagnetic Resonance*, **2016**.
[34] S. Schott, U. Chopra, V. Lemaur, A. Melnyk, Y. Olivier, R. Di Pietro, I. Romanov, R. L. Carey, X. Jiao, C. Jellett, M. Little, A. Marks, C. R. McNeill, I. McCulloch, E. R. McNellis, D. Andrienko, D. Beljonne, J. Sinova, H. Sirringhaus, *Nat. Phys.* **2019**, *15*, 814–822.
[35] H. Tanaka, S. Nishio, H. Ito, S.-I. Kuroda, *Appl. Phys. Lett.* **2015**, *107*, 243302.
[36] H. Tanaka , S. Kuroda, M. Kozuka, S. Watanabe, H. Ito,Y. Shimoi, K. Takimiya, *Phys. Rev. B* **2011**, 081306-1-4.
[37] A. Aguirre, P. Gast, S. Orlinskii, I. Akimoto, E. J. J. Groenen, H. El Mkami, E. Goovaerts, S. van Doorslaer, *Phys. Chem. Chem. Phys.* **2008**, *10*, 7129–7138.
[38] M. Arvind, C. E. Tait, M. Guerrini, J. Krumland, A. M. Valencia, C. Cocchi, A. E. Mansour, N. Koch, S. Barlow, S. R. Marder, J. Behrends, D. Neher, *J. Phys. Chem. B* **2020**, *124*, 7694–7708.
[39] R. Fujimoto, S. Watanabe, Y. Yamashita, J. Tsurumi, H. Matsui, T. Kushida, C. Mitsui, H. T. Yi, V. Podzorov, J. Takeya, *Org. Electron.* **2017**, *47*, 139–146.
[40] J. Gao, B. W. Stein, A. K. Thomas, J. A. Garcia, J. Yang, M. L. Kirk, J. K. Grey, *J. Phys. Chem. C* **2015**, *119*, 16396–16402.
[41] K. Hatada, T. Kitayama, *NMR Spectroscopy of Polymers*, Springer, Berlin and Heidelberg, **2004**.
[42] J. H. Gross, *Massenspektrometrie, Spektroskopiekurs kompakt*, Springer Berlin Heidelberg, **2019**.
[43] O. Fenwick, S. Fusco, T. N. Baig, F. Di Stasio, T. T. Steckler, P. Henriksson, C. Fléchon, M. R. Andersson, F. Cacialli, *APL Mater.* **2013**, *1*, 032108.
[44] S. Trimpin, S. Keune, H. J. Räder, K. Müllen, *J. Am. Soc. Mass Spec.* **2006**, *17*, 661–671.
[45] W. F. Edwards, L. Jin, M. C. Thies, *Carbon* **2003**, *41*, 2761–2768.
[46] N. Mermilliod, N. Sellier, *Org. Mass Spectrom.* **1984**, *19*, 563–568.
[47] R. Beckert, E. Fanghänel, W. D. Habicher, H.-J. Knölker, P. Metz, K. Schwetlick, *Organikum*, 24th ed., Wiley-VCH Verlag, Weinheim, **2015**.
[48] C. E. Tait, A. Reckwitz, M. Arvind, D. Neher, R. Bittl, J. Behrends, *Phys. Chem. Chem. Phys.* **2021**.
[49] B. Yurash, D. X. Cao, V. V. Brus, D. Leifert, M. Wang, A. Dixon, M. Seifrid, A. E. Mansour, D. Lungwitz, T. Liu, P. J. Santiago, K. R. Graham, N. Koch, G. C. Bazan, T.-Q. Nguyen, *Nat. Mater.* **2019**, *18*, 1327–1334.
[50] K. Rasmussen, G. Grampp, M. van Eesbeek, T. Rohr, *ACS Appl. Mater. Interfaces* **2010**, *2*, 1879–1883.
[51] R. Stösser, M. Siegmund, *J. Prakt. Chem.* **1977**, *319*, 827–834.
[52] Y.-H. Kim, S.-D. Jung, M.-A. Chung, K.-D. Song, D.-W. Cho, *Bull. Korean Chem. Soc.* **2008**, *29*, 948–952.
[53] Y. Qi, U. Mazur, K. W. Hipps, *RSC Adv.* **2012**, *2*, 10579.
[54] E. H. Suh, Y. J. Jeong, J. G. Oh, K. Lee, J. Jung, Y. S. Kang, J. Jang, *Nano Energy* **2019**, *58*, 585–595.
[55] N. E. Polyakov, V. V. Konovalov, T. V. Leshina, O. A. Luzina, N. F. Salakhutdinov, T. A. Konovalova, L. D. Kispert, *J. Photochem. Photobiol. A* **2001**, *141*, 117–126.
[56] M. Abe, *Chem. Rev.* **2013**, *113*, 7011–7088.
[57] B. M. Hoffman, R. C. Hughes, *J. Chem. Phys.* **1970**, *52*, 4011–4023.
[58] D. T. Scholes, P. Y. Yee, J. R. Lindemuth, H. Kang, J. Onorato, R. Ghosh, C. K. Luscombe, F. C. Spano, S. H. Tolbert, B. J. Schwartz, *Adv. Funct. Mater.* **2017**, *27*, 1702654.

[59] A. Hamidi-Sakr, L. Biniek, J.-L. Bantignies, D. Maurin, L. Herrmann, N. Leclerc, P. Lévêque, V. Vijayakumar, N. Zimmermann, M. Brinkmann, *Adv. Funct. Mater.* **2017**, *27*, 1700173.
[60] L. Ma, P. Hu, C. Kloc, H. Sun, M. E. Michel-Beyerle, G. G. Gurzadyan, *Chem. Phys. Lett.* **2014**, *609*, 11–14.
[61] L. Misseeuw, A. Krajewska, I. Pasternak, T. Ciuk, W. Strupinski, G. Reekmans, P. Adriaensens, D. Geldof, F. Blockhuys, S. van Vlierberghe, H. Thienpont, P. Dubruel, N. Vermeulen, *RSC Adv.* **2016**, *6*, 104491–104501.
[62] R. D. Rataiczak, M. T. Jones, J. R. Reeder, D. J. Sandman, *Mol. Phys.* **1985**, *56*, 65–77.
[63] L. Ma, P. Hu, H. Jiang, C. Kloc, H. Sun, C. Soci, A. A. Voityuk, M. E. Michel-Beyerle, G. G. Gurzadyan, *Sci. Rep.* **2016**, *6*, 28510.
[64] G. Couto Faria, *Structure and dynamics of poly(9,9-dioctylfluoren-2,7-diyl-co-benzothiadiazole) (F8BT) and correlations with its electrical properties (dissertation)*, Universidade de Sao Paulo, San Carlos, Brazil, **2011**.
[65] L.-F. Ji, J.-X. Fan, S.-F. Zhang, A.-M. Ren, *Phys. Chem. Chem. Phys.* **2018**, *20*, 3784–3794.
[66] Y. Zheng, G. N. Wang, J. Kang, M. Nikolka, H. Wu, H. Tran, S. Zhang, H. Yan, H. Chen, P. Y. Yuen, J. Mun, R. H. Dauskardt, I. McCulloch, J. Tok, X. Gu, Z. Bao, *Adv. Funct. Mater.* **2019**, *29*, 1905340.
[67] D. Venkateshvaran, M. Nikolka, A. Sadhanala, V. Lemaur, M. Zelazny, M. Kepa, M. Hurhangee, A. J. Kronemeijer, V. Pecunia, I. Nasrallah, I. Romanov, K. Broch, I. McCulloch, D. Emin, Y. Olivier, J. Cornil, D. Beljonne, H. Sirringhaus, *Nature* **2014**, *515*, 384–388.
[68] W. Zhang, J. Smith, S. E. Watkins, R. Gysel, M. McGehee, A. Salleo, J. Kirkpatrick, S. Ashraf, T. Anthopoulos, M. Heeney, I. McCulloch, *J. Am. Chem. Soc.* **2010**, *132*, 11437–11439.
[69] K. E. Watts, B. Neelamraju, M. Moser, I. McCulloch, E. L. Ratcliff, J. E. Pemberton, *J. Phys. Chem. Lett.* **2020**, *11*, 6586–6592.
[70] A. Kolbert, M. Mehring, *J. Mag. Res.* **1992**, *100*, 82–87.
[71] J. Li, M. J. Lear, Y. Hayashi, *Angew. Chem. Int. Ed.* **2016**, *55*, 9060–9064.
[72] L. R. Melby, R. J. Harder, W. R. Hertler, W. Mahler, R. E. Benson, W. E. Mochel, *J. Am. Chem. Soc.* **1962**, *84*, 3374–3387.

List of Figures

List of Tables

8 Appendix

ESR

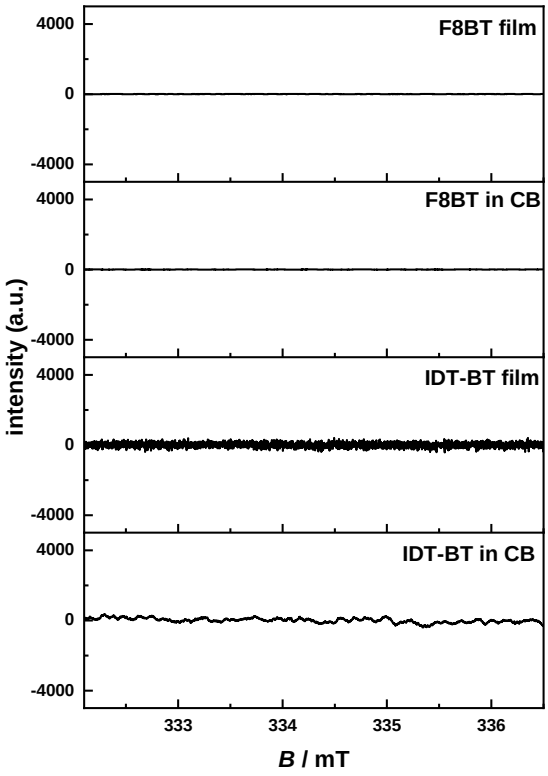

Figure 8.1: Liquid state ESR spectra of **IDT-BT**/ **F8BT** in CB as well as solid-state ESR of the polymer films, annealed from CB at 363 K for 1 h.

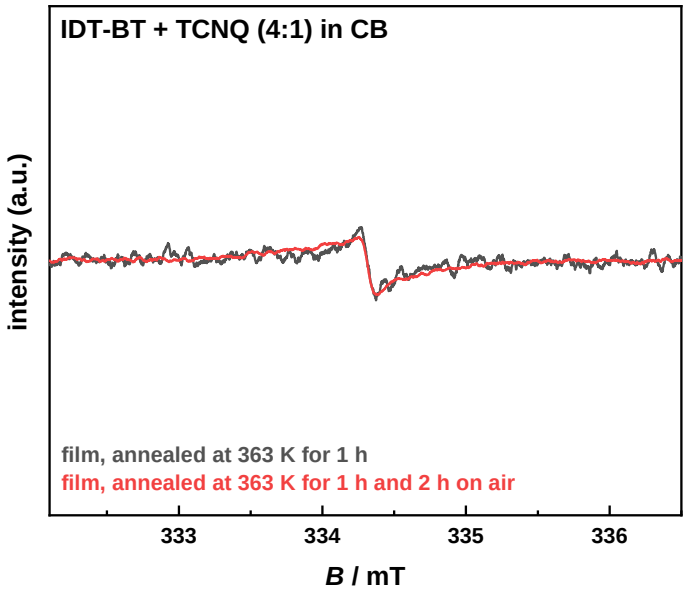

Figure 8.2: ESR spectra of IDT-BT/ TCNQ films with molar ratios of polymer:dopant = 4:1, which were annealed from CB at 363 K for 1 h. One of the film then was allowed to remain in air for 2 h prior to the measurement. The spectra were recorded at rt and $g = 2.0032 \pm 0.0003$.

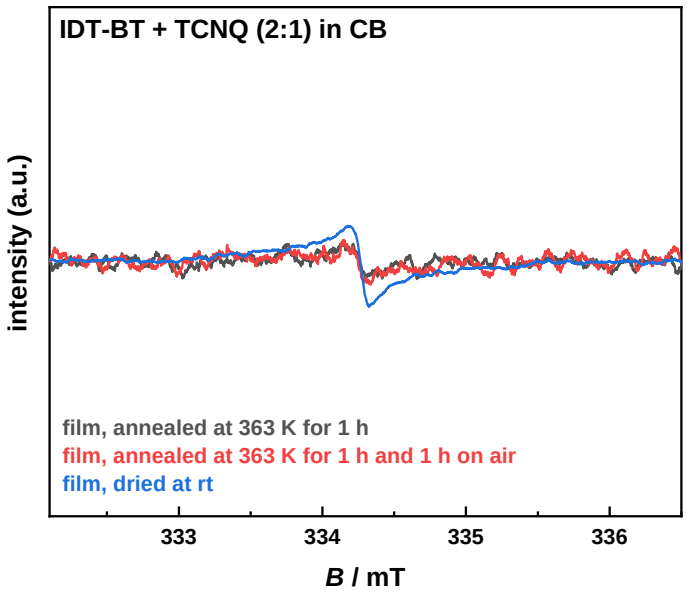

Figure 8.3: ESR spectra of IDT-BT/ TCNQ films annealed from CB at 363 K for 1 h as well as dried at rt with molar ratios of polymer:dopant = 2:1. One of the annealed films then was allowed to remain in air for 1 h prior to the measurement. The spectra were recorded at rt and $g = 2.0032 \pm 0.0003$.

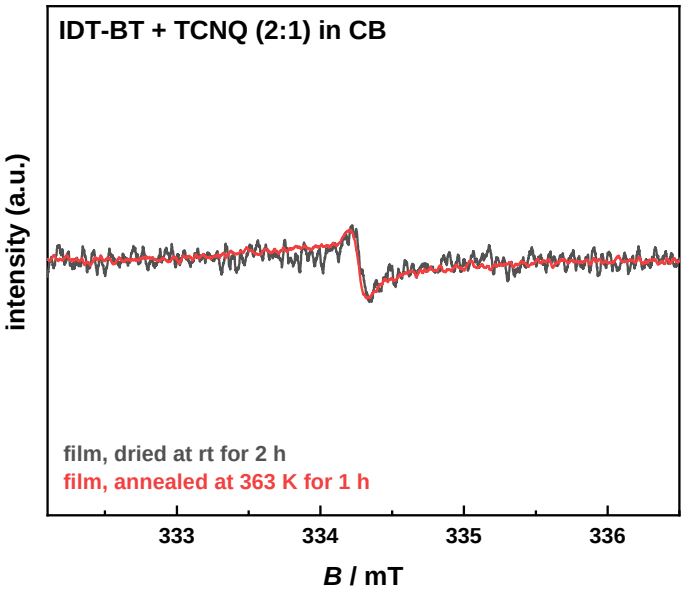

Figure 8.4: ESR spectra of IDT-BT/ TCNQ films annealed from CB at 363 K for 1 h as well as dried at rt with molar ratios of polymer:dopant = 4:1 at rt and $g = 2.0032 \pm 0.0003$.

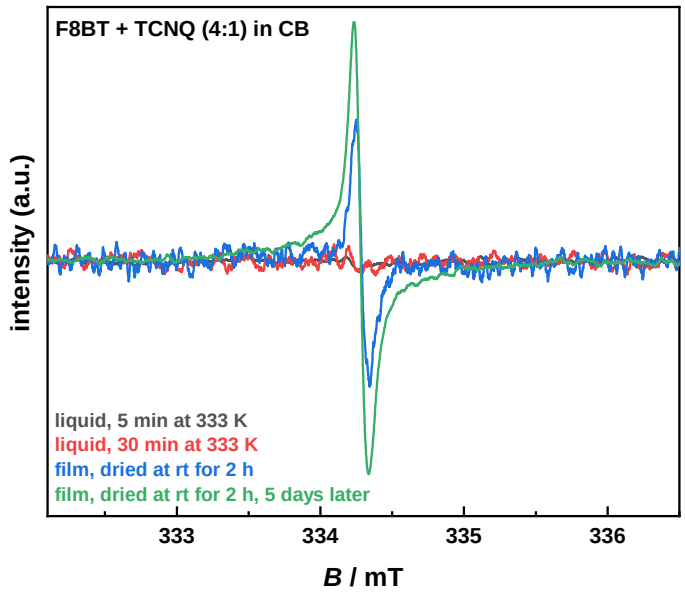

Figure 8.5: Liquid state ESR spectra of F8BT and TCNQ in CB and films annealed from this solution at 363 K for 1 h as well as dried at rt with molar ratios of polymer:dopant = 4:1. The spectra were recorded at rt and $g = 2.0032 \pm 0.0003$.

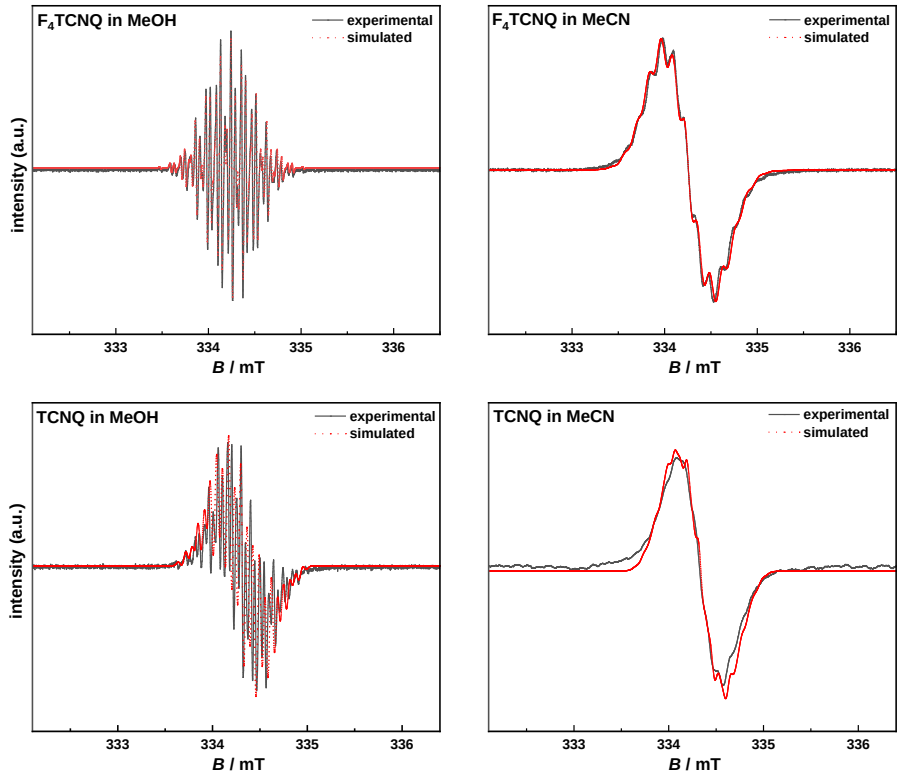

Figure 8.6: Experimental and simulated spectra of F_4TCNQ and TCNQ in methanol and acetonitrile using *EasySpin*.

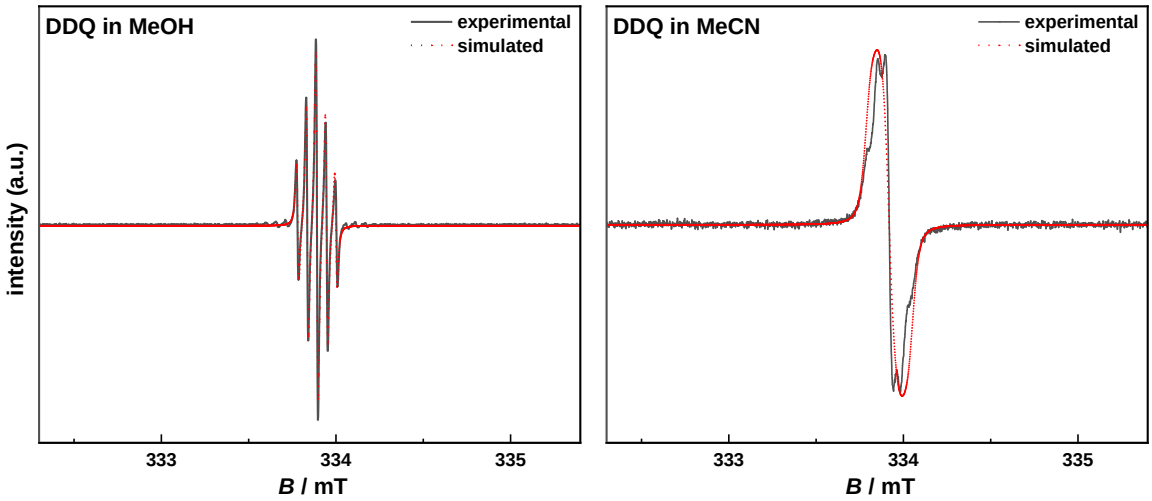

Figure 8.7: Experimental and simulated spectra of DDQ in methanol and acetonitrile using *EasySpin*.

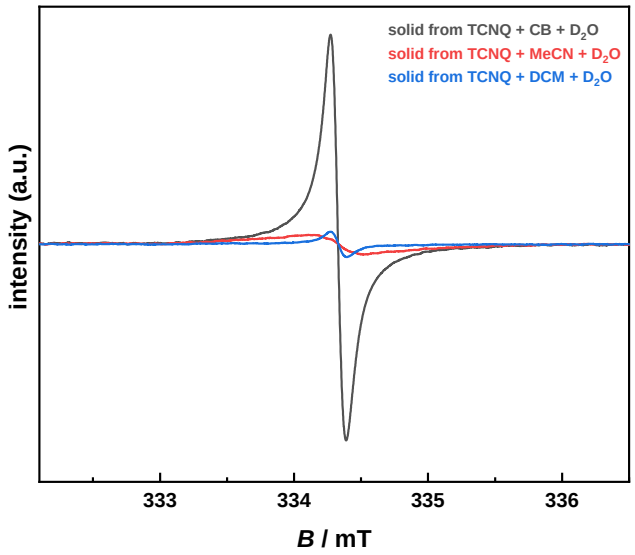

Figure 8.8: ESR spectra of solids obtained after stirring TCNQ in chlorobenzen, acetonitrile and dichloromethane with an excess of D_2O for 48 h at rt. The spectra were recorded at rt and $g = 2.0032 \pm 0.0003$.

NMR

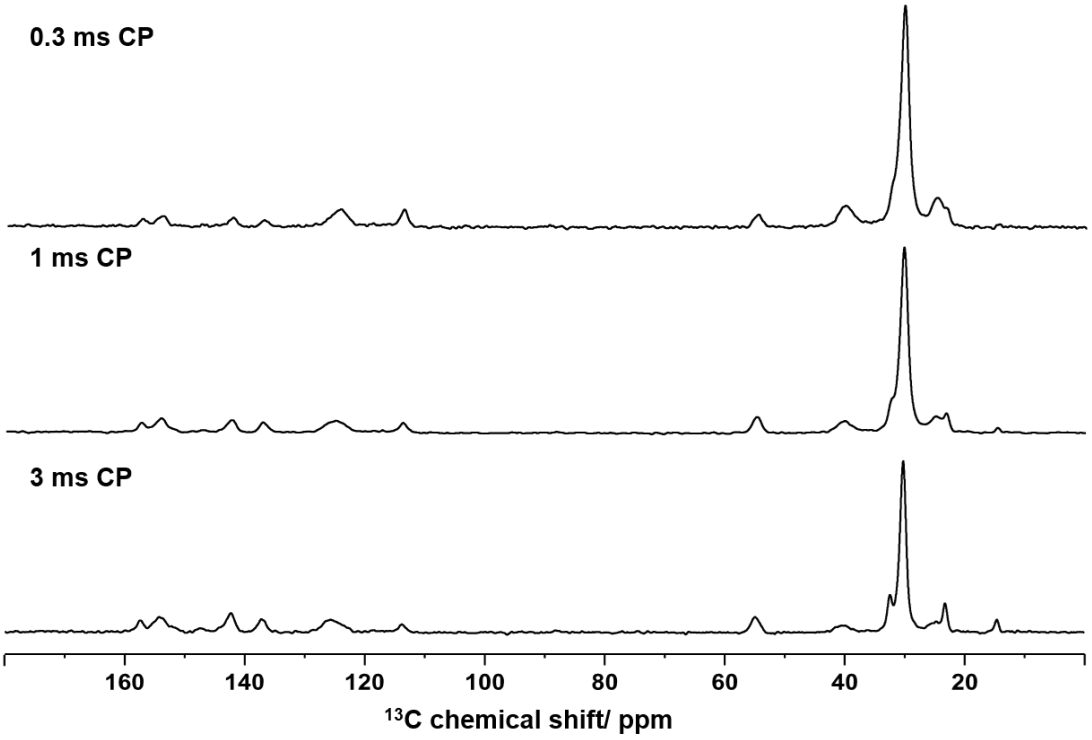

Figure 8.9: $\{^1H\}$-^{13}C CP MAS spectra of pristine IDT-BT at different CP contact times.

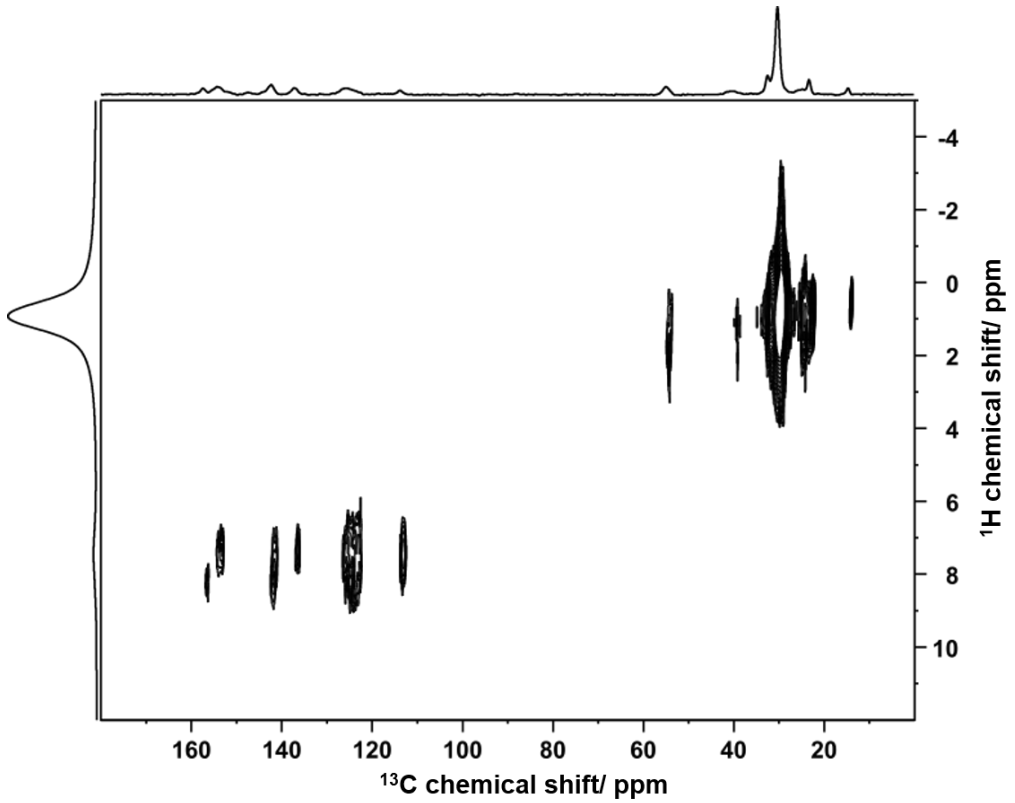

Figure 8.10: ^{1}H-^{13}C HETCOR spectrum of pristine IDT-BT.

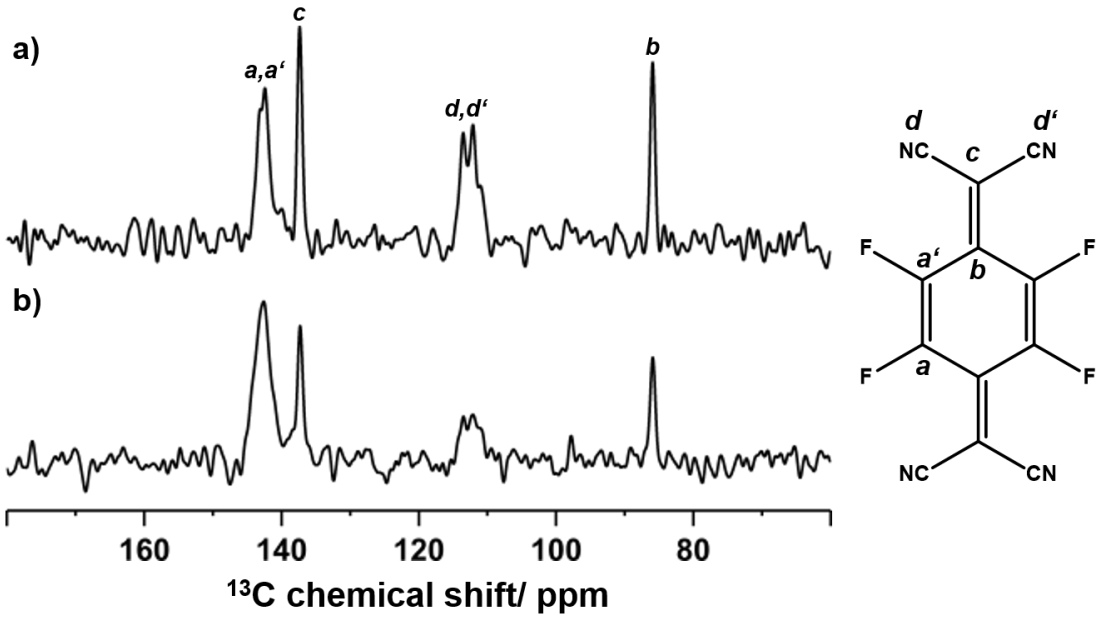

Figure 8.11: {^{19}F}-^{13}C CP MAS spectra of F_4TCNQ annealed from chlorobenzene **a)** using a glass syringe and **b)** suing a plastic syringe.

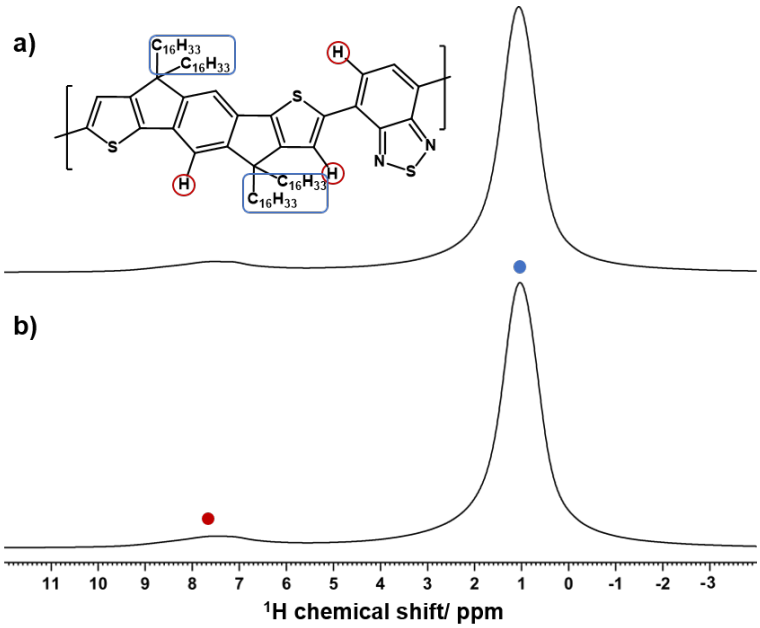

Figure 8.12: ^{1}H MAS of IDT-BT/F_4TCNQ blends: **a)** after annealing at 373 K, 383 K, 393 K, 403 K for one hour each and **b)** after preperation at rt.

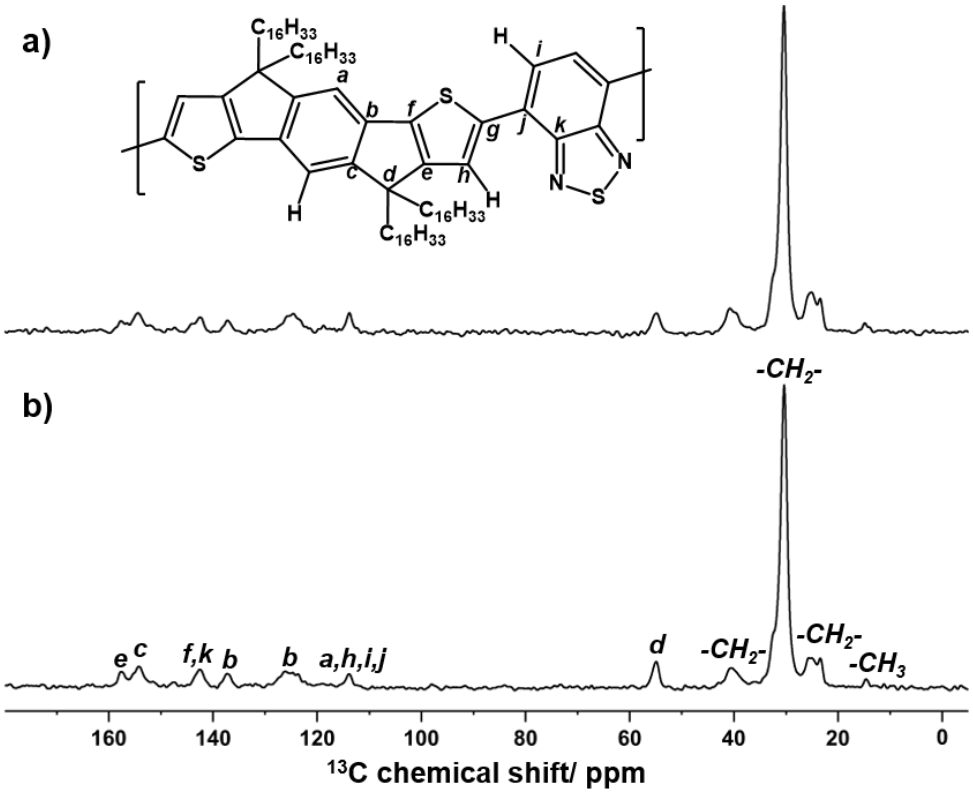

Figure 8.13: {^{1}H}-^{13}C CP MAS of IDT-BT/F_4TCNQ blends: **a)** after annealing at 373 K, 383 K, 393 K, 403 K for one hour each and **b)** after preperation at rt.

MALDI

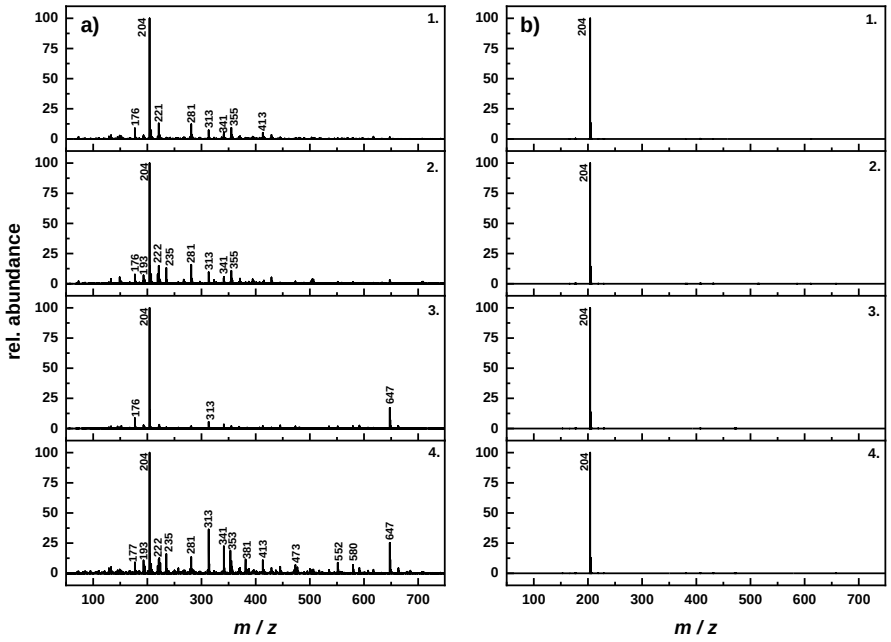

Figure 8.14: MALDI-TOF spectra in **a)** positive and **b)** negative refelctron ion mode. **1.** TCNQ and IDT-BT (10:1) in CB with excess H_2O annealed at 363 K for 1 h, **2.** TCNQ and IDT-BT (10:1) in CB with excess H_2O dried at rt, **3.** TCNQ in CB with excess H_2O annealed at363 K for 1 h hour and **4.** TCNQ in CB with excess H_2O dried at rt.

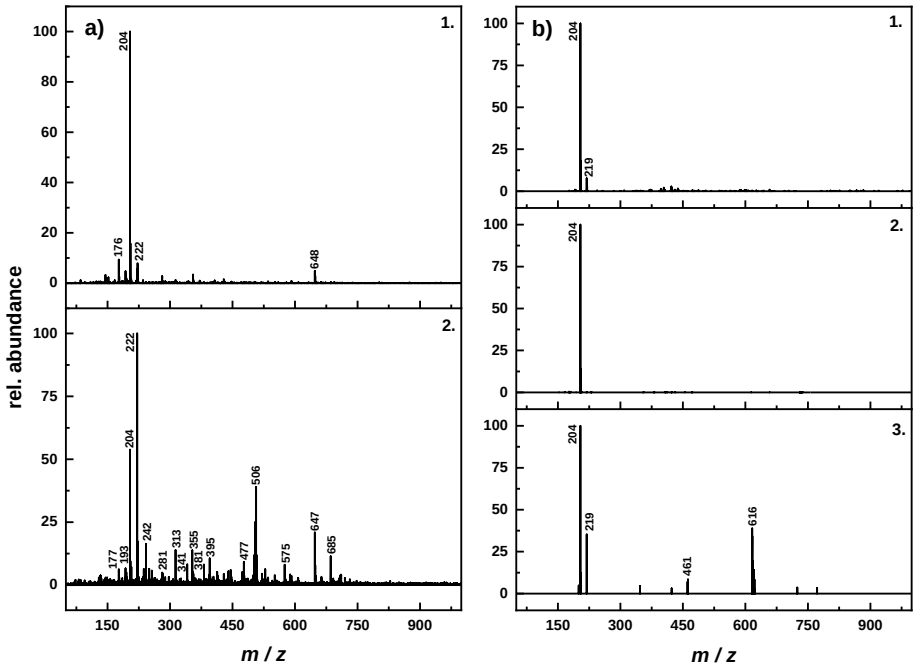

Figure 8.15: MALDI-TOF spectra in **a)** positive and **b)** negative reflectron mode. **1.** water phase obtained from combining TCNQ in CB with exces H_2O, annealed at 363 K for 1 h and **2.** water phase obtained from combining TCNQ in CB with excess H_2O dried at rt.

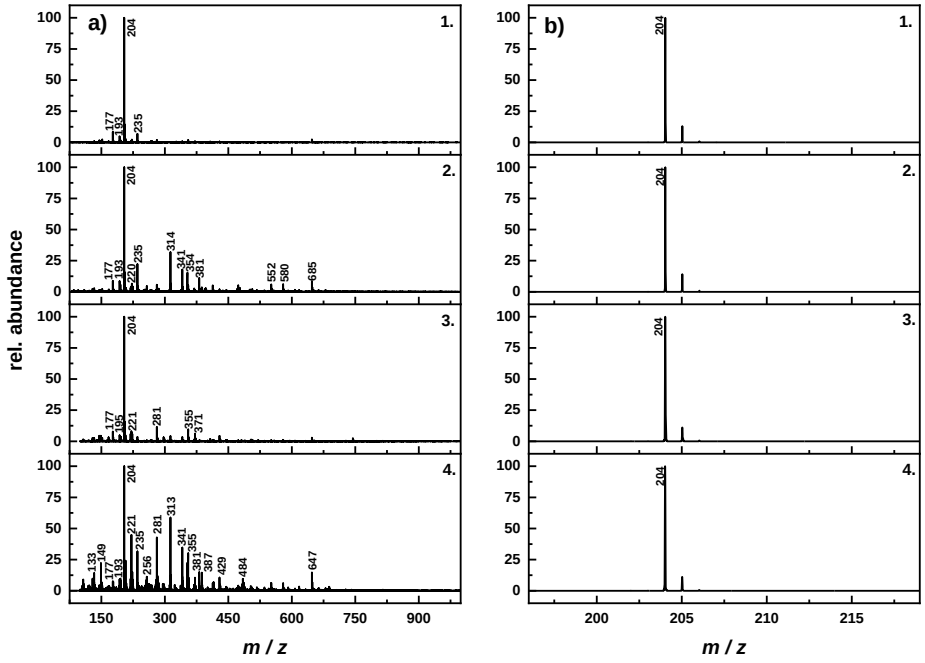

Figure 8.16: MALDI-TOF spectra in **a)** positive and **b)** negative reflectron mode. **1.** TCNQ in CB annealed at 363 K for 1 h, **2.** TCNQ in CB dried at rt, **3.** TCNQ and D_2O (1:1) in CB annealed at 363 K for 1 h and **4.** TCNQ and D_2O (1:1) in CB dried at rt.

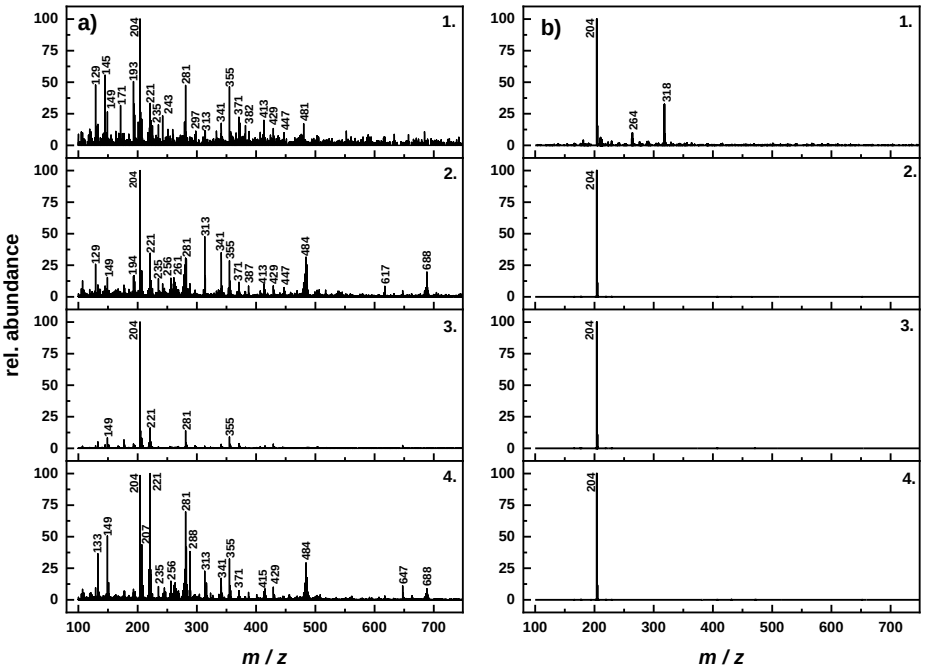

Figure 8.17: MALDI-TOF spectra in **a)** positive and **b)** negative relectron ion mode. **1.** TCNQ and IDT-BT (10:1) in CB with excess D_2O annealed at 363 K for 1 h, **2.** TCNQ and IDT-BT (10:1) in CB with excess D_2O TCNQ and IDT-BT (10:1) with excess D_2O, **3.** TCNQ in CB with excess H_2O annealed at 363 K for 1 h and **4.** TCNQ in CB with excess D_2O.

Table 8.1: $\frac{m}{z}$ and relativ abundances (r. a.) corresponding to Figure 8.16, Figure 8.14 and Figure 8.15.

Figure 4.4a 2.		Figure 4.4a 1.		Figure 4.4a 4.		Figure 4.4a 4.		Figure 8.14a)4.		Figure 8.14a 3.		Figure 8.14a 2.		Figure 8.14a 1.		Figure 8.15a 2.				Figure 8.15a 1.	
$\frac{m}{z}$	r. a.	$\frac{m}{z}$	r. a.	$\frac{m}{z}$	r. a.	$\frac{m}{z}$	r. a.	$\frac{m}{z}$	r. a.	$\frac{m}{z}$	r. a.	$\frac{m}{z}$	r. a.	$\frac{m}{z}$	r. a.	$\frac{m}{z}$	r. a.	$\frac{m}{z}$	r. a.	$\frac{m}{z}$	r. a.
167	2.4	177	8.2	167	1.1	177	8.0	167	2.8	177	8.3	151	1.5	151	1.2	156	2.2	430	2.4	177	9.3
168	2.1	193	5.4	177	9.3	193	2.0	177	8.8	193	2.9	167	1.00	177	8.3	166	2.0	439	3.0	193	4.8
177	8.3	194	3.4	178	5.9	194	1.5	178	2.7	194	2.1	177	7.7	193	3.4	177	6.1	445	6.1	194	3.5
178	2.7	204	100	192	1.3	204	100	193	10.8	204	100	178	2.4	194	2.2	178	2.9	447	3.7	204	100
179	2.2	207	3.1	193	5.1	221	2.1	194	7.2	221	2.00	192	1.3	204	100	185	1.8	477	9.3	221	5.7
192	1.1	220	1.4	194	3.2	222	3.3	195	6.0	222	3.5	193	2.6	207	7.1	185	2.7	483	1.7	222	8.0
193	8.6	221	1.5	195	1.4	313	7.2	204	100.0	313	5.7	193	7.1	208	1.5	192	1.6	484	2.8	647	5.0
194	5.6	222	2.5	195	3.4	341	7.7	206	3.0	341	5.3	194	3.8	221	13.3	193	6.6	485	2.2		
195	6.1	235	7.1	204	100.0	413	4.1	207	7.6	591	2.7	204	100	222	5.7	194	4.6	500	4.0		
204	100.0	647	2.6	207	1.1	647	5.9	208	3.1	647	18.6	207	7.8	281	12.2	195	5.1	503	12.4	Figure 8.15b 1.	
206	3.3			207	1.7			219	6.8	662	2.5	207	1.2	282	3.6	196	3.0	504	6.0	m /z	r.a.
207	3.3			208	1.9			220	3.8			208	1.5	313	7.4	204	53.4	505	26.8	204	100
208	3.2			219	2.2			221	12.7			208	1.8	341	3.8	206	2.9	506	12.4	219	7.7
219	4.0			220	2.3			222	12.4			219	7.8	341	7.5	207	7.2	507	39.5	422	2.8
220	4.2			221	1.4			223	5.1			220	2.2	355	9.6	208	2.2	508	1.5		
221	6.1			221	1.7			235	16.0			221	15	356	3.2	220	2.1	521	4.3	Figure 8.15b 3.	
222	8.5			222	2.0			236	3.5			222	3.8	413	5.3	221	100	529	6.5	204	100
223	2.7			222	1.9			281	13.5			222	2.3	429	3.7	223	5.7	551	4.0	461	7.0
235	21.9			223	1.3			282	3.5			223	3.6	430	1.7	224	3.1	575	8.4	616	15.3
236	4.4			235	14.3			313	36.6			235	13.3	480	1.1	237	6.2	576	3.1	616	39.1
256	1.2			313	7.5			341	25.5			281	15.8			238	2.8	588	4.3	616	34.6
281	5.7			341	5.1			353	18.5			282	4.4			242	16.2	589	3.3	617	4.5
282	1.8			355	3.9			354	4.2			313	9.7			250	6.5	591	3.8	617	3.7
313	31.9			552	3.2			355	10.5			341	4.7			256	5.8	647	21.5	617	19.4
341	21.1			580	4.0			355	5.8			341	5.7			257	3.1	662	2.6	618	3.6
353	15.5			647	8.1			356	5.5			342	1.8			263	2.7	663	3.2	619	10.3
354	3.6			648	4.0			381	11.5			355	10.9			281	5.1	685	11.8	619	6.6
355	5.2							382	3.1			356	4.4			282	2.5	705	1.6	620	5.4
356	1.9							387	3.9			371	4.4			282	4.5	706	2.5		
381	11.2							413	10.9			372	1.9			283	2.1	707	2.4		
382	2.7							429	4.6			394	3.7			313	13.8	708	2.3		
383	2.0							445	5.6			395	1.1			341	9.1	709	3.8		
387	3.7							473	7.1			415	2.8			353	14	710	4.3		
394	2.4							477	5.1			429	5.3			354	3.9				
395	1.2							552	8.9			430	2.0			355	5.1				
396	3.1							580	7.5			503	2.3			356	4.5				
413	5.3							591	4.5			504	1.2			381	8.1				
473	5.4							647	26.2			505	3.8			392	2.1				
477	3.2							648	11.9			507	3.7			393	3.3				
501	1.9							662	2.6			552	1.6			395	10.4				
552	6.0							663	4.6			647	3.1			396	4.4				
580	6.3											707	1.4			418	2.0				
647	8.9											708	1.1			423	1.7				
662	1.1											709	1.8			429	4.5				

Table 8.2: $\frac{m}{z}$ and relativ abundances (r. a.) corresponding to Figure 8.16 and Figure 8.17.

Figure 8.16a 2.		Figure 8.16a 1.		Figure 8.17a 4.				Figure 8.17a 3.		Figure 8.17a 2.					
$\frac{m}{z}$	r. a.	$\frac{m}{z}$	r. a.	$\frac{m}{z}$	r. a.	$\frac{m}{z}$	r. a.	$\frac{m}{z}$	r. a.	$\frac{m}{z}$	r. a.	$\frac{m}{z}$	r. a.	$\frac{m}{z}$	r. a.
149	23.8	149	4.9	128	3.2	288	38.5	149	8.8	105	6.2	245	6.5	242	1.6
150	4.2	150	1.2	129	10.3	293	2.8	150	1.5	106	2.3	246	2.9	242	10.3
151	8.8	151	1.8	130	1.7	294	1.9	151	2.9	109	5.3	247	3.5	243	5.8
167	5.3	167	3.8	131	3.5	295	4.0	167	2.2	110	1.8	250	2.1	244	2.2
168	5.3	168	2.4	132	2.2	296	2.0	168	1.6	113	2.4	250	1.5	475	2.1
177	7.6	177	7.7	133	37.2	297	4.2	177	6.7	119	5.8	251	2.7	476	1.6
178	7.5	178	3.5	134	5.1	297	3.9	193	3.7	120	1.6	253	1.8	477	1.8
179	3.7	193	5.0	135	7.8	298	1.7	194	2.7	123	4.2	256	14.6	478	3.1
192	3.1	194	4.2	136	1.8	302	2.9	195	2.8	124	1.8	257	1.5	479	6.5
193	9.9	195	5.2	139	2.3	303	1.7	204	100.0	127	2.2	257	10.3	480	11.0
194	8.0	204	100.0	140	2.1	313	23.1	207	8.0	128	4.4	258	3.3	481	10.2
195	11.9	207	4.8	141	2.2	316	13.4	208	1.6	129	26.4	260	1.7	482	17.8
204	100.0	208	1.1	142	3.8	317	3.1	219	4.4	131	3.1	261	14.9	483	10.2
205	23.9	219	6.0	149	52.5	323	5.6	220	1.4	132	1.8	263	11.2	484	31.8
206	5.6	220	2.2	150	8.1	341	17.3	221	16.3	133	8.9	265	8.0	485	14.6
207	25.5	221	9.6	151	15.8	341	14.9	222	4.8	133	6.9	266	1.8	486	25.2
208	6.8	222	7.3	152	5.3	342	5.7	223	5.3	134	2.1	267	3.4	501	2.1
219	10.4	223	6.1	153	2.8	343	4.0	224	1.0	135	6.3	267	4.7	502	1.5
220	8.4	224	1.3	154	2.7	344	2.4	281	14.0	136	2.5	268	5.5	503	5.1
221	46.2	281	11.5	155	2.5	345	2.3	282	4.0	141	2.0	269	5.4	504	2.3
222	18.9	282	3.4	156	2.3	346	2.6	341	3.2	141	3.7	274	1.6	504	2.4
223	16.8	355	9.6	163	5.7	353	4.0	355	9.1	142	3.6	274	3.2	516	1.9
224	9.6	356	3.3	164	1.5	354	2.0	356	3.2	149	15.7	275	2.6	517	5.2
235	32.2	371	6.2	165	2.9	355	32.8	371	3.8	149	5.5	276	7.6	525	1.5
256	8.6	372	2.5	166	1.8	356	11.2	372	1.6	150	2.9	277	6.3	526	1.6
278	5.0	407	1.9	167	4.0	357	7.5	429	3.3	151	4.8	278	17.2	535	2.1
280	9.2	429	4.4	168	3.8	371	7.5	430	1.4	151	4.1	279	7.4	536	2.1
281	43.0	430	1.7	169	3.2	372	3.2	647	2.5	152	4.6	280	25.1	537	2.3
281	3.8	647	3.0	170	3.4	373	2.9			152	1.8	281	30.5	540	4.1
282	11.1	744	2.4	177	6.9	387	6.3			153	2.1	281	5.4	541	2.8
282	11.5			178	6.9	401	4.1			153	2.1	282	9.4	545	3.5
283	6.7			179	2.8	401	1.8			154	2.3	282	29.5	559	1.7
284	5.1			180	2.6	402	1.6			155	2.2	283	5.8	580	2.3
313	59.6			181	1.8	411	1.5			156	2.0	284	1.9	616	3.4
341	11.6			184	2.8	412	2.2			161	4.3	284	6.2	617	8.3
341	38.8			191	2.9	413	6.8			162	1.7	285	6.1	632	2.3
353	22.8			192	2.9	414	2.5			163	5.4	288	2.1	647	4.9
354	5.2			193	9.2	415	8.7			164	1.6	288	10.3	662	2.4
355	30.2			194	5.1	416	3.7			165	1.8	289	2.3	684	4.1
356	10.6			195	6.5	429	10.1			166	2.3	289	2.5	685	5.0
371	10.7			196	6.9	430	4.3			166	3.2	294	2.5	686	7.2
372	4.2			197	1.6	439	1.9			167	6.7	301	2.0	687	5.9
381	15.3			203	3.2	440	1.5			167	2.8	311	5.5	688	19.5
387	14.9			204	98.6	455	4.1			168	4.5	312	1.6	690	4.5
429	10.7			205	21.9	456	5.1			169	3.9	313	47.5	703	1.8
430	5.1			206	4.2	457	2.6			169	2.3	314	16.2	706	1.5
482	5.6			207	44.0	458	2.1			170	2.6	323	1.9	742	1.7
483	3.3			208	8.9	467	2.2			170	2.0	328	1.5	764	3.0
484	9.8			209	12.2	468	1.9			171	1.9	333	1.9	765	2.6
485	4.5			217	5.0	469	3.4			171	3.7	337	4.8	821	2.9
647	15.0			218	1.7	478	2.0			172	1.6	338	2.0	890	2.4
				219	24.2	479	2.7			173	2.2	341	6.1	891	2.3
				220	8.4	480	5.9			174	2.0	341	35.4	963	1.8
				221	100.0	481	4.6			177	9.1	342	2.4	978	2.7
				222	25.6	482	13.5			178	6.8	342	8.7	979	2.2
				223	21.3	483	8.2			179	2.2	343	3.2		
				224	5.6	484	30.4			179	1.9	344	3.1		
				235	11.1	485	12.8			180	3.0	345	1.6		
				236	2.9	486	17.9			181	2.4	353	6.6		
				239	1.7	487	6.5			184	1.7	355	28.4		
				240	2.0	495	1.8			185	5.9	356	12.1		
				243	5.3	496	1.5			186	3.0	357	5.0		
				244	1.6	497	1.8			189	2.6	357	1.7		
				245	9.4	498	2.1			190	2.4	358	1.9		
				246	2.1	499	2.6			193	16.0	358	2.0		
				247	6.2	500	2.3			194	16.8	369	4.0		
				251	1.9	501	3.1			195	12.2	371	11.4		
				256	14.7	503	3.3			198	3.3	372	3.8		
				257	6.1	504	1.5			201	4.9	380	1.6		
				258	1.6	508	4.2			202	2.3	381	1.7		
				259	5.7	617	3.5			203	5.0	381	2.6		
				260	2.3	647	11.6			204	100.0	381	4.0		
				261	11.8	648	5.4			205	20.3	386	1.7		
				262	3.4	662	2.1			206	5.5	387	8.4		
				263	13.8	663	3.7			207	20.5	401	1.8		
				264	3.4	684	2.2			207	2.5	407	4.5		
				265	9.1	685	2.5			208	2.5	408	2.7		
				267	6.3	686	5.1			209	4.0	411	1.8		
				268	1.6	687	4.2			209	1.9	412	2.3		
				269	7.4	688	9.1			219	6.6	413	9.9		
				274	2.8	689	5.0			220	4.6	429	8.6		
				275	3.6	690	3.7			221	34.7	430	5.2		
				276	7.4	764	2.6			222	9.1	440	3.1		
				277	3.7	765	2.1			223	13.2	441	1.7		
				278	13.2	766	2.7			224	2.6	442	1.6		
				279	4.0					224	1.8	443	2.0		
				280	24.2					231	3.3	447	7.2		
				281	4.8					232	1.8	457	2.1		
				282	40.2					233	2.8	458	3.4		
				283	12.1					234	2.2	465	2.6		
				283	9.4					235	14.2	466	2.1		
				284	2.8					236	3.3	467	1.6		
				284	7.8					236	1.9	468	1.8		

Table 8.3: $\frac{m}{z}$ and relativ abundances (r. a.) corresponding to Figure 8.17.

Figure 8.17a 1.				Figure 8.17b 1.	
$\frac{m}{z}$	r. a.	$\frac{m}{z}$	r. a.	$\frac{m}{z}$	r. a.
109	5.1	371	22.0	204	100
110	3.4	372	11.2	264	10
117	7.8	380	4.1	318	33
118	3.6	381	3.3		
127	3.0	381	8.5		
128	5.5	381	4.5		
129	47.5	387	4.2		
130	14.6	397	4.3		
141	4.6	401	3.7		
141	8.2	407	10.0		
142	5.8	411	7.8		
145	55.3	412	4.1		
146	9.6	426	5.3		
149	26.0	427	3.7		
149	4.7	428	3.7		
150	5.0	429	13.1		
151	4.6	439	5.5		
154	3.5	440	3.2		
165	4.5	445	4.0		
166	3.7	446	5.1		
167	4.6	465	5.9		
168	8.9	466	3.2		
169	5.6	473	3.8		
170	3.2	476	8.4		
171	31.2	477	3.6		
174	8.7	477	7.9		
177	3.7	480	16.9		
178	3.6	503	7.5		
193	50.3	503	3.2		
194	32.4	504	6.0		
201	18.2	505	6.3		
202	16.5	521	3.8		
202	4.7	522	3.0		
203	12.2	527	3.6		
204	100.0	589	8.1		
205	25.9	590	5.9		
207	20.3	615	5.6		
210	3.5	616	6.6		
220	13.6	632	3.5		
221	32.9	912	3.3		
221	3.8				
222	16.4				
222	4.2				
223	19.2				
224	3.6				
225	7.4				
225	15.2				
228	4.5				
233	5.7				
234	3.9				
235	15.9				
249	6.2				
250	5.6				
254	4.5				
258	4.6				
259	12.3				
269	3.4				
274	5.5				
274	4.6				
275	7.1				
276	6.4				
281	47.2				
282	10.0				
283	3.6				
283	3.8				
293	3.6				
297	8.2				
310	6.2				
313	11.2				
317	3.3				
326	3.1				
327	3.8				
332	4.0				
333	11.0				
333	4.8				
335	4.3				
336	5.0				
340	4.7				
341	9.0				
342	5.3				
343	6.1				
344	3.7				
344	4.2				
355	46.4				
357	10.5				
358	8.9				
359	4.4				
360	5.3				
364	3.5				
365	4.8				